Robust Repetitive Control and Applications

Submitted in total fulfilment of the requirements of the degree of
Doctor of Philosophy

Edi Kurniawan

Faculty of Engineering and Industrial Sciences
Swinburne University of Technology
Melbourne, Australia
2013

Abstract

Repetitive Control (RC) has been widely used to track a periodic reference signal, or to reject periodic disturbance. Digital RC is usually designed by assuming a constant period of reference/disturbance signal, which then leads to the selection of a fixed sampling period. However, in practice, both reference signal and disturbance may vary in period. In order to overcome this problem, the sampling period is carefully adjusted to maintain a constant number of samples per period. This sampling period adjustment causes a change in the parametric model of the plant. This thesis aims to develop novel RC designs for a tracking/ rejecting periodic signal with time-varying frequency. We present three main designs in this thesis: a robust RC design, an adaptive RC design, and a MIMO RC design.

The first design developed was the robust RC for linear systems with time varying sampling periods. Firstly, it develops a new frequency domain method for the nominal sampling period to design a low order, stable, and causal IIR repetitive compensator that uses an optimization method to achieve fast convergence and high tracking accuracy. A new stable and causal compensator can be implemented independently to reduce the design complexity, as most existing repetitive compensators are either unstable or non-causal, which makes the implementation difficult. A comprehensive analysis and comparison study is presented. Then this thesis extends the method to design a robust RC, which compensates time varying periodic signals in a known range. In the design, the time-varying parts due to sampling period interval variation are treated as parametric uncertainties, and the robust RC is designed as close as possible to the nominal one, thus ensuring that the system is stable for any sampling period in the given interval. A complete series of experiments on a servo motor was successfully carried out to demonstrate the effectiveness of the proposed algorithms.

The second design developed was the Adaptive Repetitive Control (ARC) for unknown linear systems subject to time varying periodic disturbances. It was assumed that the sampling period would be locked to the period of disturbance signal to preserve a constant number of samples per disturbance period, as required by the RC. The sampling period adjustment results in a discrete plant with time-varying coefficients. By considering the direct adaptive control, it is possible to adapt the parameters of the controller to handle the time varying plant. Thus, the ARC has been proposed, based on the direct adaptive control and the internal model principle. The internal model can reject the disturbance perfectly, since the number of samples per period remains fixed. The time-varying plant parameters are handled by the direct adaptive control, as it tunes the controller parameters such that the closed-loop system is stable and the plant output tracks the reference. The effectiveness of the ARC has been verified in simulations and experiments on a servo motor system.

The third design developed was the decentralized RC (DRC) for linear multiple inputs multiple outputs (MIMO) systems. The design is based on decentralized control that treats the MIMO system as a set of single input single output (SISO) systems. A Relative Gain Array (RGA) analysis is first performed to determine the dynamics that result in dominant interactions. A set of low order, stable and causal repetitive compensators are then designed to compensate the dominant dynamics that have been determined by the RGA. The compensators, which ensure the system stability, are obtained by solving an optimization. Various numerical examples are presented to demonstrate the effectiveness of the proposed DRC. The comprehensive analysis and comparison study is given. The novelty of the design was also verified in experiments on a 2 DOF robot.

Acknowledgement

I shall always be deeply indebted to my principal supervisor, Dr. Zhenwei Cao, for her constant support and guidance during the past 3.5 years of my research. She has given remarkable help during my research, with insightful opinions in every discussion. I am also very grateful to her for introducing me to the field of Repetitive Control, and for encouraging me in my study of many control schemes. I would like to thank my co-supervisor, Prof. Zhihong Man, who has always been ready to provide academic and financial advice. Without their constant help, this work would not have been completed.

I gratefully acknowledge the funding for 3.5 years that made my Phd research possible, namely Swinburne University of Technology (SUT). Thanks to SUT for awarding me a SUPRA scholarship and providing me with a constructive research environment. I am also indebted to the senior technical staff, Walter and Phil, who resolved any issues related to working in the Lab.

To my dear comrades in AD222, Aiji, Himani, Ehsan, Hai Wang, Fei Siang, and Hossein, thanks for making my PhD life a little more vibrant. Our gatherings in the office always end up with such a fun discussion.

I would really like to thank my parents, my sisters, and my brothers-in-law for their love and encouragement. Finally, this thesis would not have been possible without the love and support of my dear wife and daughter.

Declaration

This is to certify that:

1. This thesis contains no material which has been accepted for the award to the candidate of any other degree or diploma, except where due reference is made in the text of the examinable outcome.

2. To the best of the candidate's knowledge, this thesis contains no material previously published or written by another person except where due reference is made in the text of the examinable outcome.

3. The work is based on the joint research and publications; the relative contributions of the respective authors are disclosed.

4. This thesis has been professionally proofread by Christine De Boos.

Edi Kurniawan, 2013

Contents

CHAPTER 4:

CHAPTER 5:

List of Figures

List of Tables

List of Abbreviations and Acronyms

ADC – analog to digital converter

ARC – adaptive repetitive control

DAC – digital to analog converter

DOF – degrees of freedom

DRC – decentralized repetitive control

DSP – digital signal processor

FIR – finite impulse response

HIL – hardware in the loop

IIR – infinite impulse response

IMP – internal model principle

LMI – linear matrix inequality

LTI – linear time invariant

MIMO – multiple inputs multiple outputs

MRAC – model reference adaptive control

MRC – model reference control

MRRC – model reference repetitive control

PLL – phase-lock loop

PCI – phase cancelation inverse

PRC – prototype repetitive control

RC – repetitive control

RMS – root mean square

SISO – single input single output

ZPETC – zero phase error tracking controller

CHAPTER 1

INTRODUCTION

1.1 MOTIVATION

Repetitive Control (RC) has been successfully used for many applications, such as in a hard disc, for robot control, for altitude stabilization of satellite, etc [1, 2]. A well-known use of a repetitive controller is to both track a periodic reference signal and reject periodic disturbance, as tracking and rejecting periodic signals are common tasks in many control applications. RC is related to learning control [3, 4] and originated from the idea of the Internal Model Principle (IMP) of Wonham and Francis [5]. The IMP is attached inside a feedback loop, and behaves as the generator of a periodic signal in order to achieve a zero tracking error. Many researchers have worked in the field of RC, and some issues have already been investigated. Inoue et al [6] originally formulated a repetitive model that deals with disturbances with a known period. This was followed successfully by Chew and Tomizuka [7], who applied RC in computer disk drives. The recent RC design to reject disturbances with multiple periods has been done by [8]. The RC consists of two main parts; the internal model to generate a periodic signal, and a compensator to stabilize the closed-loop system.

A number of important works related to the design of a compensator have been discussed in [9-18]. The compensator is often designed as the inverse of the plant model in order to cancel whole system dynamics [9-11]. The inverse of the plant is sometimes not available due to uncertainties and disturbance [15]. Moreover, the inverse of discrete time plant models are almost unstable as the zeros of discrete time plant models are very close to the unit circle [19]. This makes the design of a compensator is sometimes not feasible [14]. The design of a compensator based on pole placement was developed in [12, 13]. The compensator parameters are obtained by solving the Diophantine Equation, where the order of compensator is similar to the order of the IMP. An unstable IIR filter composed of stable and unstable poles was found to model the inverse of the plant [12]. This filter requires special implementation, where the unstable part operates in reverse time. In [14], the design of compensator became a problem of minimization in the frequency domain, where a compensator was in the form of a non-causal FIR filter. The design required a high order of FIR filter to stabilize the system, which meant that a large number of parameters needed to be optimized [14]. A compensator in the form of phase lead $k_r z^m$, where k_r is a gain, and m is an integer value, was proposed in [15, 16]. These approaches [15, 16] use a non-causal operator z^m that gives inflexible phase compensation.

Furthermore, in most designs of discrete RC, it is assumed that the frequency of the periodic signal is a constant and the sampling period is fixed to give an integer number of samples per period. However, in practice, the periodic signal may have a time varying period. Such a periodic signal, where its frequency is time-varying in nature, appears on a compact disc mechanism [20], vibrations control [21], rotational machinery [22], and an active suspension system [23]. If the sampling period is kept fixed while the period of repetitive signal changes, then the RC performance will significantly decay [24].

A number of RC designs have been proposed to compensate periodic signals with uncertain or time-varying periods [22-27]. An adaptive RC algorithm to recursively identify the period of disturbance then update either the delay length or sampling period has been proposed in [22, 25]. Landau et al [23] presented a direct adaptive RC to reject time-varying periodic disturbances. However, this can only be used for narrow band disturbances that give a lower order of the internal model RC. Steinbuch [26] proposed a RC with multiple periodic signal generators to reject the disturbance when its period is only slightly changed or less varying. Cao and Narasimhulu [27] proposed a digital PLL-based RC, where the sampling period was locked to the period of the disturbance signal to maintain a constant number of samples per period, as required by RC. This sampling period adjustment results in a discrete plant with time-varying coefficients, especially when the periodic signal has a time varying period. The approaches in [22-27] also assume that the plant is known.

The motivation of this research is to develop novel RC designs for a tracking/ rejecting periodic signal with time-varying frequency. To overcome time-varying frequency problem, it has been assumed that the sampling period is locked to the period of repetitive signal to maintain a constant number of samples per period. This sampling period adjustment causes the change of parametric model of the plant. The RC has to be changed accordingly to achieve a stable system. This thesis firstly proposes digital designs of RC for linear systems with time-varying sampling periods. Then, this thesis extends the method to the design of RC for linear MIMO systems.

The major contributions of this thesis are outlined as follows:

- The development of a new design methodology to obtain a low order, stable, and causal RC compensator.
- The design of a robust RC compensator that accommodates the sampling period variation in the known bound.
- The design of an adaptive RC (ARC) for unknown linear systems with time-varying sampling periods.
- The design of a decentralized RC (DRC) for linear MIMO systems.

1.2 ORGANIZATION OF THE THESIS

The thesis is organized as follows

Chapter 1: Introduction.

This chapter gives the motivation for the research. Some important works related to the compensator design and RC design for tracking/rejecting time-varying periodic signal, are presented.

Chapter 2: Literature Review.

This chapter presents both earlier and the latest applications of RC, and discusses various RC designs. In this chapter, the previous RC designs are classified into 4 main categories: Basic RC Design, Robust RC Design, Adaptive RC Design, and MIMO RC Design.

Chapter 3: Experimental System.

This chapter describes the experimental system used for testing the control algorithms proposed in this thesis. The details of the system hardware and software are explained in this chapter.

Chapter 4: Design of Robust RC with Time-Varying Sampling Periods.

This chapter firstly proposes a design methodology using optimization to obtain a low order, stable, and causal RC compensator. The chapter then presents a robust RC design to achieve a stable system when the sampling period varies in a defined range. Some simulation and experimental results are also presented to validate the effectiveness of the proposed design. A comparison study is also given in this chapter.

Chapter 5: Design of Adaptive RC of Linear Systems with Time-Varying Periodic Disturbances

This chapter proposes two algorithms: Model Reference Repetitive Control (MRRC) and Adaptive Repetitive Control (ARC). MRRC is employed when the plant model is known and subject to periodic disturbance with fixed frequency, while ARC is applied when the plant model is unknown and subject to time-varying periodic disturbance. Simulation and experimental results are presented in this chapter.

Chapter 6: Design of Decentralized RC of Linear MIMO Systems

This chapter proposes the design of decentralized RC (DRC) for linear MIMO systems. The design is based on decentralized control that treats the MIMO system as a set of SISO systems. Two design approaches are proposed in this thesis. Various numerical examples are presented to demonstrate the effectiveness of the proposed DRC. A comprehensive analysis and comparison study is given. The effectiveness of the design is also verified in experiments on a 2 DOF robot.

Chapter 7: Conclusion and Future Works.

This chapter summarizes all of the proposed algorithms in the research. Some comparisons for each algorithm are also presented. The chapter closes with some suggestions for the future works.

The publications based on this research are given at the end of this thesis. In addition, the list of Matlab codes and Simulink models used in simulations and real-time experiments are provided in the Appendix.

CHAPTER 2

LITERATURE REVIEW

2.1 INTRODUCTION

Repetitive Control (RC) is a learning control scheme that is designed to track / reject a repetitive signal. RC has a superior performance compared to the non-predictive control schemes such as PI and PID [2]. This is due to the capability of RC to learn the repetitive signal values, and then generate them as an output. For tracking or rejecting non-periodic signals, RC is not suitable due to the delay component of RC which gives large transient time.

Tracking and rejecting repetitive signal are common tasks in many control applications. The first use of RC was to control a power supply of proton synchrotron to follow a periodic reference [6]. Then, Chew and Tomizuka [7] successfully used RC to reject periodic disturbance in disk drives. Other early applications of RC, as listed in [2], are in a compact disc (CD) player, a peristaltic pump, robot control, continuous steel casting, thickness control in cold rolling, noise cancellation, active vibration compensation, and attitude stabilization of satellites. In 2004, Cuiyan et al [1] also listed applications of RC and included speed control of ultrasonic motors, suppression of torque vibration in motors, reduction of waveform distortion in pulse width-modulation (PWM) inverters, current compensation in active filters, suppression of harmonic current in an interior permanent magnet synchronous motor (IPMSM), accurate position control of piezoelectric actuators, control of electro hydraulic actuators, acoustic impedance matching control in a standing wave tube, turning process, and current control of a photovoltaic generation system .

Recently, RC has been used for the reduction of total harmonic distortion (THD) in a grid-connected inverter [28-32], in a constant-voltage constant frequency (CVCF) PWM converter [15, 33-36], for compensation of the current harmonics in a power correction factor (PFC) converter [37-40], in an Active Power Filter (APF) [41-43], for the improvement of scanning performance in an imaging atomic force microscope (AFM) [44, 45], for the suppression of topography disturbances in metrological AFM [46], for tracking control in an Ionic polymer-metal composite (IPMC) actuator [47], for disturbance rejection due to breathing in a flexible endoscopy system [48, 49], for position control of an electro-hydraulic engine valve system (EVHS) [50, 51], for tracking of contouring tasks in an industrial biaxial precision gantry [52], for compensation of fluctuating DC link voltage in a AC-fed railway traction drives [53], and for suppression of human tremor in functional electrical stimulation (FES) [54].

The list of applications above shows that RC has been widely used in many applications. Moreover, since RC has been introduced, various RC designs have been developed. In this chapter, a review of various RC designs is presented. Section 2 reviews basic RC designs. A review of both robust and adaptive RC designs is given in Sections 3 and 4 respectively. Section 5 presents a review of MIMO RC designs. Section 6 draws the conclusion.

2.2 BASIC RC DESIGN

This section reviews various designs for basic RC. The RC designs that will be reviewed in this section refer to internal model based RC, where the model of repetitive signal is included in the basic feedback loop. This is to differentiate it from the external model based RC as proposed in [55] where the periodic signal model is placed outside the feedback loop, and a periodic signal is injected to cancel the disturbance. The RC is originated from the idea of the Internal Model Principle (IMP) of Wonham and Francis [5], which states that the periodic signal model needs to be included in the closed-loop system in order to achieve perfect tracking or rejection of the periodic signal.

Inoue et al [6] first proposed an internal model based RC for tracking any repetitive signal with known period T_r, and successfully implemented it to control a proton synchrotron magnet power supply that required high precision tracking .

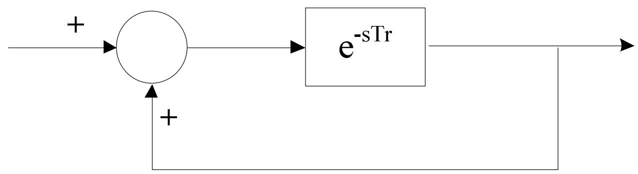

Figure 2.1 A continuous time-delay internal model

The internal model in [6] is constructed from a continuous time-delay with positive feedback, as shown in Figure 2.1, which can be represented in the following transfer function:

$$I(s) = \frac{e^{-sT_r}}{1 - e^{-sT_r}} \tag{2.1}$$

where T_r is the period of the reference signal, and e^{-sT_r} is a continuous time-delay with the length T_r.

An important feature of this internal model is that it is able to compensate fundamental frequency and all harmonics frequency components in a repetitive signal. The internal model above also shows an infinite dimensional structure as it has infinite poles at the imaginary axis: $\pm jn\omega$, where $n = 1,2,\ldots,\infty$. Since the poles are located at the imaginary axis, the internal model is marginally stable.

In [56], the stability condition of an RC system with the internal model (2.1) was assessed by using small gain theorem, and it was revealed that the internal model worked only for stable plant with a relative degree of zero. This gives restriction to the class of plants that can utilize this internal model.

Hara et al [57] proposed a modified internal model by cascading the time-delay with a low pass filter $q(s)$. This modified internal model helped to improve robustness of an RC system at the expense of tracking performance at high-frequencies.

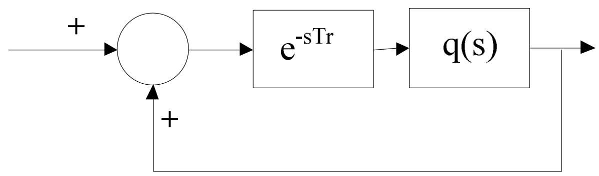

Figure 2.2 A continuous time-delay internal model with low pass filter

The modified internal model, as shown in (2.2), still has an infinite dimensional structure. However, the addition of the low pass filter $q(s)$ pushes the poles of $I(s)$ to the open left half plane (LHP). Thus, the modified internal model is open loop stable.

$$\mathrm{I(s)} = \frac{\mathrm{q(s)e^{-sT_r}}}{1 - \mathrm{q(s)e^{-sT_r}}} \tag{2.2}$$

where q(s) is a proper stable rational filter such that $|\mathrm{q(j\omega)}| < 1$ for ω is larger than the cut-off frequency.

In practice, the infinite dimension internal model was difficult to realize and sometimes some signals were concentrated in the low to medium frequency range [1, 58]. The finite order internal model to track/reject repetitive signal that was composed of fundamental frequency up to the finite number of harmonics was then proposed by Ghosh and Paden [58], and was successfully implemented in the servomechanism [59]. Ghosh and Paden [58] approximated the infinite internal model above by using the following model:

$$\mathrm{I(s)} = \frac{1}{\mathrm{s}\prod_{n=1}^{m}(s^2 + n^2\omega^2)} \tag{2.3}$$

where m is a finite integer representing the preferred highest harmonics.

Different to the internal models (2.1)-(2.2) which has infinite poles, this internal model only has $2m$ poles located at $\pm jn\omega$, where $n = 1,2, \dots, m$

Nagahara et al [60] replaced the time-delay e^{-sT_r} in (2.1) with an optimal controller to avoid infinite dimensionality.

$$\mathrm{I(s)} = \frac{K(s)}{1 - G(s)K(s)} \tag{2.4}$$

where K(s) is an optimal controller, $G(s)$ is a plant model,

The optimal controller K(s) is designed to approximate a linear phase characteristic of e^{-sT_r} by solving the following optimization:

$$\min_{\mathrm{K(s)}} \| [e^{-sT_r} - G(s)K(s)]W(s) \|_\infty \tag{2.5}$$

where $\|.\|_\infty$ is the infinity norm operator, and $W(s)$ is a weighting function, which is a low pass filter with a cut-off frequency larger than the targeted harmonics.

Since the introduction of the digital computer, the use of digital control has greatly expanded for several reasons, such as being cheaper, smaller, and more flexible than analogue hardware. RC designs in the discrete time domain have also been studied extensively. The first digital RC was given in [61]. In a discrete-time, the internal model to generate periodic signal with period T_r is formulated as follows:

$$\mathrm{I(z)} = \frac{\mathrm{z^{-N}}}{1 - \mathrm{z^{-N}}} \tag{2.6}$$

where $\mathrm{N} = \frac{\mathrm{T}_r}{\mathrm{T}} \in \mathbb{N}$, N being the number of samples per period, where it is also referred to as the order of the internal model, $\mathrm{T_r}$ being the period of the repetitive signal, T being the sampling period, and $\mathbb{N}$ is the integer value.

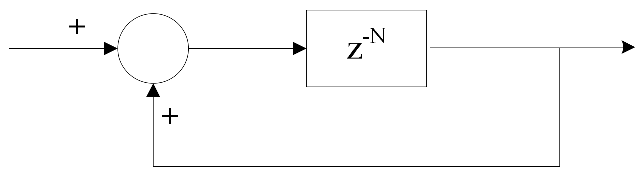

Figure 2.3 A discrete time-delay internal model

The discrete internal model above has a finite dimensional structure, because it has N evenly spaced poles at the unit circle. This internal model gives a null tracking error for repetitive signal with frequency $\frac{n}{T_r}$, where $n = 1,2,..,\frac{N}{2}$. In other words, it only compensates fundamental frequency and its harmonics up to the Nyquist components of the repetitive signal.

The system with the discrete internal model (2.6) is stable if the plant model is sufficiently accurate. To improve robustness, a low-pass filter $Q(z)$ was cascaded with discrete time delay z^{-N} [62]. As a result, the robustness was improved but the tracking accuracy at high harmonics was sacrificed.

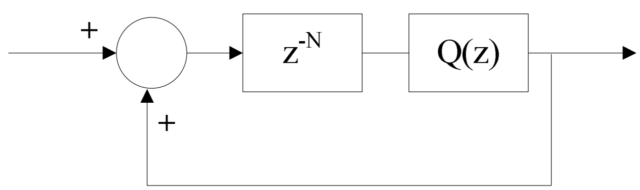

Figure 2.4 A discrete time-delay internal model with Q-filter

This Q-filter here is a zero phase low pass filter with unity gain at low frequencies, and is often chosen as a moving average filter as follows:

$$\mathrm{Q(z)} = \sum_{i=0}^{m} \alpha_i z^{i} + \sum_{i=1}^{m} \alpha_i z^{-i} \tag{2.7}$$

where m is the order of filter, $\alpha_0 + 2\sum_{i=1}^{m} \alpha_i = 1$, and $\alpha_i > 0$

Hillerstrom and Sternby [63] proposed a low order discrete internal model for rejecting band-limited periodic disturbances. Compared to the internal model (2.6) that models repetitive frequency and its harmonics up to Nyquist frequency, the low order internal model only represents some dominant harmonics.

$$\mathrm{I_{low}(z)} = \frac{1}{(1-\mathrm{z}^{-1})\prod_{\mathrm{k}\in\mathrm{K}}(1-2\cos(\mathrm{k}\omega_{\mathrm{o}}T)\,\mathrm{z}^{-1}+\mathrm{z}^{-2})} \tag{2.8}$$

where $\omega_{\mathrm{o}} = \frac{2\pi}{T_r}$ is a fundamental frequency of repetitive signal in rad, T is the sampling period, and K denotes preferred harmonics indices.

The order of the internal model here depends on the number of dominant harmonics, where each harmonic component is modeled by second order system.

In the power systems, the references and disturbances usually contain only odd-harmonic frequencies. The internal model that is specifically used to track/attenuate odd harmonic periodic references or disturbances was proposed by Grino and Costa-Castello [64]. The proposed internal model is shown in Figure 2.5.

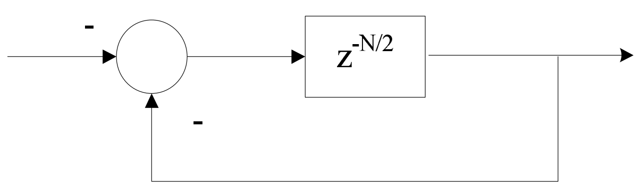

Figure 2.5 A discrete internal model for odd harmonic signals

$$\mathrm{I(z)} = -\frac{\mathrm{z}^{-\mathrm{N}/2}}{1+\mathrm{z}^{-\mathrm{N}/2}} \tag{2.9}$$

Instead of using positive feedback, this internal model uses negative feedback, and requires only $\mathrm{N}/2$ integrators, which is half of the discrete internal model (2.6).

A discrete internal model to reject a repetitive signal that consists of two dominant fundamental frequencies and their harmonics has been proposed by Woo Sok and Il Hong [65]. The design came to be called as multi-periodic RC, and was further developed [66-68]. The successful implementation of multi periodic RC in hard disk drive has been shown in [8, 69]. An internal model is determined according to the number of targeting fundamental frequencies.

$$I(z) = \frac{1}{\prod_{k=1}^{L} 1 - Q_k(z) z^{-N_k}} \tag{2.10}$$

where $N_k = T_{rk}/T$,T_{rk} being k-th repetitive signal period, T being the sampling period, L being the number of fundamental frequencies, $Q_k(z)$ being the low pass filter for k-th period.

The discussion above reviews various designs of the internal model. The internal model is a key feature of RC because of its capability as a periodic signal generator. However, there is another important part in the RC, namely the compensator. A compensator is needed to stabilize the closed-loop system. The general structure of a discrete RC system for tracking periodic reference is shown in Figure 2.1.

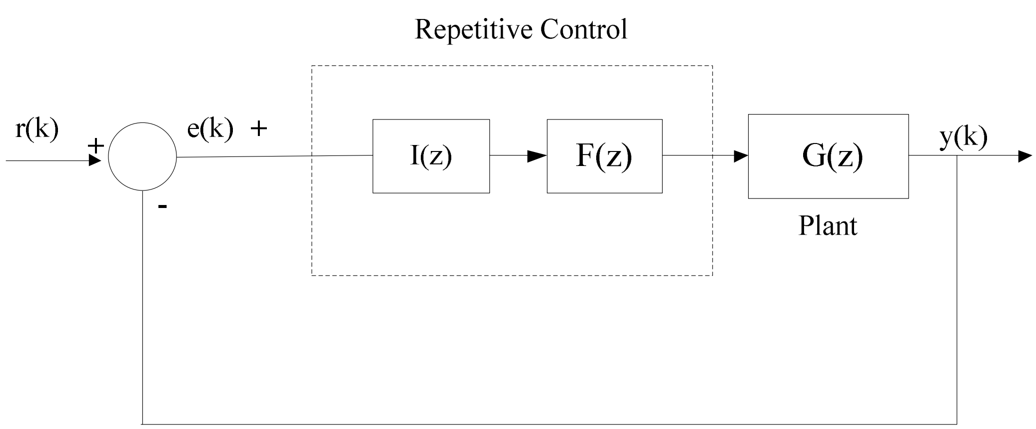

Figure 2.6 Block diagram of the discrete RC system

Figure 2.6 shows that RC basically consists of two main parts; the internal model $I(z)$ and a compensator $F(z)$. The compensator $F(z)$ plays a significant role in RC as it determines the stability of a closed-loop system. A number of important works related to the design of compensator have been discussed in [9-18, 70-75].

The design of an RC compensator based on Zero Phase Error Tracking Controller (ZPETC) of [11] was proposed by Tomizuka et al [10]. The design is also known as a prototype repetitive controller (PRC) that features a compensator of similar order to the plant. The aim of the design is to perfectly cancel the phase of the plant, so the phase of the product of $F(z)$ and $G(z)$ is zero for all frequencies. The compensator design works for both stable minimum and non-minimum phase plant. For stable minimum phase plant, the compensator can be simply the inverse of $G(z)$, as its inverse has stable poles.

$$\mathrm{F(z)} = G^{-1}(z) = \frac{A(z)}{B(z)} \tag{2.11}$$

where $\mathrm{G}(z) = \frac{B(z)}{A(z)}$, and $B(z)$ and $A(z)$ are the numerator and denumerator of $G(z)$ respectively.

For stable non-minimum phase plant, the compensator was proposed as follows:

$$\mathrm{F(z)} = \frac{\mathrm{k_r}}{b}\frac{\mathrm{A(z)B^-(z^{-1})}}{\mathrm{B^+(z)}} \tag{2.12}$$

where

$B^+(z)$ and $B^-(z)$ are stable and unstable parts of $B(z)$, $B^-(z^{-1})$ is $B^-(z)$ with the backward shift operator z^{-1} , k_r is a RC gain, and b is a scalar value.

The polynomial $A(z)$ and $B^+(z)$ in (2.12) cancel the stable poles and zeros of $G(z)$ respectively, while $B^-(z^{-1})$ and b cancel the phase and the magnitude of the unstable zeros respectively. The gain k_r is a limited controller gain, which affects the convergence rate. The choice of k_r and b are given as follows:

$$\mathrm{k_r} \in (0,2) \tag{2.13}$$

$$\mathrm{b} \geq \max_{\omega\epsilon[0,\pi]} \left|\mathrm{B^-}\left(\mathrm{e^{j\omega}}\right)\right|^2 \tag{2.14}$$

Yamada et al [70] replaced the gain $\frac{k_r}{b}$ in (2.12) with a zero-phase low pass filter $f(z)$ to obtain a minimum radius for the dominant poles of the RC system. This results in a faster convergence rate of the tracking error.

$$\mathrm{F(z)} = f(z)\frac{\mathrm{A(z)B^{-}(z^{-1})}}{\mathrm{B^{+}(z)}} \tag{2.15}$$

Cosner et al [9] formulated plug-in discrete RC, as shown in Figure 2.7, where it was successfully applied to robot manipulators. The compensator design is based on the system model which is a closed-loop response, not just the plant model and conventional controller in the series.

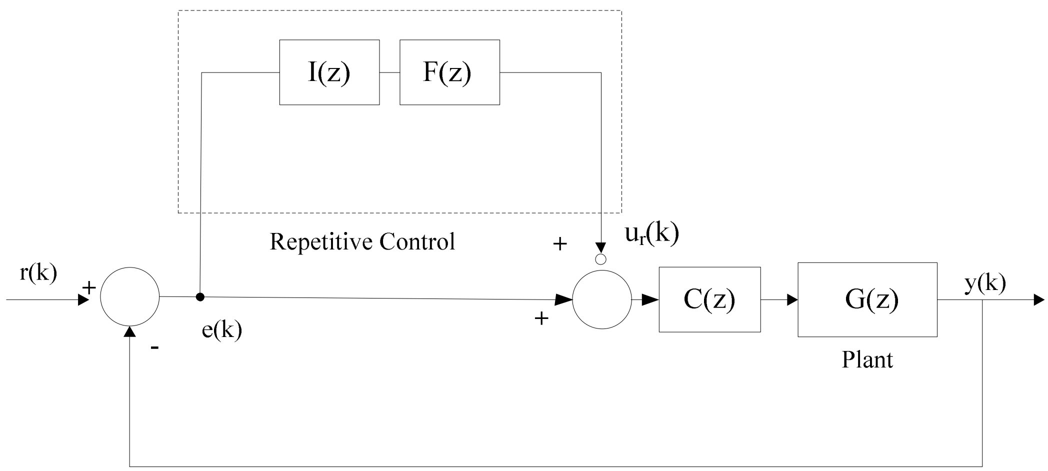

Figure 2.7 Plug-in discrete RC system

where $\mathrm{C(z)}$ is a conventional/nominal controller used to stabilize system without RC.

Now, the compensator $F(z)$ is not designed to compensate $G(z)$, but to compensate the closed-loop system $\mathrm{G_s(z)}$ as follows:

$$\mathrm{G_s(z)} = \frac{\mathrm{G(z)C(z)}}{1 + \mathrm{G(z)C(z)}} \tag{2.16}$$

The design of a compensator based on pole placement was developed in [12, 13]. Ledwich et al [12] designed an RC compensator based on pole placement that is used to track periodic reference. The RC structure proposed in [12] is shown in Figure 2.8.

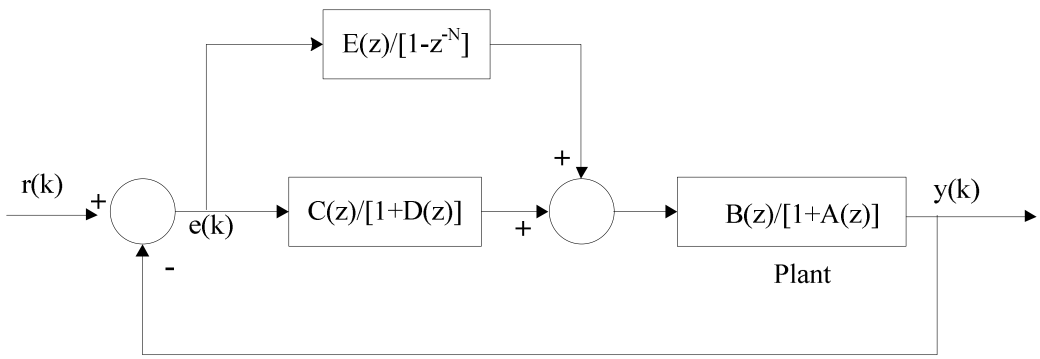

Figure 2.8 Pole placement based RC system with plug-in structure

where $B(z)[1+A(z)]^{-1}$ is an open loop plant model, $C(z)[1+D(z)]^{-1}$ is a conventional controller, and $E(z)[1-z^{-N}]^{-1}$is a plug-in RC

The design task is to obtain the polynomials $D(z), C(z)$, and $E(z)$ shown in Figure 2.8 by solving the polynomial fitting as follows:

$$[1+A(z)][1+D(z)][1-z^{-N}]-B(z)L(z)=(1+T(z)) \tag{2.17}$$

where $(1+T(z))$ represents the desired characteristic polynomial, and $L(z)$ is a polynomial equal to:

$$L(z)=[1+D(z)]E(z)+C(z)[1-z^{-N}] \tag{2.18}$$

The polynomials $D(z)$ and $L(z)$ are firstly obtained by solving polynomial fitting (2.17), then solving (2.18) gives both $E(z)$and $C(z)$. The polynomial $(1+T(z))$ is chosen to have $(N+M)$ poles, where N and M are the order of the internal model and the plant respectively. This selection number of poles gives M-th order polynomial $D(z)$ and N-th order polynomial $E(z)$. The polynomial $E(z)$ can be considered as the RC compensator, in which it has the same order of the internal model.

Hillerstrom [13] designed a pole placement based RC compensator that is used to reject periodic disturbance. An RS polynomial structure as shown in Figure 2.9, was used in the design.

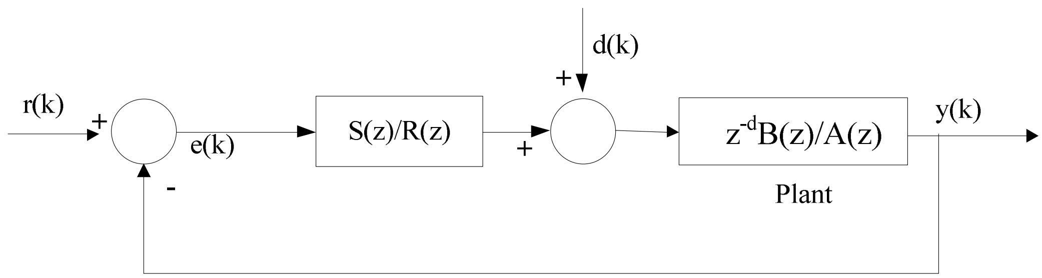

Figure 2.9 Pole placement based RC system with RS polynomial structure

where $d(k)$ is disturbance and d is a system time-delay.

First, the disturbance model, denoted as $H(z)$, should be included in the polynomial $R(z)$, as indicated in (2.19).

$$\frac{S(z)}{R(z)} = \frac{S(z)}{R'(z)H(z)} \tag{2.19}$$

Then, the transfer function $\frac{S(z)}{R'(z)}$ which behaves as a compensator is designed. The numerator $S(z)$ and denumerator $R'(z)$ are obtained by solving the Diophantine Equation as follows:

$$A(z)H(z)R'(z) + z^{-d}B(z)S(z) = A_m(z) \tag{2.20}$$

where $A_m(z)$ is the desired characteristic polynomial.

Solving (2.18) results in the polynomial $S(z)$ with a similar order to the order of the disturbance model $H(z)$.

An RC compensator in the form of an unstable IIR filter was proposed by Ledwich et al [12]. An unstable IIR filter composed of stable and unstable poles was found to model the inverse of the plant.

$$F(z) = \frac{(z - z_1)(z - z_2)}{(z - p_i)(z - p_o)} \approx \frac{1}{G(z)} \tag{2.21}$$

where p_i and p_o are a pole inside and outside the unit circle respectively.

Since the compensator has an unstable pole, the design requires special implementation, where the unstable part operates in reverse time.

An interesting form of RC compensator as shown in Figure 2.10 was introduced by Zhang et al [15]. Instead of using the inverse of the plant, Zhang et al [15] used a compensator in the following form:

$$F(z) = k_r z^m \tag{2.22}$$

where k_r is an RC gain, and m is a lead step.

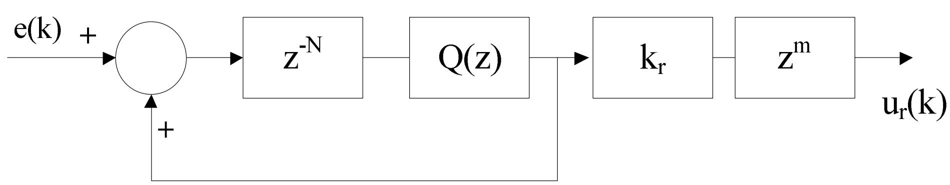

Figure 2.10 RC with phase lead compensator $k_r z^m$

The order m is firstly chosen to give larger stable bandwidth that satisfies the following condition:

$$|\theta_g(e^{j\omega}) + m\omega\,| < 90^\circ - \varepsilon \tag{2.23}$$

where $\theta_g(e^{j\omega})$ is the phase response of the plant, and ε is the positive constant for a stable margin.

Then, the gain k_r is chosen for fast convergence, and determined according to the design criterion as follows

$$k_r < \frac{2cos(\theta_g(e^{j\omega}) + m\omega)}{M_g(e^{j\omega})} \tag{2.24}$$

where $M_g(e^{j\omega})$ is the magnitude response of the plant, and m is the selected lead step.

Another design of RC compensator in the form of a phase lead z^m was proposed by Wu et al [16]. A block diagram of the proposed RC is shown in Figure 2.11. As shown in Figure 2.11, the low pass filter $q(z)$ is not placed inside the internal model loop, which make it differs to the design [15]. The exclusion of $q(z)$ in the internal model loop aims to preserve the tracking performance at high frequencies, and the $q(z)$ here is not necessarily a zero phase filter.

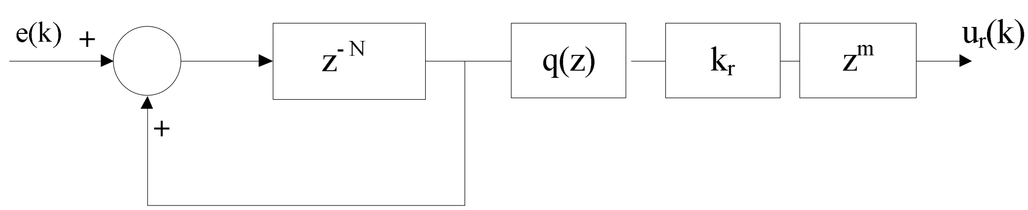

Figure 2.11 RC with phase lead compensator $q(z)\ k_r z^m$

$$F(z) = q(z)k_r z^m \tag{2.25}$$

where $q(z)$ is a low-pass filter to reject the noise and improve the system stability, k_r is an RC gain, and z^m here is phase angle compensator to compensate the phase delay by $q(z)$ and the plant.

The design procedure starts by choosing filter $q(z)$ that gives the desired cut-off frequency. Then, the order m is selected so that inequality below is satisfied in the desired bandwidth.

$$\left|\cos\left(\theta_g\left(e^{j\omega}\right) + \theta_q\left(e^{j\omega}\right) + m\omega\right)\right| < 90^o \tag{2.26}$$

where $\theta_g\left(e^{j\omega}\right)$ and $\theta_q\left(e^{j\omega}\right)$ are the phase response of the plant and $q(z)$ respectively Then, the gain k_r is chosen to satisfy the following condition:

$$k_r < \frac{2\min[\cos\left(\theta_g\left(e^{j\omega}\right) + \theta_q\left(e^{j\omega}\right) + m\omega\right)]}{\max[M_g(e^{j\omega})M_q(e^{j\omega})]} \tag{2.27}$$

where $M_g\left(e^{j\omega}\right)$ and $M_q\left(e^{j\omega}\right)$ are the magnitude of the plant and $q(z)$ respectively, and m is the selected order.

For Panomruttanarug and Longman [14], the design of RC compensator became a problem of minimization in the frequency domain, where the compensator was in the form of non-causal FIR filter as shown in (2.28). The design problems are choosing the order n, m, and obtaining the gains $a_1, a_2, \dots a_n$ by trying to match the inverse of the plant over the frequency range up to Nyquist.

$$F(z) = a_1 z^{m-1} + a_2 z^{m-2} + \cdots + a_m z^0 + \cdots + a_{n-1} z^{-(n-m-1)} + a_n z^{-(n-m)} \tag{2.28}$$

The gains $a_1, a_2, \dots a_n$ are obtained by solving the following optimization:

$$\min_{(a_1,\dots,a_n)} \sum_{j=0}^{179} \left[\frac{1}{k_r} F\left(e^{i\omega_j T}\right) - G^{-1}\left(e^{i\omega_j T}\right)\right] W_j \left[\frac{1}{k_r} F\left(e^{i\omega_j T}\right) - G^{-1}\left(e^{i\omega_j T}\right)\right]^* \tag{2.29}$$

where subscript * means complex conjugate, k_r is a RC gain , T is sampling period, and W_j is the weight for j-th frequency.

Equation (2.29) shows that the objective function is composed of 180 frequencies which are chosen every one degree in the z domain. This also means that the phase and magnitude value of $G^{-1}(z)$ at every one degree are required in order to construct the above objective function.

In [73, 75], the compensator in the form of non-causal FIR filter was designed based on Taylor expansion. The design is accomplished by approximating the terms $\left[\frac{1}{\mathrm{z}-z_i}\right]$ and $\left[\frac{1}{\mathrm{z}-z_o}\right]$ shown in (2.30) by a finite Taylor series.

$$\mathrm{F(z)} = \left[\frac{(z-p_1)(z-p_2)(z-p_3)}{k_g}\right]\left[\frac{1}{\mathrm{z}-z_i}\right]\left[\frac{1}{\mathrm{z}-z_o}\right] \tag{2.30}$$

where p_1, p_2, p_3 are stable poles in the plant, k_g is the plant gain, and z_i, z_o are stable and unstable zero respectively.

$$\frac{1}{\mathrm{z}-z_i} = \left(\frac{1}{z}\right)\left[\frac{1}{1+(a_i/z)}\right] \approx \left(\frac{1}{z}\right)\sum_{\mathrm{k}=0}^{\mathrm{n}}\left(-(a_i/z)\right)^{\mathrm{k}} \tag{2.31}$$

$$\frac{1}{\mathrm{z}-z_o} = \left(\frac{1}{a_o}\right)\left[\frac{1}{1+(z/a_o)}\right] \approx \left(\frac{1}{a_o}\right)\sum_{\mathrm{k}=0}^{\mathrm{n}}\left(-(z/a_o)\right)^{\mathrm{k}} \tag{2.32}$$

where $a_i = -z_i$, $a_o = -z_o$, and n is the highest power of the Taylor series.

The digital RCs discussed above require a priori knowledge of the period of repetitive signal and the plant model. The information regarding the period of repetitive signal is used to design the internal model, while knowledge of the plant model is required to design the compensator. The compensator designs in [9, 10] result in a low order and non-causal compensator. The order of the compensator is similar to the order of the compensated plant (open loop plant/stabilized plant). The compensator designs based on pole placement [12, 13] give a non-causal compensator with the similar order to the internal model. The order of the internal model N can be large [76]. For example, if a robot performing a repetitive task with a period of 1s, the RC with a sampling period of 1 ms means $N = 1000$. Therefore, the pole placement assignment gives a high order of compensator. In [12], the compensator is unstable and requires special implementation where the unstable part operates in reverse time. In [14], the compensator is in the form of a non-causal FIR filter. The design requires high order of FIR filter to stabilize the system, which means that a large number of parameters are required to be optimized [14]. The design approaches [15, 16] use a non-causal operator z^m that gives inflexible phase compensation. The non-causal compensators are still implementable because they are merged with the internal model.

It becomes a challenge to design a low order, stable, and causal compensator. The advantage of causal compensator is that it can be implemented independently without being merged to the internal model. This reduces the design complexity, especially when the internal model has a high order. Motivated by this challenge, a new RC design that results in low-order, stable, and causal compensator, is proposed. The proposed design is presented in Chapter 4.

2.3 ROBUST RC DESIGN

In real situations, the actual plant model and period of repetitive signal are not accurately known. The plant may be subject to input/output constraints and model uncertainties (eg. parametric uncertainties, non-parametric uncertainties, uncertain plant delay). Moreover, the repetitive signal itself may vary in period. Under those conditions, the basic RC may fail to achieve perfect tracking/rejection, and may become unstable. This section discusses some robust RC designs that aim to handle either uncertain plant or uncertain period of repetitive signal.

A design of robust RC for an uncertain plant with known parameter bounds was proposed by Roh and Chung [72]. A robust compensator in the form of a proportional derivative (PD) controller was designed to compensate that uncertain plant. The choice of compensator gains becomes a problem of minimization in the frequency domain. The minimization problem is formulated based on both RC stability criteria and Kharitonov's theorem. The complexity of the optimization problem depends on the polynomial order of the plant.

The basic RC works well for plants with relatively small time-delays. However, it will fail in the realm of process control applications and requirements due to the typical presence of time-delay and large phase lag [77]. Tan et al [77] proposed a robust RC for the plant with a long and imprecise time delay. Unlike most RC designs that offer phase lead compensation, the proposed method uses phase lag compensation by cascading an additional time-delay with duration M to the RC, as shown in Figure 2.12. The stability of the RC system has been assessed, and it was revealed that the proposed RC yields a wider range of learning gain compared to the usual RC.

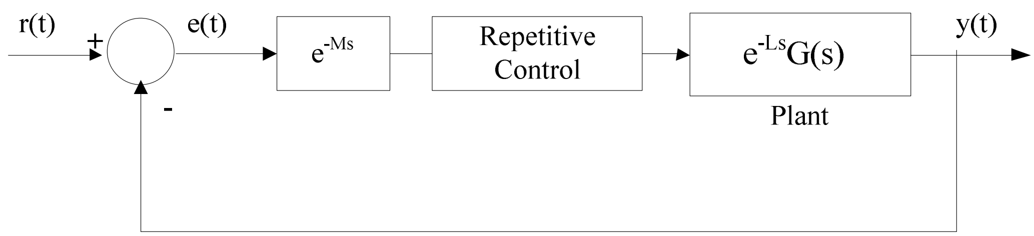

Figure 2.12 RC system for the plant with long-time delay

where $M = T_r - L$, T_r being a repetitive signal period, and L is a large time-delay .

When the actual period of repetitive signal is subject to slight variation, a small period mismatch happens. This condition makes the RC gains significantly drop to a low level magnitude. As a consequence the tracking/rejecting performance is significantly decayed. Steinbuch [26] proposed an internal model with multiple periodic signal generators with weighting factors to improve RC capabilities when the periodicity changes slightly. In the presence of period-time variations, the use of multiple memory loops helps to improve the RC gains at the harmonics.

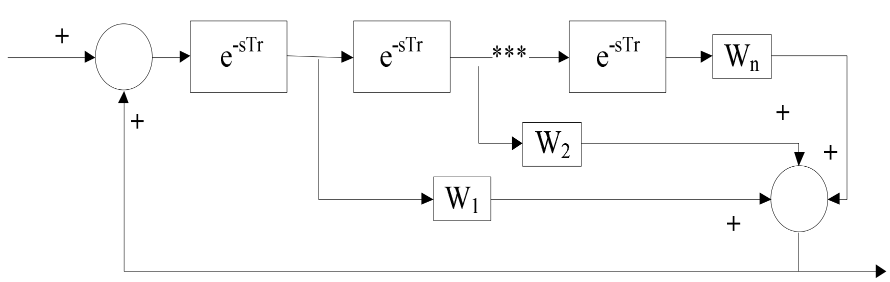

Figure 2.13 A continuous internal model with multiple loops

$$I(s) = \frac{\sum_{i=1}^{n} W_i\, e^{-isTr}}{1 - \sum_{i=1}^{n} W_i\, e^{-isTr}} \tag{2.33}$$

where n is the number of periodic signal generators, W_i is the weighting factor, and T_r is the known period of signal

Kim and Tsao [78] proposed an RC design to deal with near periodic time varying reference signals. Near periodic means that the reference signal $r(t)$ has a priori known period, T_r, and that $|r(t) - r(t + T_r)|$ is small in a certain sense. This near periodic phenomena happens due to the reference signal slowly changing in its magnitude and phase. In [78], a new integrated feed forward controller and RC was presented. The RC part enables the control system to learn and track the periodic component of the reference signal while the feed forward action compensates for the slow changes in magnitude and the phase of the reference signal. The control design problem is formulated in the linear fractional transformation (LFT) form and solved by μ-synthesis. In [78], the order of the resulting controller is significantly high, and controller order reduction must be performed for real-time implementation.

A low-pass filter $q(s)$ in the modified internal model is used to give more robustness to the RC system. However, the inclusion of this filter affects tracking accuracy. Finding the largest bandwidth of low-pass filter is very important, especially for a system requiring good tracking precision. She et al [79] proposed an algorithm to simultaneously optimize the low-pass filter and obtain state feedback compensator, when the plant contains a class of uncertainties. The configuration of the RC system is shown in Figure 2.14. Two robust-stability conditions based on LMI were formulated, and the conditions were transformed into; a generalized eigenvalue minimization problem that is used to calculate the maximum bandwidth of low-pass filter, and a H_∞ control problem that is used to find the state-feedback gains.

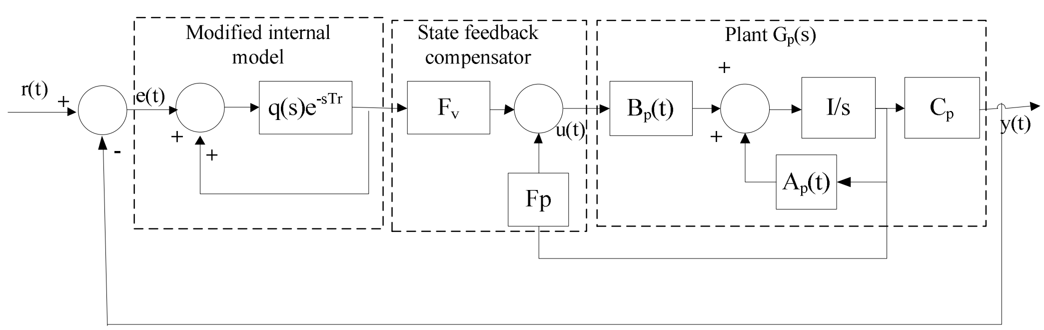

Figure 2.14 RC system with state feedback controller

where F_v and F_p are state-feedback gains, and $A_p(t)$, $B_p(t)$, and C_p are state-space representations of uncertain plant $G_p(s)$.

In the presence of control saturation, the inclusion of an internal model is insufficient to guarantee perfect tracking/rejecting of a repetitive signal. In the RC system, windup can be a potential problem due to the marginally stable characteristic of the internal model. For some reference signals, the presence of control saturation can even lead to divergent trajectories [80]. An RC design that addresses the problem of tracking/rejecting repetitive signal for the plant subject to actuator saturation were proposed in [80, 81]. Sbarbaro at al [81] proposed anti-windup strategy for RC system shown in Figure 2.15. The design aims to maintain all the internal signals bounded independently of the reference, and to shape the response during the transients. The proposed design cancels the internal model dynamics during saturation. The dynamics associated with the internal model can be modified by selecting the polynomials $M(z)$ and $N(z)$. The polynomials $M(z)$ and $N(z)$ are chosen so that the roots of $M(z) + N(z)$ are inside the unit circle. This will guarantee that the actuator input, plant input and plant output will be bounded.

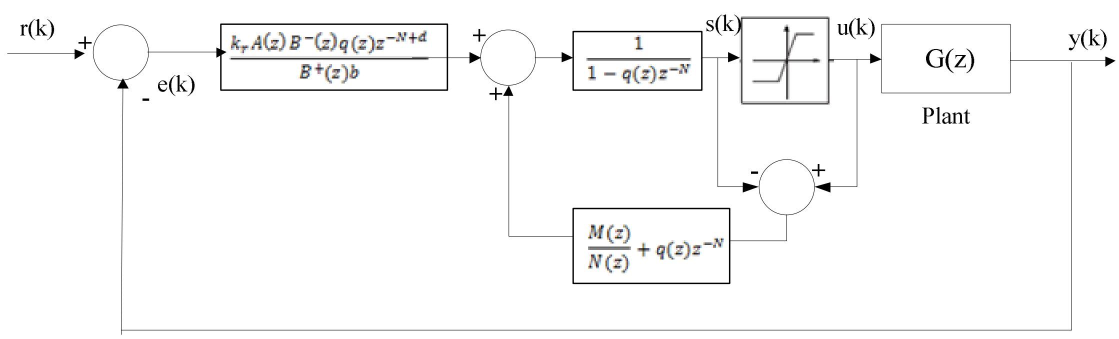

Figure 2.15 RC system with anti-windup compensator

In [80], the design objective was to handle both control saturation and plant uncertainty. In the design, a state-space RC structure was considered, and stability conditions in LMI form were formulated to calculate a stabilizing state feedback gain and anti-windup gain. Provided the states, the references and the disturbances belong to certain admissible sets, the chosen gains will ensure the reference tracking/disturbance rejection.

Lin and Liu [82] integrated RC with model predictive control (MPC) for tracking control and constraint handling of mechatronics systems. The design aims to preserve the desired properties of RC with the given input constraints. In [82], a state observer was required to provide the estimated plant states for MPC , and a Quadratic Programming (QP) problem was formulated to obtain the optimal change of control input sequence.

A robust RC scheme for three-phase CVCF PWM inverters was presented in [83]. The plant was subject to non-linear loads and parametric model uncertainties causing periodic tracking error. The design combines RC and robust optimal feedback controller, where the feedback controller is obtained by transforming the plug-in RC structure to a LFT form then applying μ-synthesis.

The designs [72, 77, 79, 83] aim to handle uncertain plants, while the designs [80, 81] address windup problems. Robust RC designs to compensate uncertain periods and the uncertain magnitude of a repetitive signal were discussed respectively in [26] and [78]. In [26], the period of the repetitive signal was slightly changed or less varying. In [78], the period of repetitive signal might be fixed but the magnitude and phase of repetitive signal slowly changed. A robust RC design to handle a large time-varying repetitive signal still remains open. One of the solutions to overcome a large time-varying repetitive signal is to use a digital PLL-based RC [27], where the sampling period is locked to the period of the repetitive signal to maintain a constant number of samples per period, as required by RC. However, the discrete plant parameters change as the sampling period varies. The change of plant parameters can result in an unstable closed-loop RC system. Motivated by this problem, a robust RC compensator that accommodates the sampling period variation in a known relatively large bound, is proposed. In the design, the time-varying parts due to sampling period interval variation are treated as parametric uncertainties. The proposed design is presented in Chapter 4.

2.4 ADAPTIVE RC DESIGN

The design of RC when the plant model and period of repetitive signal are both known is straightforward. The internal model can be easily designed based on the information of the repetitive signal period and the choice of sampling period, while the RC compensator can be designed based on the known plant model. A problem arises when the period of repetitive signal is unknown, or known but time-varying. A slight mismatch between the internal model period and the actual repetitive signal period significantly degrades the performance of the RC [25]. Another problem also arises when the plant is subject to non-repeatable disturbance. These problems make the design of RC more complex. Several solutions based on an adaptive scheme have been proposed in [22-25, 84-92]. This section discusses some adaptive RC designs that are specifically proposed to handle the problems mentioned above.

An adaptive RC algorithm to recursively identify the period of repetitive signal then update either the delay length or sampling period has been proposed [22, 25, 84]. The period estimation scheme is based on the minimization of a quadratic energy function of the periodic signal. This is an indirect adaptive RC that firstly estimates the period of the periodic signal, then based on the identified period either the delay length is updated and the sampling period is kept fixed, or the sampling period is adjusted and the delay length kept constant.

When the period of reference/disturbance varies but the requirement forces a fixed sampling period for nominal controller and plant, the number of samples per period may change and be non-integer. An adaptive RC design to address such a problem was proposed by Cao and Ledwich [85]. There are two portions of controller, as illustrated in Figure 2.16, where each portion has a different sampling period. The sampling period of the RC is adapted to maintain N samples per reference period, while the sampling period of the nominal controller is kept fixed. Interpolations are utilized to synchronize those two portions.

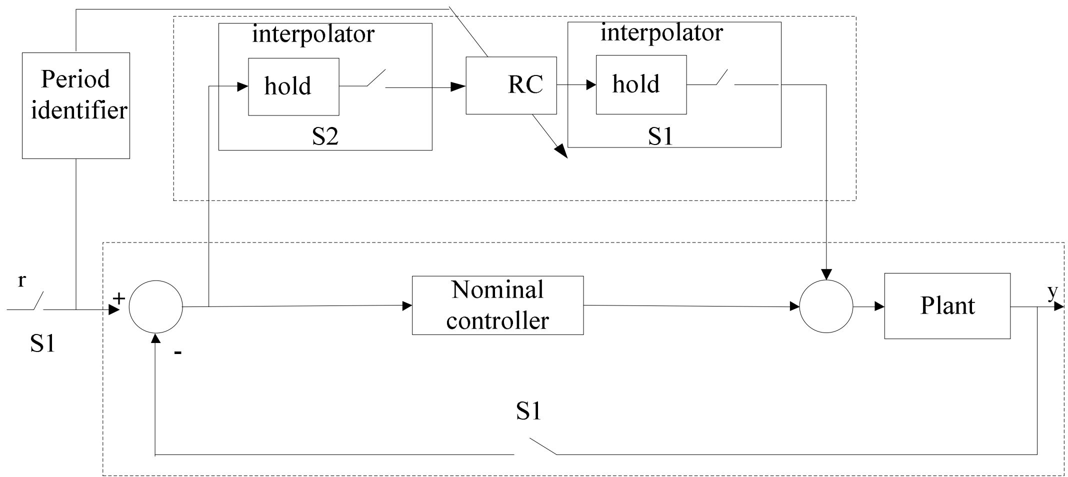

Figure 2.16 Adaptive RC to track variable periodic signals with fixed Sampling period

where S1 and S2 are samplers 1 and 2 respectively.

Kim et al [86] designed an adaptive RC algorithm to reduce a single frequency disturbance in hard disk drives. The disturbance frequency is unknown and adaptive peak frequency identification is employed to determine the dominant disturbance frequency. The proposed design uses a low order internal model targeting a single fundamental frequency. Problems occur when there are some harmonics or significant peaks disturbances.

A self-tuning digital RC that is comprised of a gradient descent disturbance model estimation and a Pseudo Feed Forward (PFF) controller was proposed by Hillerstrom and Sternby [87]. The design consists of two main ideas; online identification to estimate the fundamental frequency of the disturbance by minimizing the output energy of the filtered disturbance, and the PFF controller that uses the filtered plant input and output to reject the disturbance signal affecting the system. The PFF controller is designed based on the identified disturbance model. A nice property of PFF controller is that it does not affect the closed-loop system stability, as the cancellation signal is injected from outside the feedback loop. A low order disturbance model that represents some dominating harmonics is used here. Therefore, the design only works for band-limited disturbance.

N´estor et al [88] designed a control strategy to reject both the repeatable and non-repeatable run out disturbances affecting the hard disk drive (HDD). The control scheme integrates the internal model to reject repeatable disturbance and an adaptive component based on minimum variance regulation to eliminate the non-repeatable disturbance.

Lin et al [89] integrated RC and adaptive FIR filter based on a recursive least-squares lattice filter to suppress random jitter while tracking a reference trajectory generated by a deterministic dynamic model. RC based ZPETC is employed to achieve asymptotic tracking performance, while an adaptive FIR filter is used to minimize the steady-state variance of plant output.

Lu et al [90] proposed a continuous adaptive RC to eliminate periodic disturbance with an unknown period. In the design, a finite-dimensional internal model was used. The adaptive algorithm tunes the finite-dimensional internal model parameters to match with the actual disturbance model. Since the proposed method uses a finite-dimensional internal model, then the design works only for band-limited disturbance.

A direct adaptive RC based on pole placement, as shown in Figure 2.17, has been proposed in [23]. Landau et al [23] presented a discrete adaptive RC to reject unknown narrow band disturbances. The proposed method identified the model of disturbance and updated the repetitive controller at each sampling time. The proposed design showed that it is possible to build an adaptive control where the parameters of the repetitive controller are directly adapted in order to have the desired internal model.

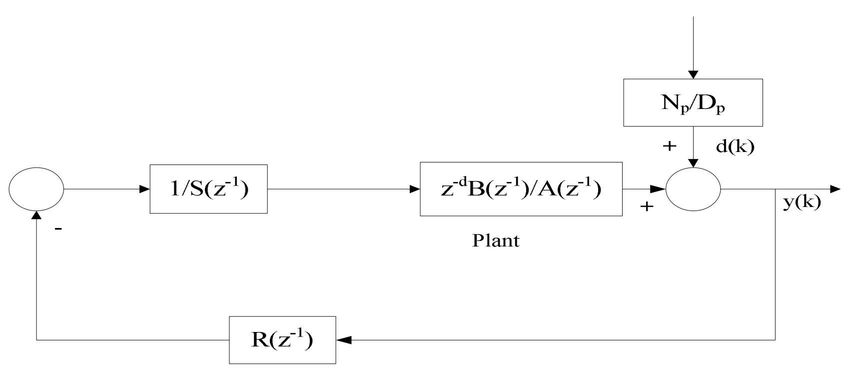

Figure 2.17 Adaptive RC system with RS polynomial control structure

where$D_p(z^{-1})$ is disturbance model ,

By using Youla-Kucera parameterization, polynomials $R(z^{-1})$ and $S(z^{-1})$ can be decomposed to:

$$S(z^{-1}) = S_o(z^{-1}) - z^{-d}B(z^{-1})Q(z^{-1}) \tag{2.34}$$

$$R(z^{-1}) = R_o(z^{-1}) + A(z^{-1})Q(z^{-1}) \tag{2.35}$$

Since the plant model is known and the central controller $R_o(z^{-1})$ and $S_o(z^{-1})$ can be computed by closed-loop pole assignment as follows:

$$P(z^{-1}) = A(z^{-1})S_o(z^{-1}) + z^{-d}B(z^{-1})R_o(z^{-1}) \tag{2.36}$$

, then the design problem is obtaining polynomial $Q(z^{-1})$ such that the $S(z^{-1})$ includes the internal model of disturbance $d(k)$

In [23], the disturbance model was unknown, but its order was known. Therefore, it was possible to tune polynomial $Q(z^{-1})$ at each sampling time until the polynomial $S(z^{-1})$ incorporated the internal model of disturbance.

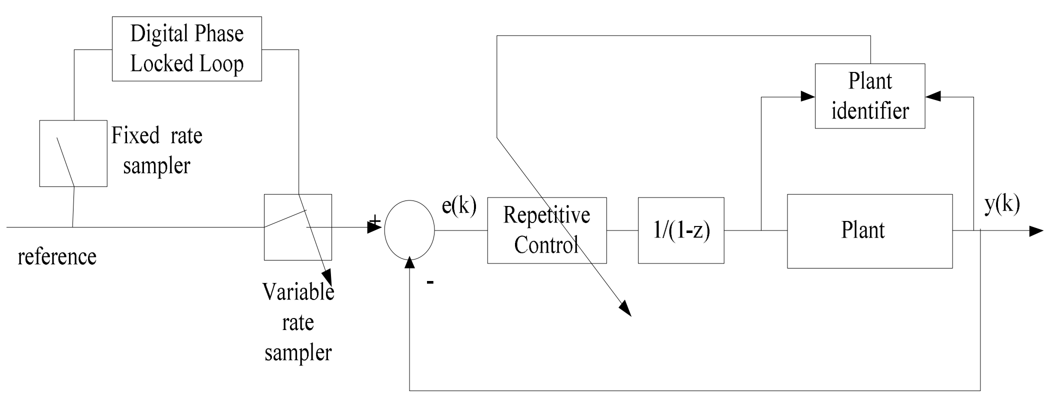

Figure 2.18 Digital PLL-based RC

Cao and Narasimhulu [27] proposed a digital PLL-based adaptive RC as shown in Figure 2.18. In the presence of a periodic signal with time-varying frequency, the sampling period was locked to the period of the reference/disturbance signal to maintain a constant number of samples per period, as required by RC. The use of PLL to estimate the time-varying frequency of disturbance and synchronize the sampling period also has been investigated by Cataliotti et al [93]. The sampling period adjustment in [27] changes the discrete plant coefficients. Then, the RC compensator needs to be adjusted accordingly to achieve a stable system.

An adaptive RC design to compensate parametric changes of the plant caused by sampling period adjustment was proposed by Olm et al [91]. The proposed method was comprised of two steps: an RC compensator design based on ZPETC at the selected nominal sampling period, and a controller design to keep the closed-loop model fixed at the selected nominal sampling period even though the sampling period varies. The design strategy is depicted in Figure 2.19 below:

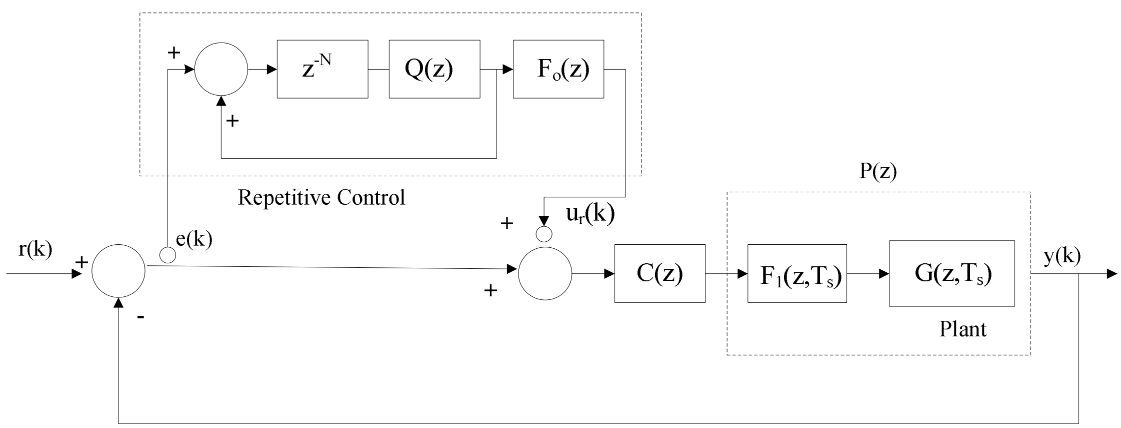

Figure 2.19 Adaptive RC with time-varying sampling period

where $F_o(z)$ is the RC compensator at the nominal sampling period T_n , which is formulated as follows:

$$F_o(z) = k_r \left[\frac{C(z)G(z,T_n)}{1 + C(z)G(z,T_n)}\right]^{-1} \tag{2.37}$$

$F_1(z,T)$ being a controller that makes $P(z)$ fixed and equal to the discrete plant model at the nominal sampling period $G(z,T_n)$

$$F_1(z,T) = G(z,T_n)[G(z,T)]^{-1} \tag{2.38}$$

, and T being the current sampling period that maintains the constant number of samples per period N.

The implementation of the design is quite complex, especially when updating the controller $F_1(z,T)$ that requires the calculation of the discrete model of $G(s)$ at the current sampling period T

A stability analysis of closed-loop system containing RC under time-varying sampling period [91] was presented by Ramos et al [94]. An analysis was carried out using LMI gridding approach.

A number of adaptive RC designs to track/reject repetitive signals with unknown or time-varying period have been discussed above. Most of the approaches assume that the plant is known. An indirect adaptive RC algorithm to recursively identify the period of disturbance then update either the delay length or sampling period was proposed in [22, 25, 84]. An indirect adaptive RC to identify the period of disturbance then update the external model of disturbance was presented by Hillerstrom and Sternby [87]. Landau et al [23] presented a direct adaptive RC to reject time-varying periodic disturbances. However, it can only be used for narrow band disturbances that give a lower order of the internal model RC. A direct adaptive RC design to reject time-varying periodic disturbances without knowledge of the plant model has not been proposed yet. Therefore, the design of adaptive RC for unknown linear systems subject to time-varying periodic disturbances, is proposed in this thesis. The proposed adaptive RC is based on the direct adaptive control scheme and the internal model principle. The design aims to reject disturbance frequency and its harmonics up to Nyquist. The proposed method is presented in Chapter 5.

2.5 MIMO RC DESIGN

An extensive study of RC was done for a SISO system, as discussed in previous sections. There are still few RC designs for the MIMO system to be found. This section presents some work on MIMO RC designs.

Sadegh [95] synthesized the discrete-time RC of a linear MIMO system, which aimed to preserve tracking performance over the sampling bandwidth. The compensator was designed based on a priori knowledge of the plant frequency response and the range of learning gain was formulated by using Nyquist stability criteria.

Jeong and Fabien [96] proposed the design of a Phase Cancellation Inverse (PCI) Matrix that operates by cancelling the phase lag in the diagonal elements and eliminating the-off diagonal elements of the plant model. The idea was initiated using a Zero Phase Tracking Error Controller (ZPETC) by Tomizuka [11], which aims to exactly cancel the phase response of the plant model. For the plant $G(z)$ with a square matrix transfer function, where its elements have a non-causal FIR filter form, the PCI matrix is given by:

$$F_{pci}(z) = Adj(G(z))\frac{\beta^{+}(z^{-1})}{\beta^{-}(z)} \tag{2.39}$$

where $F_{pci}(z)$ is PCI matrix, $Adj(G(z))$ is an adjoint of $G(z)$, $\beta^{+}(z), \beta^{-}(z)$ are the uncancellable and cancellable parts of $det(G(z))$, and $det(G(z))$ stands for determinant of $G(z)$.

The PCI matrix for a non-square matrix was also given Jeong and Fabien [96]. The design ends up with a non-causal PCI matrix, which is allowed due to the high causal term of the internal model.

In some situations, the repetitive signals consist of unrelated fundamental frequencies. A so-called multi periodic RC is required to address these situations. Owens et al [97] presented stability conditions for multi-periodic RC of a continuous-time MIMO system using Lyapunov analysis. As illustrated in Figure 2.20, the multi-periodic RC here was constructed from several internal models with different time-delays arranged in parallel. In [97], stability conditions of this RC system were derived. It has been shown that asymptotic stability is guaranteed if the plant model is positive real (PR), and exponential stability is ensured if the plant is strictly positive real (SPR).

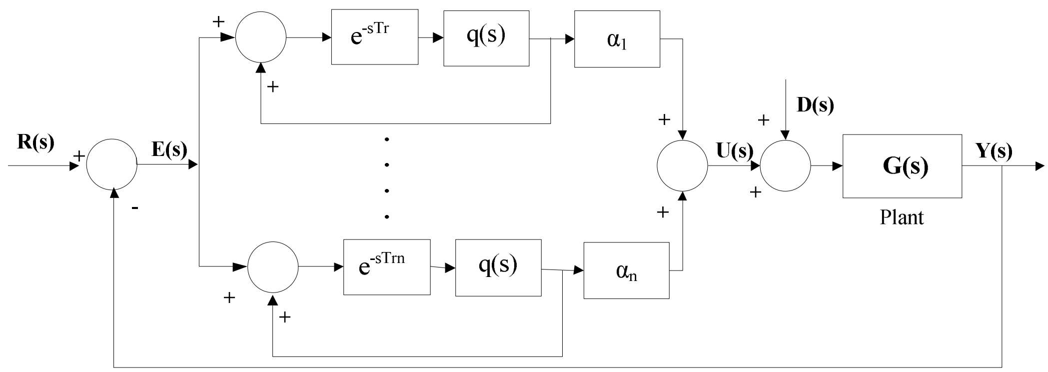

Figure 2.20 MIMO multi periodic RC system

where $G(s)$ is a continuous –time plant with a mxm transfer function matrix ($G(s) \in \mathbb{C}^{mxm}$), n is the number of unrelated fundamental frequencies, $q(s)$ is a low-pass filter, α is the gain given to each internal model, and the reference R , disturbance D, tracking error E , control U , and output Y belong to the set $\mathbb{R}^m$.

The design of an adaptive multi-periodic RC of continuous-time MIMO system was proposed by Dang and Owens [98]. The design objective was to adapt feed-forward controller such that the plant output tracks/rejects a multi periodic repetitive signal without information of the plant model. The MIMO plant is not necessarily positive real. However, it needs to be a strictly minimum-phase system. A direct adaptive scheme was employed, and the system stability was analysed using the Lyapunov method. The design was also extended to MIMO plant under certain nonlinear perturbations and the stability was also discussed.

An RC design that addresses the problem of tracking/rejecting repetitive signal for a MIMO system subject to control saturation was proposed by Flores et al [99]. The modified internal model allows tracking/rejecting of a repetitive signal of different fundamental frequencies on each channel that is used. In the design, LMI conditions are also proposed to compute the stabilizing state feedback gain and the antiwindup gain, which ensures that the outputs, states, references, and disturbances belong to certain admissible sets.

Another RC design for tracking the reference signal of a MIMO system subject to control saturation was also proposed by Wang et al [100]. The frequency of all reference signals were first decomposed via Fourier analysis and the dominant frequencies were chosen based on the reconstruction of reference signals with a predefined accuracy. A low order internal model was used to model each dominant frequency. The use of model predictive control (MPC) enabled it to put constraints on the plant inputs.

Xu [73] proposed an optimization based compensator to mimic each component of the inverse matrix of a plant. Given a mxm MIMO system (m^2 transfer functions), then there were m^2 compensators that needed to be designed.

$$G(z) = \begin{bmatrix} g_{11}(z) & \cdots & g_{1m}(z) \\ \vdots & \ddots & \vdots \\ g_{m1}(z) & \dots & g_{mm}(z) \end{bmatrix} \tag{2.40}$$

$$F(z) = \begin{bmatrix} f_{11}(z) & \cdots & f_{1m}(z) \\ \vdots & \ddots & \vdots \\ f_{m1}(z) & \dots & f_{mm}(z) \end{bmatrix} \tag{2.41}$$

where $G(z)$ is the plant matrix, and $F(z)$ is a compensator matrix

Each component of $F(z)$ is designed by minimizing the objective function as follows:

$$J_{ij} = \sum_{k=0}^{M-1} \left\{ \left[1 - \left(h_{ij}(z)\right)^{-1} f_{ij}(z)\right] \mathrm{W}_k \left[1 - \left(h_{ij}(z)\right)^{-1} f_{ij}(z)\right]^* \right\}_{z=e^{i\omega_k T}} \tag{2.42}$$

where $i = 1,2, \dots, m$, $j = 1,2, \dots, m$, k is indices of the chosen frequency up to Nyquist, W_k is weight for kth frequency, $h_{ij}(z)$is a component of $G^{-1}(z)$ at i-th row and j-th column, and $G^{-1}(z)$ is the inverse matrix of $G(z)$, f_{ij} is a compensator in the form of a non-causal FIR filter.

$$G^{-1}(z) = \frac{1}{\det\big(G(z)\big)} Adj(G(z)) = \begin{bmatrix} h_{11}(z) & \cdots & h_{1m}(z) \\ \vdots & \ddots & \vdots \\ h_{m1}(z) & \dots & h_{mm}(z) \end{bmatrix} \qquad (2.43)$$

This makes m^2 separate SISO objective functions to obtain a compensator matrix $F(z)$. Since the design procedure requires the calculation of the determinant of the matrix, then this design only works for a square matrix $G(z)$. Moreover, complexity in the design increases when the dimension of the matrix is significantly large.

Most of the designs for discrete-time MIMO are based on the full MIMO approach, which results in a compensator with the same dimensions as the plant. This implies that if we have an mxm MIMO system (m^2 transfer functions), then we need to design m^2 RC compensators. Moreover, the designs also end up with a non-causal compensator that needs to be merged with the internal model to make it realizable. The fact that most of MIMO control problems can be treated on a decentralized basis [101], gives a motivation to design decentralized RC of MIMO system. Decentralized control means that the MIMO system should be considered as a set of SISO systems. In chapter 6, a design for an RC compensator for a MIMO system is proposed, based on decentralized control. The stability of decentralized RC is also discussed.

2.6 SUMMARY

This chapter has presented a review of various RC designs. The designs were classified into four categories: Basic RC design, Robust RC design, Adaptive RC design, and MIMO RC design.

In Section 2, various designs for both an internal model and a compensator were presented. For digital RC, most existing compensators are either non-causal or unstable. The non-causal compensator is implementable because it is merged with the internal model, while the unstable compensator requires special implementation where the unstable poles operate in reverse time. In Chapter 4, a stable, low order, and causal compensator is proposed that can be implemented independently without being merged with the internal model. This reduces the complexity of the design, especially when the internal model has a high order.

In Section 3, various robust RC designs were discussed. The RC designs addressed; uncertain plant, control saturation, uncertain period of repetitive signal. Robust RC design to handle large time-varying repetitive signal has not been discussed yet. To overcome a repetitive signal with large variations in a period, the sampling period needs adjustment to maintain a constant number of samples per period. However, the discrete plant model changes as the sampling period varies In Chapter 4, a robust RC compensator is proposed that accommodates sampling period variation in a known relatively large bound.

In Section 4, various adaptive RC designs were reviewed. Most of the designs use an indirect scheme, and require information of the plant, which is required either to design the compensator of the internal model based RC or to estimate the disturbance signal in the external model based RC. In Chapter 5, a direct adaptive RC scheme is proposed that is able to simultaneously track and reject a time-varying periodic signal without knowledge of the plant model. The design is based on direct adaptive control and the internal model principle.

In Section 5, several MIMO RC designs were presented. There has still been little work on MIMO RC designs. Most of the designs for discrete-time MIMO have been based on the full MIMO approach, resulting in a compensator with the same dimensions as the plant. This implies an mxm MIMO system (m^2 transfer functions), requires the design of m^2 RC compensators. In Chapter 7, a decentralized RC design is presented, as most MIMO control problems can be treated on a decentralized basis. This reduces the complexity of the design since we only need to design m RC compensators for an mxm MIMO plant Another advantage of the proposed design is that it ends up with a causal compensator that can be implemented independently rather than being merged with the internal model.

CHAPTER 3

EXPERIMENTAL SYSTEM

3.1 INTRODUCTION

The fastest and most convenient approach to test the effectiveness of the design is to simulate the system on a computer via software. Computer simulations can quickly demonstrate the performance of the system, as the simulations are only processed and calculated in the computer. However, simulations cannot replace the real-time experiments, in which the tests represent the real situations that may be affected by disturbances, uncertainties, and nonlinearities.

This chapter describes the experimental system used for testing the control algorithms proposed in this thesis. System hardware and software are given in Sections 2 and 3 respectively. Section 4 concludes the chapter.

3.2 SYSTEM HARDWARE

The experimental system used here consists of the following hardware components:

1. Host PC: This hardware is the computer that hosts the software simulator, editor, compiler, and debugger.
2. Target System: This is the computer that runs the code generated by the host PC. This hardware interfaces directly to the plant. In this experiment, both host PC and target system were the same machine (single-PC solution).
3. Signal Conditioning Hardware: This hardware amplifies, attenuates, and filters signals sent between the software execution hardware and the plant
4. Plant: This is the hardware to be controlled.

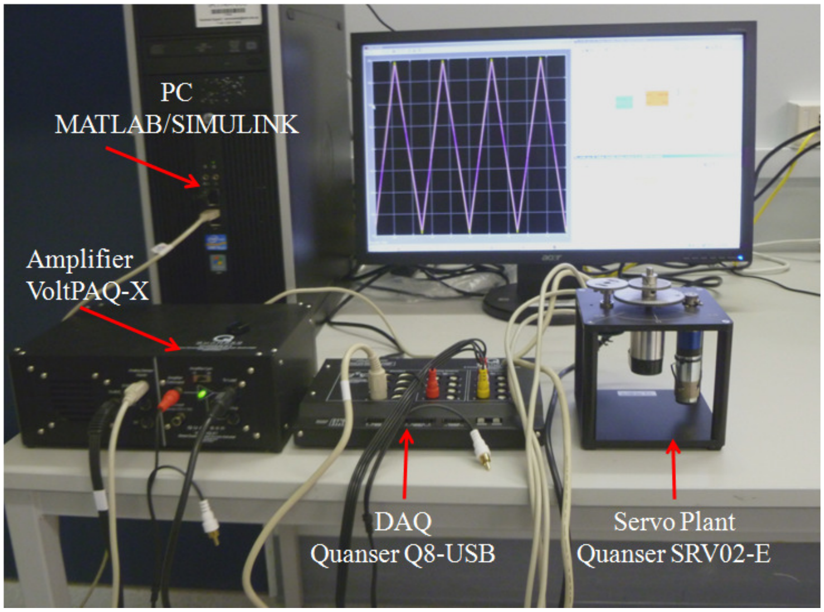

Figure 3.1 Experimental setup for the servo plant

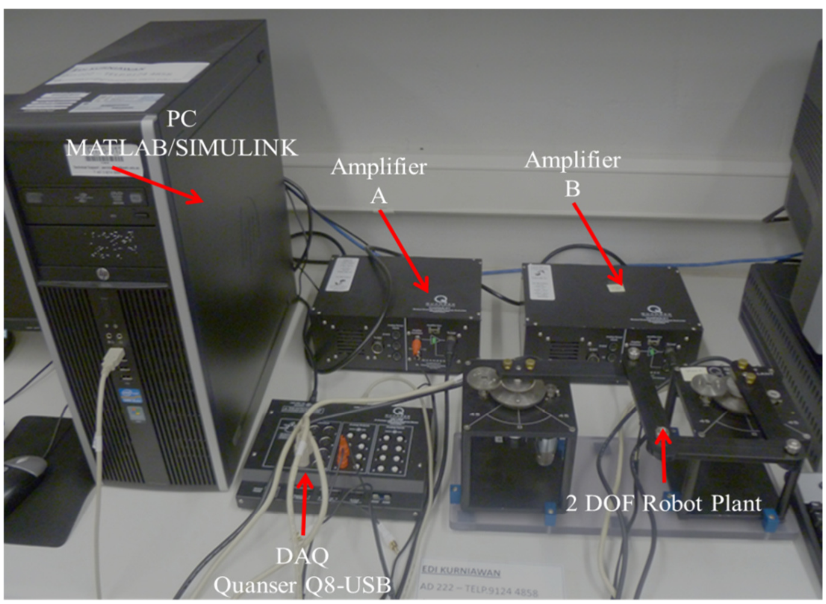

Figure 3.2 Experimental setup for 2 DOF robot plant

Figures 3.1 and 3.2 show the experimental setup for the servo plant and 2 DOF robot plant respectively. The block diagram of the experiment is shown in Figure 3.3. A PC and a set of hardware manufactured by Quanser are used to control the position of servomotor. The system hardware used in the experiment consisted of a PC, a servomotor, a 2 Degrees of Freedom (DOF) robot, an amplifier, and a data acquisition board. A PC with the specifications; Intel Core i5 processor, and 2GB RAM, was used for both Host and Target system.

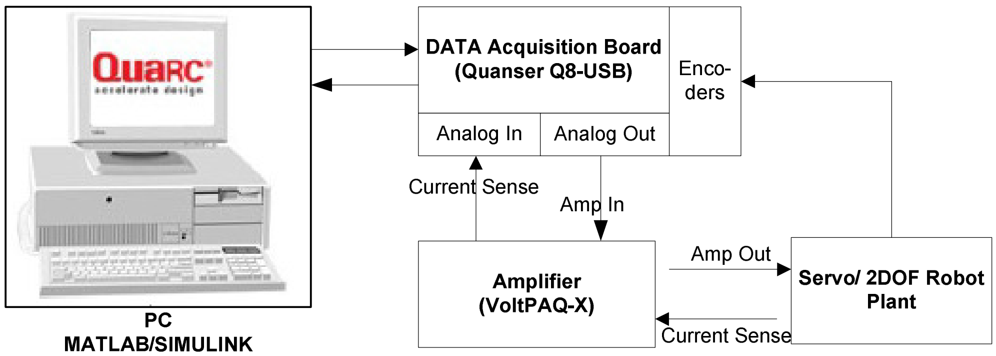

Figure 3.3 Experimental system block diagram

3.2.1 SERVOMOTOR

The first plant to be controlled is a rotary servo SRV02-E manufactured by Quanser. The Quanser SRV02-E, pictured in Figure 3.4, consists of a DC motor that is equipped with a planetary gearbox, a potentiometer sensor that is used to measure angular position of the load gear, and an encoder that can be used to obtain a digital position measurement. The potentiometer sensor provides an absolute position measurement as opposed to relative measurement from the encoder.

The open-loop SRV02-E has the following model

$$G(s) = \frac{V_o(s)}{\theta_o(s)} = \frac{K}{\tau s^2 + s} \tag{3.1}$$

where $V_o(s)$ is open-loop voltage, $\theta_o(s)$ is load gear position, parameter K and τ are experimentally identified based on the frequency response, and are shown in Table 3.1

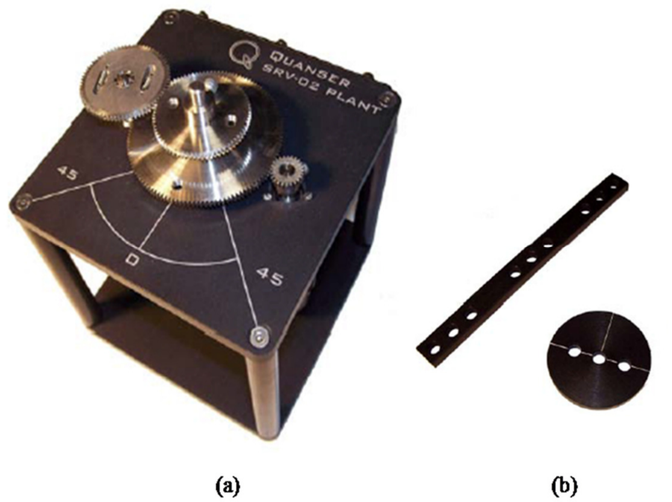

Figure 3.4 (a) Quanser SRV02-E servo plant (b) Bar and disc load supplied with SRV02-E system [102]

Table 3.1 Parameter **K** and **τ** for different loads

Load	K= steady-state gain (rad/sV)	τ = time constant (s)
No Load	1.7400	0.0268
Bar	1.7400	0.0275
Disc	1.7500	0.0255

Real-time experiments using this plant were conducted to verify the control algorithms proposed in Chapter 4 and 5. The experiments aimed to control the angle position of Quanser SRV02-E to exactly track the periodic reference signal.

3.2.2 A 2 DOF Robot

The second plant used in the experiment is Quanser 2 DOF robot, pictured in Figure 3.5. Two servo motors mounted at a fixed distance control two arms coupled via two non-powered two-link arms. The system has 2 actuated and 3 unactuated revolute joints. The 4-bar linkage system gives coupling effect to the actuated joints. The 2 DOF robot is a 2x2 MIMO system, and its transfer functions are experimentally modeled using time-domain data. The 2 DOF robot has the following transfer functions:

$$G(s) = \frac{V_c(s)}{\theta_o(s)} = \begin{bmatrix} g_{11}(s) & g_{12}(s) \\ g_{21}(s) & g_{22}(s) \end{bmatrix} \tag{3.2}$$

where $V_c(s)$ is close-loop voltages, $\theta_o(s)$is load gear positions

$$g_{11}(s) = \frac{1.0210}{0.0059s^2 + 0.1191s + 1} \tag{3.3}$$

$$g_{12}(s) = \frac{-0.0144\, s \; + \; 0.3975}{26.430s^2 + 7.2020s + 1} \tag{3.4}$$

$$g_{21}(s) = \frac{-0.0029\, s}{0.0069s^2 + \; 0.1201s + 1} \tag{3.5}$$

$$g_{22}(s) = \frac{1.0030}{0.0051\, s^2 + 0.1151s + 1} \tag{3.6}$$

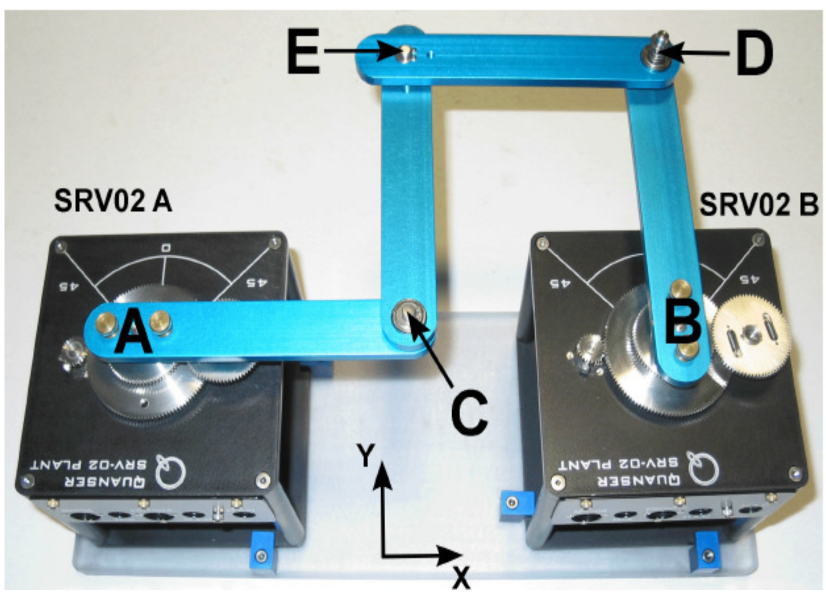

Figure 3.5 2 DOF Quanser robot plant [103]

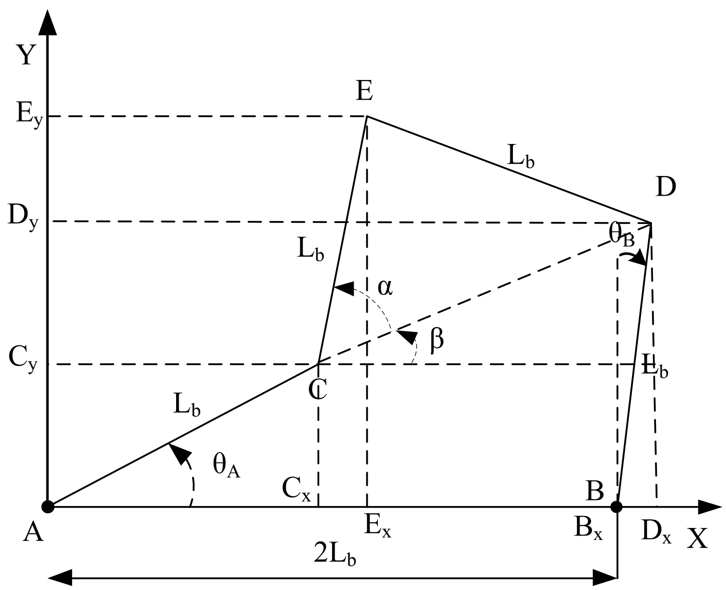

Figure 3.6 Schematic of 2 DOF robot

A schematic of the 2 DOF robot is shown in Figure 3.6. Figure 3.6 shows that the two servomotors are represented as the actuated revolute joints A and B. All four bars have the same length L_b. The robot end effector is depicted by joint E. The two actuated angles are denoted by θ_A and θ_B, and they are the angles position of SRV02-E A and SRV02-E B respectively. The goal of the system is to control the X-Y coordinates of a 4-bar linkage end effector joint E. The given references are periodic signals of X-Y Cartesian coordinate, while the control inputs and measured outputs are angles position. To obtain control inputs in angles, and tracking outputs in Cartesian, some conversions are required. Hence, the forward and inverse kinematics need to be derived. The X-Y Cartesian coordinate of joint E is represented as (E_x, E_y).

The forward kinematics calculate the Cartesian coordinates of robot end effector from the actuated angles (θ_A , θ_B). The known quantities in forward kinematics are θ_A, and θ_B. By assuming that the joint A is at the origin, the Cartesian coordinate of joint C, namely C_x and C_y are

$$C_x = L_b cos(\theta_A) \tag{3.7}$$

$$C_y = L_b sin(\theta_B) \tag{3.8}$$

Similarly, the Cartesian coordinate of joint D, namely D_x and D_y are

$$D_x = B_x + L_b sin(\theta_B) \tag{3.9}$$

$$D_y = L_b cos(\theta_B) \tag{3.10}$$

where $B_x = 2L_b$ (3.11)

The distance between point C and D, is given by the following equation:

$$CD = \sqrt{(D_x - C_x)^2 + \left(D_y - C_y\right)^2} \tag{3.12}$$

From Figure 3.6 and doing some trigonometry, the following expressions are derived:

$$\alpha = arccos\left(\frac{CD}{2L_b}\right) \tag{3.13}$$

$$\beta = arctan\left(\frac{D_y - C_y}{D_x - C_x}\right) \tag{3.14}$$

Thus, the Cartesian coordinate of joint E, namely E_x and E_y can be expressed respectively as follows:

$$E_x = C_x + L_b cos(\alpha + \beta) \tag{3.15}$$

$$E_y = C_y + L_b sin(\alpha + \beta) \tag{3.16}$$

The inverse kinematics convert from the Cartesian coordinates of joint E to the actuated angles (θ_A , θ_B). From [103], the inverse kinematics are given as follows:

$$\theta_A = arctan\left(\frac{E_y}{E_x}\right) - \frac{\pi}{2} + \frac{\lambda_A}{2} \tag{3.17}$$

$$\theta_B = arctan\left(\frac{B_x - E_x}{E_y}\right) - \frac{\pi}{2} + \frac{\lambda_B}{2} \tag{3.18}$$

where the angles λ_A and λ_B are given by

$$\lambda_A = arccos\left(\frac{2L_b^2 - \left(E_x^2 + E_y^2\right)}{2L_b^2}\right) \tag{3.19}$$

$$\lambda_B = arccos\left(\frac{2L_b^2 - \left[(E_x - B_x)^2 + E_y^2\right]}{2L_b^2}\right) \tag{3.20}$$

3.2.3 DATA ACQUISITION BOARD (DAQ)

A data acquisition board (DAQ) is used to interface between the target system and the plant. The DAQ basically performs analogue to digital (A/D) conversions, and digital to analogue (D/A) conversions. The DAQ used in the experiments is Q8-USB board , manufactured by Quanser. The Q8-USB board supports a rapid prototyping and Hardware-in-the-Loop (HIL) control environment. This board does not require digital signal processor (DSP), because a CPU does all processing. The others features include a USB connection, 8 16-bit ADCs, 8 16-bit DACs, 8 encoder inputs, supporting both QUARC Windows and NI LabView targets [104].

3.2.4 POWER AMPLIFIER

A linear power amplifier, VoltPAQ-X1 manufactured by Quanser, was used in the experiment. This is signal conditioning hardware that powers one load only. An analog control signal from DAC is fed to the amplifier before it is sent to the plant. The same goes for the analog measurement signal from the plant, which is sent to the amplifier before going to ADC. The main specifications of VoltPAQ-X1 are shown in the table below [105].

Table 3.2 VoltPAQ-X1 Specifications

Amplifier Specifications	Value
Output Voltage	$\pm 24\ V$
Continuous Current Output	$\pm 4.16\ A$
Voltage Gain	$1x\ or\ 3x$
Current Sense	$1A/\ V$
Amplifier Command Voltage	$\pm 10\ V$

3.3 SYSTEM SOFTWARE

System software used in the experiment consists of the following components:

1. **Software Development**

The software development used in the experiment, and which ran on the host computer, consisted of Microsoft Windows XP SP2, QUARC$^{@}$2.1, and MATLAB R2009b, which includes Simulink, and Real-Time Workshop (RTW). Windows XP SP2 is an operating system on which the QUARC and MATLAB run.

QUARC$^{@}$ 2.1 is a rapid prototyping software for real-time control, developed by Quanser, that generates real-time code directly from Simulink. This tool basically extends the capabilities of Real-Time Workshop by adding a Windows target. The QUARC compiles the C code generated from the Simulink model, links with libraries for the selected target, and downloads the code to the target.

Simulink is an add-on product to MATLAB that provides a graphical environment for modeling, simulating and analyzing of dynamic systems. It includes a library of pre-defined blocks to be used to create a graphical model of system. The user also can create and insert the user-defined block to the Simulink model.

Real-time workshop (RTW) generates and executes C or C++ code from Simulink diagrams, Stateflow charts, and Matlab functions. The user can generate code for any Simulink diagrams (discrete-time, continuous, or hybrid systems) that are useful for real-time or embedded applications. The generated code also can be used for non-real time applications including simulation acceleration, and HIL testing.

2. **Target Software.**

This is an operating system on which the software execution hardware runs. In this experiment, the same Windows XP SP2 was used.

The procedures of running real-time control in the experiment consisted of the following stages:

1. Creating Simulink Model

This is the process by which a system model is created, first selecting the desired blocks, then configuring the block parameters, and finally connecting the block inputs and outputs. The reference signal and controller parameters are set at this stage. For the robust RC described in Chapter 4 and the MIMO RC system described in Chapter 6, the system models were built from blocks that were already available in the library browser. All of the controller parameters were fixed and designed by using an Optimization Toolbox, MATLAB [106]. The controller parameters were set offline before running the model. For the adaptive RC system in Chapter 5, besides the blocks provided from the libraries, user-defined blocks were created. These blocks embed C-S functions. The C-S function is a user-defined code written in C environment. This C-S function gives more flexibility than the common blocks provided in the Library, because it enables the controller parameters to be updated at each sampling time when the model is already running.

2. Configuring Model

This is the stage of configuring the Simulink parameters after the model is created. The key parameters for building and running the model are Solver parameters and a System target file. The fixed-step type solver, which has a constant step size, was chosen, as this was the only solver that could support code generation. A variable-step type solver may be chosen, if the models run in the normal simulation. The solver is a numerical method used to compute the model's states when the model is running. A first order solver, ode1 (Euler's Method), was used because it gives less computation time in real-time code. Another important parameter is the System target file. The target file determines the target type for which the real-time code will be generated. The target file *quarc_windows.tlc* was chosen, in which it indicates the Quarc Windows target.

3. Building Model

This stage is required if the model is to run in real-time. In a normal simulation, a building model is not necessary because simulation does not need real-time code. The building model basically consists of the following operations; Model compilation, Code generation, Customized makefile generation, Real-time code generation, and a Downloading real-time code.

Model compilation is the operation in which RTW examines the Simulink model and builds a database describing every single block and line in the model. Code generation is the process of generating C code for the model. Customized makefile generation is the process in which QUARC creates a customized makefile using a template associated with the specified target file. In real-time code generation, the generated C code is compiled, the object files and libraries are linked, and a real-time code is obtained for the specified target type. The real-time code is the executable file that will run on the target machine. The executable file has an extension *.rt-windows*, where windows indicates the Quarc windows target. Once the real-time code is generated, then the code is ready to be downloaded to the target machine.

4. Connecting to a Model's Real-Time Code

Downloading real-time code as part of build process does not make the code is loaded into memory. Connecting to the real-time code here is needed to make the target load the code into memory, and initialize it. However, this does not start the model.

5. Starting/Stopping

The user must input the start/stop command to run/stop the model.

3.4 SUMMARY

This chapter has presented the experimental system used to validate the proposed algorithms. The system hardware and software used in the experiments have been described in this chapter.

The system hardware consists of a PC, a servomotor, a 2 DOF robot, an amplifier, and a data acquisition board. The first experimental system has used a servomotor as the plant. The goal of the system is to control the angle position of the servomotor in order to be exactly track the periodic reference signal. A 2 DOF robot was used for the second experimental system. The system aims to control the X-Y Cartesian coordinates of the end effector. For the system software, the following software was used; Microsoft Windows XP SP2, QUARC@2.1, and MATLAB R2009b.

CHAPTER 4

DESIGN OF ROBUST RC WITH TIME-VARYING SAMPLING PERIODS

4.1 INTRODUCTION

In most designs of discrete RCs, it is assumed that the frequency of the compensated signal is a constant, and the sampling rate is fixed to give an integer number of samples per period. However, in practice, the reference or disturbance may have a time varying period. If the sampling period remains fixed, the number of samples per period will change. This may decay the tracking performance [24]. To overcome this problem, a digital PLL-based repetitive control was proposed [27], in which the sampling period was locked to the period of the reference/disturbance signal to maintain a constant number of samples per period. However, the discrete plant model changes as the sampling period varies. The RC has to be changed accordingly in order to achieve a stable system.

In this chapter, a design of robust RC with time varying sampling periods is proposed. A new design methodology was developed first in order to obtain a stable, robust and causal IIR compensator that achieves fast convergence and high tracking accuracy. The new stable and causal RC compensator is implemented independently to reduce the design complexity, as most existing repetitive compensators are either unstable or non-causal, which makes implementation difficult. A comprehensive analysis and comparison study is presented. A robust compensator is then proposed, which accommodates the sampling period variation in the known bound. In the design, the time-varying parts due to sampling period interval variation are treated as parametric uncertainties.

This chapter is organized as follows. In Section 2, the design of a new compensator using an optimization method is presented. Section 3 covers how to model the uncertainties. In Section 4, the robust design is described. Simulation and experimental results are given in Section 5 and Section 6 respectively. A comparison study is also presented in Section 5. Section 7 concludes the chapter.

4.2 A NEW DESIGN OF RC COMPENSATOR

The general structure of a digital plug - in RC system is shown in Figure 4.1 [9], where $G_{rc}(z)$ is the digital repetitive control, $C(z)$ is the feedback controller, $G(z)$ is the plant model, $r(k)$ is the periodic reference signal, $e(k)$ is the tracking error, $u_p(k)$ is the control signal, and $y_p(k)$ is the tracking output.

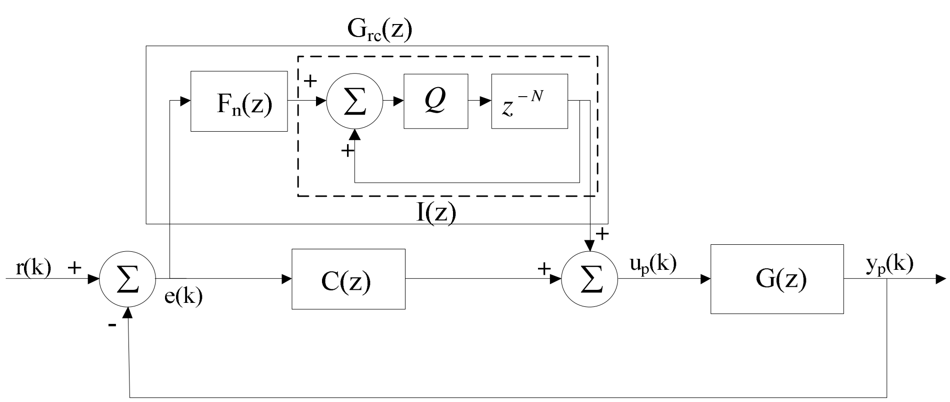

Figure 4.1 General structure of the plug –in RC system

The digital RC has a generic transfer function as follows:

$$G_{rc}(z) = F_n(z)\frac{Q(z)z^{-N}}{1 - Q(z)z^{-N}} \tag{4.1}$$

where $F_n(z)$ is the compensator, $Q(z)$ is the zero phase low pass filter with unity gain, T_r is the period of the reference, T is the sampling period, $N = T_r/T \in \mathbb{N}$, N is the integer number of samples per period and is also the order of the internal model.

For the plug-in RC system shown in Figure 4.1, the compensator $C(z)$ is firstly designed to achieve a stable system with the closed loop transfer function of $G_c(z)$:

$$G_c(z) = \frac{G(z)}{1 + C(z)G(z)} \tag{4.2}$$

The RC compensator is then designed to cancel the dynamics of $G_c(z)$, in which the plant model is usually required [9-11]. However, the accurate plant model is sometimes not available due to uncertainties and disturbance [15]. Here, we propose a new form of compensator, which is a proper and stable m-th order IIR filter $F_n(z)$ as:

$$F_n(z) = \frac{q_0 z^m + q_1 z^{m-1} + \cdots + q_m}{z^m + r_1 z^{m-1} + \cdots + r_m}\ , m > 0 \tag{4.3}$$

The characteristic equation of the system shown in Figure 4.1 can be derived as:

$$1 + \left(C(z) + F_n(z) \frac{Q(z)z^{-N}}{1 - Q(z)z^{-N}} \right) G(z) = 0 \tag{4.4}$$

$$[1 + C(z)G(z)] - [1 + C(z)G(z)]Q(z)z^{-N} + F_n(z)G(z)Q(z)z^{-N} = 0 \tag{4.5}$$

$$[1 + C(z)G(z)] \left[1 - Q(z)z^{-N} + \left(\frac{G(z)}{1 + C(z)G(z)} \right) F_n(z)Q(z)z^{-N} \right] = 0 \tag{4.6}$$

$$[1 + C(z)G(z)][1 - Q(z)z^{-N} + G_c(z)F_n(z)Q(z)z^{-N}] = 0 \tag{4.7}$$

$$[1 + C(z)G(z)]\left[1 - \left(1 - G_c(z)F_n(z)\right)Q(z)z^{-N}\right] = 0 \tag{4.8}$$

The overall system is stable if two conditions are satisfied [9, 15]:

1. $G_c(z)$ is a stable transfer function.

2. $\left\|\left(1 - G_c(z)F_n(z)\right)Q(z)\right\|_\infty < 1$ or $\quad (4.9)$

$$\left|\left(1 - G_c(z)F_n(z)\right)Q(z)\right| < 1 \quad \forall \quad 0 < \omega_i < \frac{\pi}{T} \tag{4.10}$$

As the controller sampling period T is specified, and the continuous model $G(s)$ is known, the discrete plant model $G(z)$ and the closed-loop transfer function $G_c(z)$ can be easily obtained. Hence, the information regarding the magnitude and phase response of $G_c(z)$ is also known.

Let $M_{Gc_i}$and θ_{Gc_i}, $M_{Q_i}$and θ_{Q_i}, $M_{F_{ni}}$ and $\theta_{F_{ni}}$are magnitude and phase response of $G_c(z)$, Q-filter and F_n at frequency ω_i respectively. As the parameters of F_n are unknown, then $M_{F_{ni}}$ and $\theta_{F_{ni}}$ are nonlinear scalar functions that have $(2m + 1)$ variables denoted as $r_{1,}r_2, \dots, r_m, q_0, \dots, q_m$. The stability condition (4.10) at frequency ω_i can be expressed as:

$$\left|1 - M_{F_{ni}} e^{j\theta_{F_{ni}}} M_{Gc_i} e^{j\theta_{Gc_i}}\right|\left|M_{Q_i} e^{j\theta_{Q_i}}\right| < 1 \tag{4.11}$$

Since the phase response of Q-filter is zero for all frequencies, thus (4.9) can be rewritten as:

$$\left|1 - M_{F_{ni}} e^{j\theta_{F_{ni}}} M_{Gc_i} e^{j\theta_{Gc_i}}\right| M_{Q_i} < 1 \tag{4.12}$$

$$\left[\left(1 - M_{F_{ni}} M_{Gc_i} e^{j\left(\theta_{F_{ni}} + \theta_{Gc_i}\right)}\right)\left(1 - M_{Gc_i} e^{-j\left(\theta_{F_{ni}} + \theta_{Gc_i}\right)}\right)\right]^{\frac{1}{2}} M_{Q_i} < 1 \tag{4.13}$$

Let $M_{T_i} = M_{F_{ni}} M_{Gc_i}$, $\theta_{T_i} = \theta_{F_{ni}} + \theta_{Gc_i}$, and the LHS of (4.13) denoted as :

$$h_i = \left[\left(1 - M_{T_i}\left[\cos\left(\theta_{T_i}\right) + j\sin\left(\theta_{T_i}\right)\right]\right)\left(1 - \left[\cos\left(\theta_{T_i}\right) - j\sin\left(\theta_{T_i}\right)\right]\right)\right]^{\frac{1}{2}} M_{Q_i} \tag{4.14}$$

$$= \left[1 - 2M_{T_i}\cos(\theta_{T_i}) + {M_{T_i}}^2\right]^{\frac{1}{2}} M_{Q_i} \tag{4.15}$$

h_i is a scalar function presenting the magnitude response of (4.10) at frequency ω_i. To satisfy the stability condition (4.10), h_i has to be less than one for all frequencies up to the Nyquist.

$$h_i = \left[1 - 2M_{T_i}\cos(\theta_{T_i}) + {M_{T_i}}^2\right]^{\frac{1}{2}} M_{Q_i} < 1 \tag{4.16}$$

An objective function can now be defined as:

$$h_{Total} = \sum_{i=1}^{L} h_i \ \forall\omega_i = 2\pi\frac{i}{NT} \ i = 1,2,3 \dots, L \tag{4.17}$$

where $L = N/2$ for an even N, and $L = (N-1)/2$ for an odd N.

Now, the optimization problem as follows is proposed:

$$\min_{(p_1,\dots,p_m,q_0,\dots,q_m)} h_{Total}$$

Subject to:

$$1. \begin{bmatrix} -1+\delta \\ \cdot \\ \cdot \\ -1+\delta \end{bmatrix} < \begin{bmatrix} p_1 \\ \cdot \\ \cdot \\ p_m \end{bmatrix} < \begin{bmatrix} 1-\delta \\ \cdot \\ \cdot \\ 1-\delta \end{bmatrix} \tag{4.18}$$

$$2. h_i < 1 - \tau, \forall\omega_i = 2\pi\frac{i}{NT} \ i = 1,2,3 \dots, L$$

where δ and τ are small positive constants, and $p_1, p_2, \dots, p_m$ are m real poles of $F_n(z)$.

Remark 4.1: We can assume that some poles are complex, and complex poles always come in pairs. Suppose p_1 is a complex pole, $p_1 = u + jv$, so there is a pair conjugate of this pole, $p_2 = u - jv$. In this case, the optimization problem is simply modified to:

$$\min_{(u,v,p_3,\ldots,p_m,q_0,\ldots,q_m)} h_{Total}$$

Subject to:

1. $u^2 + v^2 < 1 - \delta$
2. $\begin{bmatrix} -1+\delta \\ \cdot \\ \cdot \\ -1+\delta \end{bmatrix} < \begin{bmatrix} p_3 \\ \cdot \\ \cdot \\ p_m \end{bmatrix} < \begin{bmatrix} 1-\delta \\ \cdot \\ \cdot \\ 1-\delta \end{bmatrix}$ (4.19)
3. $h_i < 1 - \tau, \forall \omega_i = 2\pi \frac{i}{N\,T_s}\ i = 1,2,3 \ldots, L$

Remark 4.2: The first condition of (4.18) consists of m constraints which guarantees that all poles of $F_n(z)$ are inside the unit circle. The positive constant δ presents the minimum distance of all $F_n(z)$ poles from the unit circle. This condition ensures that the compensator is stable within a safe margin.

Remark 4.3: The second condition of (4.18) guarantees that the closed loop system is stable within a positive margin of τ.

The optimization problem (4.18) is a class of nonlinear optimization that finds $(2m + 1)$ optimum variables subject to m bound constraints and $N/2$ (for an even N) or $(N - 1)/2$ (for an odd N) nonlinear constraints.

4.3 UNCERTAINTY MODELING

Suppose we have a k-th order plant, the transfer function of $\mathrm{G_c(z)}$ can be expressed as:

$$\mathrm{G_c(z)} = \frac{\mathrm{b_1(T)z^{k-1} + b_2(T)z^{k-2} + \cdots + b_k(T)}}{\mathrm{z^k + a_1(T)z^{k-1} + \cdots + a_k(T)}} \tag{4.20}$$

where $\mathrm{a_1, \ldots, a_k,\ b_1, \ldots, b_k}$ are coefficients of the transfer function.

These coefficients vary when the sampling period $\mathrm{T_s}$ is changed. Assume $\mathrm{T_s}$ is varying in the known bound, $\mathrm{T \in [T_l, T_u] \subset R^+}$, where $\mathrm{T_l}$ and $\mathrm{T_u}$ are the lowest and highest sampling periods respectively. This leads to the parametric uncertainties of $G_c(z)$. Defining $G_{cl}(z)$ and $G_{cu}(z)$ as the transfer function when the plant $G_c(z)$ is sampled at T_l and T_u respectively:

$$G_{cl}(z) = \frac{b_1(T_l)z^{k-1} + \cdots + b_k(T_l)}{z^k + a_1(T_l)z^{k-1} + \cdots + a_k(T_l)} \tag{4.21}$$

$$G_{cu}(z) = \frac{b_1(T_u)z^{k-1} + \cdots + b_k(T_u)}{z^k + a_1(T_u)z^{k-1} + \cdots + a_k(T_u)} \tag{4.22}$$

Assume $G_c(s)$ is a continuous time transfer function:

$$G_c(s) = D + C(sI - A)^{-1}B \tag{4.23}$$

where A, B, C and D are the matrixes of the system state space model.

Its discrete time transfer function is:

$$G_c(z) = D + C(zI - A_d)^{-1}B_d \tag{4.24}$$

where $A_d(T) = e^{AT}$, and $B_d(T) = \left(\int_0^T e^{A\tau}\, d\tau\right)B$.

From the Taylor series,e^{AT} can be expressed as:

$$e^{AT} = I + AT + \frac{(AT)^2}{2!} + \frac{(AT)^3}{3!} + \cdots \tag{4.25}$$

Let the sampling period T take small values, $T \ll 1$, then e^{AT} can be approximated as:

$$e^{AT} \approx I + AT \tag{4.26}$$

Therefore, matrix A_d and B_d can be expressed as:

$$A_d \approx I + AT \tag{4.27}$$

The digital system matrix A_d is varying linearly with T_s. Therefore, the eigenvalues of the digital system are the linear functions of T. If a robust RC compensator is designed to make the system at T_l and T_u stable, it guarantees that the system is stable at any sampling period $T \in [T_l, T_u] \subset R^+$. In the following section, the design of such a robust RC compensator is discussed.

4.4 ROBUST RC DESIGN

Suppose that the causal and stable RC compensator $F_n(z)$ is firstly designed at the nominal sampling period T_n. Let vector $\bar{f}_n$ represent the coefficients of $F_n(z)$

$$\bar{f}_n = [r_1\ r_2 \dots r_m q_0\ \ q_1 \dots q_m]^T \tag{4.28}$$

Now the robust compensator $F_r(z)$ is designed closest to the nominal one $F_n(z)$, which ensures that the system is stable at T_l and T_u. Let vector $\bar{f}_r$ represent the coefficients of $F_r(z)$:

$$\bar{f}_r = [r_{1r} r_{2r} \dots r_{mr} q_{0r}\ \ q_{1r} \dots q_{mr}]^T \tag{4.29}$$

Therefore, the robust design can be formulated as:

$$\min_{\bar{f}_r = r_{1r} r_{2r} \dots r_{mr} q_{0r} q_{1r} \dots q_{mr})} \left\|\bar{f}_r - \bar{f}_n\right\|^2$$

Subject to:

$$1. \begin{bmatrix} -1+\delta \\ \cdot \\ \cdot \\ -1+\delta \end{bmatrix} < \begin{bmatrix} p_{1R} \\ \cdot \\ \cdot \\ p_{mR} \end{bmatrix} < \begin{bmatrix} 1-\delta \\ \cdot \\ \cdot \\ 1-\delta \end{bmatrix} \tag{4.30}$$

$$2.\ h_{li} < 1 - \tau, \forall \omega_i = 2\pi \frac{i}{N\,T_l}\ \ i = 1,2,3 \dots, N/2$$

$$3.\ h_{ui} < 1 - \tau, \forall \omega_i = 2\pi \frac{i}{N\,T_u}\ \ i = 1,2,3 \dots, N/2$$

where $p_{1r}, p_{2r}, \dots, p_{mr}$ are m real poles of $F_r(z)$,

$$, h_{li} = |(1 - F_r(z)G_{cl}(z))Q(z)|_{\omega=\omega_i} \tag{4.31}$$

$$, \text{and } h_{ui} = |(1 - F_r(z)G_{cu}(z))Q(z)|_{\omega=\omega_i} \tag{4.32}$$

The robust compensator $F_r(z)$ can be obtained by solving the above optimization problem, which minimizes a quadratic objective function subject to m bound constraints, and N nonlinear constraints (N constraints for N even and $(N-1)$ constraints for N odd).

4.5 SIMULATION RESULTS

In this section, we present the simulation results of the proposed methods; a new design of RC compensator and robust RC design. Simulation results of a new design of RC compensator and robust RC design are given in subsections 4.5.1 and 4.5.2 respectively.

4.5.1 SIMULATION OF NEW RC COMPENSATOR

This sub section covers numerical examples of the new design of compensator for both minimum and non-minimum phase plant, and also provides an analysis of the simulation results. A comparison study is also given in sub subsection 4.5.1.3.

4.5.1.1 Minimum Phase System

The continuous plant model has the following transfer function;

$$G(s) = \frac{1.74}{0.0268s^2 + s} \tag{4.33}$$

which represents the servomotor used in the experiment.

The feedback controller $C(s)$ used to stabilize open-loop model is just a proportional controller with gain 10. Let the sampling period be $T = 0.005$ s, the reference signal $r(k)$ have a fundamental frequency 0.8 Hz. The discrete closed-loop transfer function $G_c(z)$ is given as follows:

$$G_c(z) = \frac{10^{-3}(0.7634z + 0.7173)}{z^2 - 1.8222z + 0.8370} \tag{4.34}$$

$G_c(z)$ is a stable minimum phase plant, since it has stable poles and a zero located inside the unit circle.

A first order Q-filter is generally accepted in most RC designs [15]. In this case, the Q-filter $Q(z) = 0.25z + 0.5 + 0.25z^{-1}$ is chosen, as it gives a sufficient bandwidth to accommodate the reference harmonics. The small constants $\delta = 0.075$ and $\tau = 0.05$ are chosen respectively. The Optimization toolbox from MATLAB is employed to solve this optimization problem (4.16). Table 4.1 shows the objective function value of the optimized compensator for different m.

Table 4.1 The objective function value (4.18) of minimum phase for $m \in \{1,4\}$

m	1	2	3	4
The function value h_{Total}	60.01	37.03	32.39	32.35

Figure 4.2 shows the magnitude response of $\big(1 - G_c(z)F_n(z)\big)Q(z)$, while Figure 4.3 shows the phase compensation $\theta_{G_c(z)F_n(z)}$ for $m \in \{1,4\}$. The figures indicate that the designed compensator fulfills the stability criteria of (4.8), although it does not completely compensate the phase and magnitude of $G_c(z)$. The first order compensator gives a very large objective function value, which results in poor magnitude and phase compensation. The second order compensator is sufficient to compensate both the phase and magnitude. The compensated phase is significantly small at low frequency, but it drops to -90^o at high frequency. For $m \in \{3,4\}$, the compensator gives a slightly better performance compared to $m = 2$.

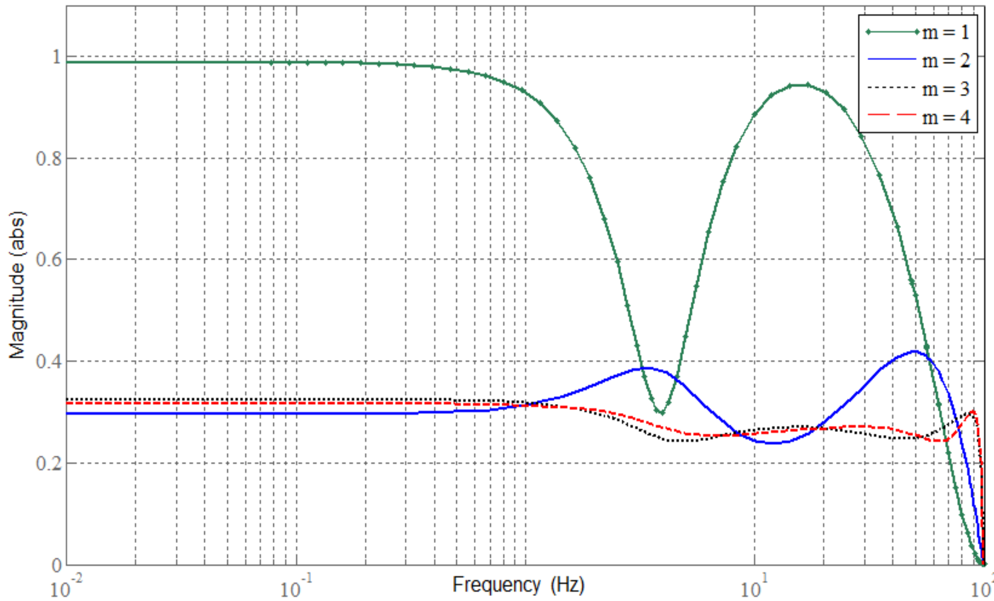

Figure 4.2 Magnitude response of $\left[\left(1 - \mathrm{G_c(z)F_n(z)}\right)\mathrm{Q(z)}\right]$ for the minimum phase system

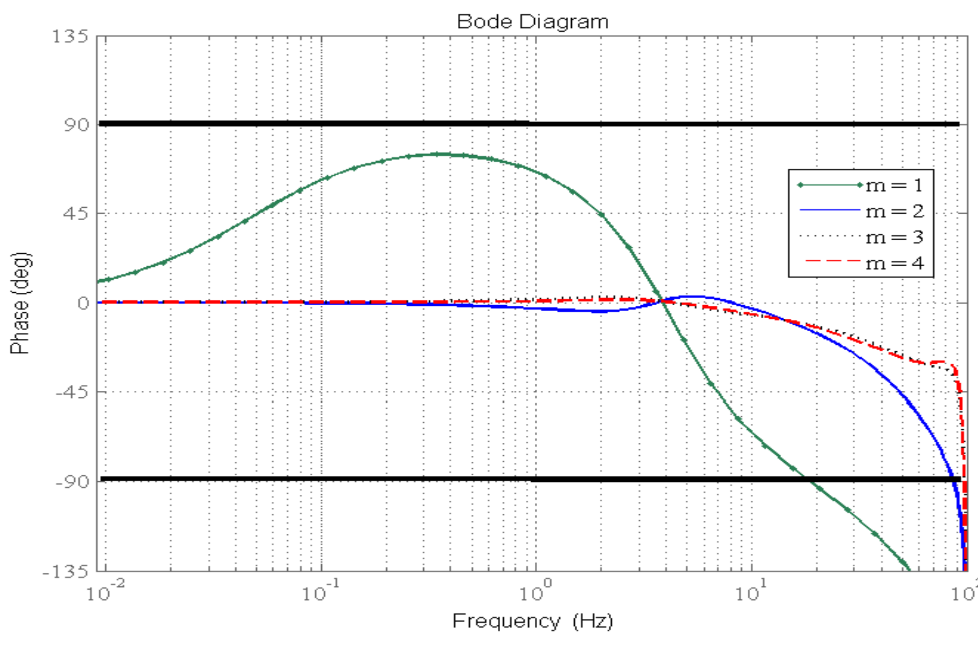

Figure 4.3 Phase response of $\mathrm{G_c(z)F_n(z)}$ for different *m*

The phase plot shown in Figure 4.3 also indicates that the $\mathrm{F_n(z)}$ has a phase lead response to compensate $\mathrm{G_c(z)}$. This basically can be explained from stability condition (4.14). Equation (4.14) can be rewritten as follows:

$$\left[1 - 2M_{T_i} cos(\theta_{T_i}) + M_{T_i}{}^2\right] < \frac{1}{M_{Q_i}{}^2} \tag{4.35}$$

where M_{Q_i} is 1 at low frequencies, and approaches zero at high frequencies.

Therefore, at low frequencies, the stability condition can be rewritten as:

$$\left[1 + M_{T_i}{}^2\right] - 2M_{T_i} cos(\theta_{T_i}) < 1 \tag{4.36}$$

Since $M_{T_i} = M_{F_{ni}} M_{Gc_i}$, is a non-negative value, the phase compensation θ_{T_i} is required to meet the following condition to satisfy the stability condition

$$\left|\theta_{T_i} = \theta_{F_{ni}} + \theta_{Gc_i}\right| < 90^0 \tag{4.37}$$

A stable discrete plant has phase lag characteristics, which means θ_{Gc_i} is negative. To meet the stability phase condition, $\theta_{F_{ni}}$ must be positive, which gives a phase lead compensator.

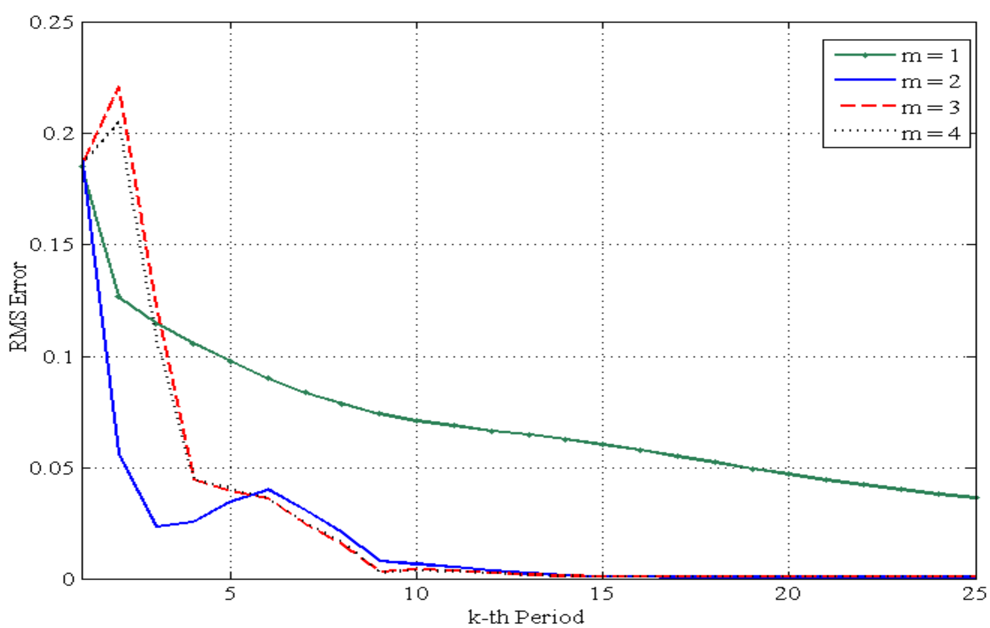

Figure 4.4 RMS errors for different m

The simulated root mean square (RMS) error for $m = 1,2,3,4$ is shown in Figure. 3.4. The reference signal is a triangle waveform with amplitude $\pi/4$ and frequency 0.8 Hz. Figure 4.4 shows that the first order compensator gives a very slow convergence rate and poor tracking accuracy. For $m = 2$, the convergence rate and tracking accuracy are significantly improved in comparison to $m = 1$. Figure 4.4 shows that the tracking error converges to zero after 15 repetitions.

Figures 4.5(a) and (b) show the tracking outputs for $m = 1$ and 2 respectively, where the second order compensator clearly gives a better performance. The tracking performance for $m = 3,4$ does not show a significant difference to the tracking performance for $m = 2$. In this case, $m = 2$ can be chosen as the optimum order of the proposed compensator. The designed compensator $\mathrm{F_n(z)}$ for m = 2 is

$$\mathrm{F_n(z)} = \frac{10^3(1.9228\mathrm{z}^2 - 3.5679\mathrm{z} + 1.6712)}{\mathrm{z}^2 + 1.85\mathrm{z} + 0.8556} \tag{4.38}$$

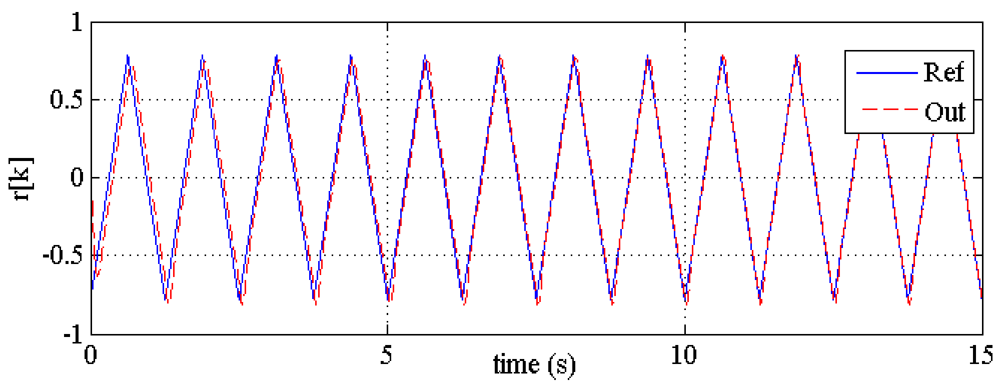

(a)

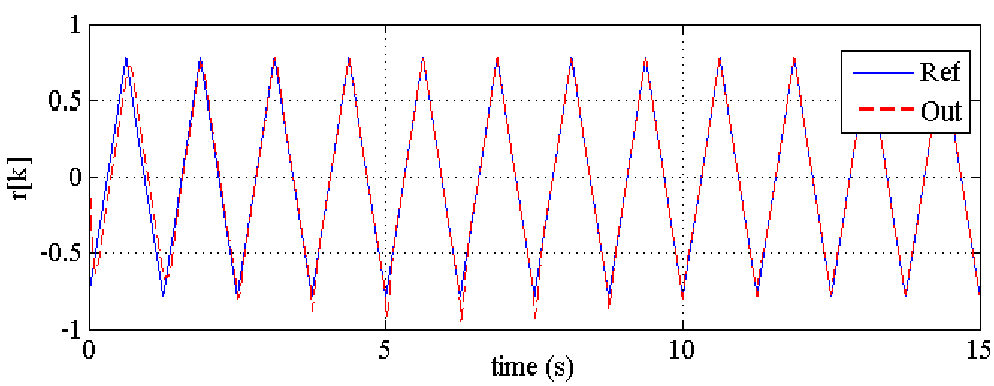

(b)

Figure 4.5 Tracking outputs for (a) m = 1, (b) m = 2

4.5.1.2 Non-Minimum Phase System

Given a third order closed-loop model $\mathrm{G_c(s)}$ as follows:

$$\mathrm{G_c(s)} = \left(\frac{8.8}{s + 8.8}\right)\left(\frac{37^2}{s^2 + 37s + 37^2}\right) \tag{4.39}$$

,which is a dynamic of 7 degrees-of-freedom (DOF) Robotics Research Corporation robot [107, 108].

At $T = 0.005\ s$, the discrete model is obtained as follows:

$$\mathrm{G_c(z)} = \frac{0.2368 \times 10^{-3}(z + 0.2533)(z + 3.519)}{(z - 0.9419)(z^2 - 1.815z + 0.844)} \tag{4.40}$$

Equation (4.40) shows that there is one zero outside the unit circle which makes the discrete model becomes a non- minimum phase system.

Using the same Q-filter, δ, and τ, the objective function value of the optimized compensator for different m is shown in Table 4.2. Table 4.2 indicates that there is no solution for $m = 1$, which means that the first order compensator is not able to compensate the third order non-minimum phase system in order to get a stable system.

Table 4.2 The objective function value (4.18) of non-minimum phase for $m \in \{1,5\}$

m	1	2	3	4	5
The function value $\mathrm{h_{Total}}$	No Solution	61.61	58.96	58.81	58.77

Magnitude response and phase response for this non-minimum system for $m \in \{2,5\}$ are shown in Figure 4.6 and 4.7 respectively. Figures 4.6 and 4.7 show that both magnitude and phase compensation are inferior compared to the minimum phase case. For a non-minimum phase plant (4.39), the discrete model has a maximum phase lag 360°. To compensate, the compensator ideally needs to have a maximum phase lead

360^o. However, this is hard to achieve due to the compensator providing stable poles, and also having the same number of poles and zeros.

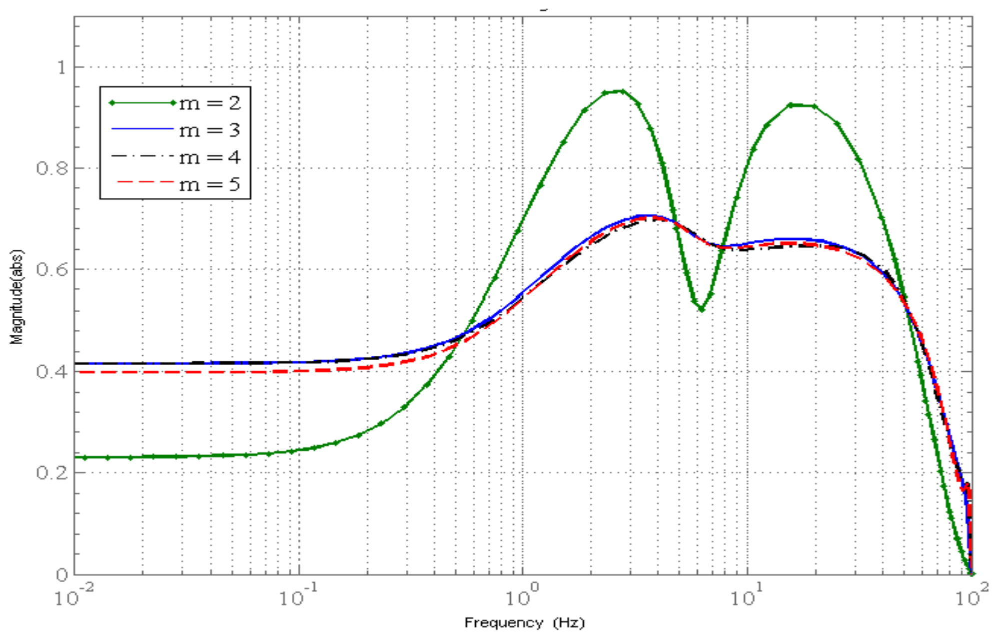

Figure 4.6 Magnitude response of $\left[\left(1 - G_c(z)F_n(z)\right)Q(z)\right]$for a non-minimum phase system

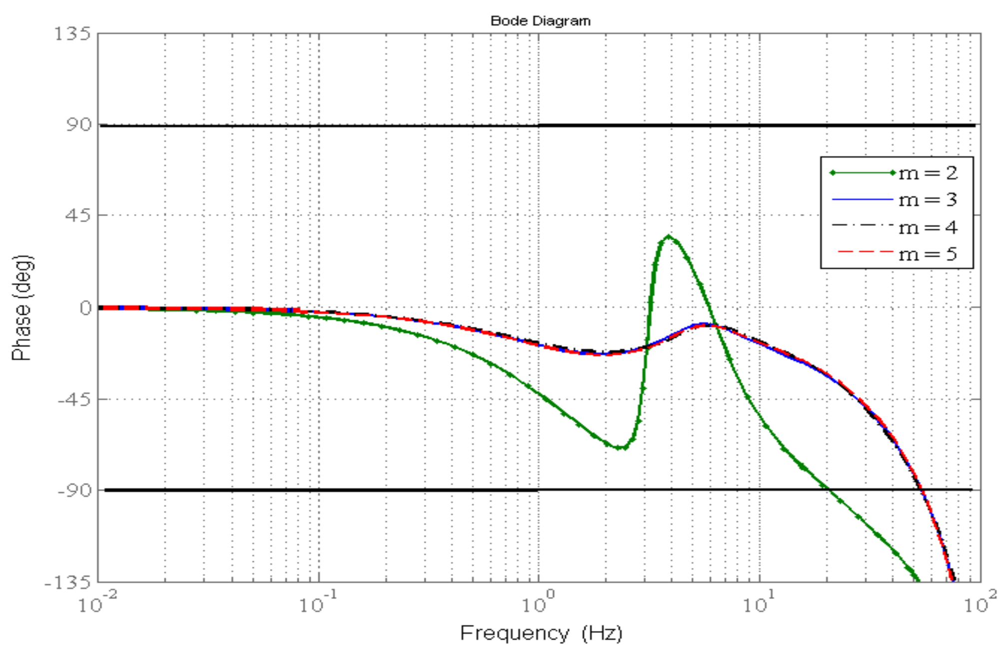

Figure 4.7 Phase response of $G_c(z)F_n(z)$for a non-minimum phase system

The tracking output of a triangle reference signal using the third order compensator is shown in Figure 4.8. Figure 4.8 shows that a good tracking performance can still be achieved for non-minimum phase plant.

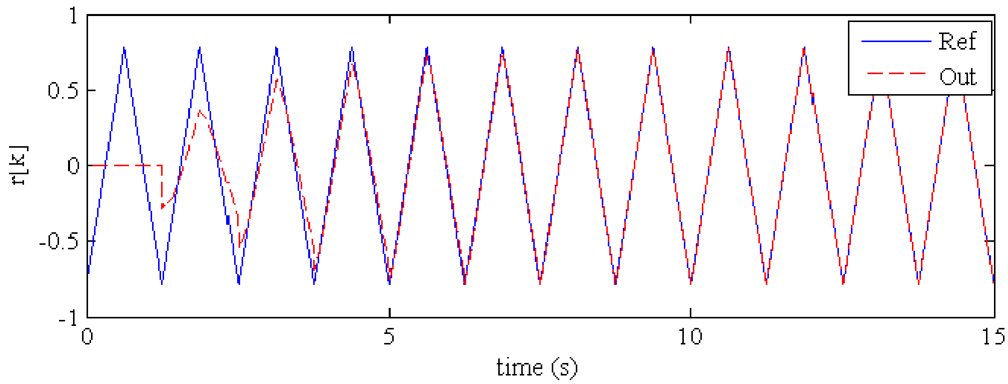

Figure 4.8 Tracking output for $m = 3$

Apart from the simulation for the plant in (4.34) and (4.40) above, the additional simulation results for different systems are given in the table below.

Table 4.3 The objective function value of (4.18) for different systems

System		The function value h_{Total}			
		$m = 1$	$m = 2$	$m = 3$	$m = 4$
n=2,mp	$G_c(z) = \dfrac{0.011(z + 0.932)}{z^2 - 1.789z + 0.8106}$ (a SCARA robot manipulator [109])	60.58	37.27	32.56	32.07
n=2,nmp	$G_c(z) = \dfrac{0.003(z + 3.778)}{z^2 - 1.796z + 0.8106}$	62.57	59.53	59.45	59.26
n=3,mp	$G_c(z) = \dfrac{0.008(z - 0.9715)(z + 0.9397)}{(z - 0.9521)(z^2 - 1.87z + 0.8789)}$ (a servomotor in (4.31) with PI controller)	No Solution	37.51	32.76	32.22

mp = minimum phase, *nmp* = non-minimum phase

This suggests that the controller has the lowest order of $n-1$, where n is the order of the plant, to be able to give the required phase compensation. However, the controller with an order of $m=n$ gives a smaller objective function value, which means better tracking performance. Therefore, the compensator order should be equal or higher than the plant order to give good phase and magnitude compensation.

4.5.1.3 A Comparison Study

A comparison study is given to show the significance of the proposed compensator. The designed compensator $\mathrm{F_n(z)}$ in (4.38) can be presented in a zero-pole format:

$$\mathrm{F_n(z)} = 1922.8\left[\frac{\mathrm{z}-(0.928+0.089\mathrm{i})}{\mathrm{z}+0.925}\right]\left[\frac{\mathrm{z}-(0.928-0.089\mathrm{i})}{\mathrm{z}+0.925}\right] \qquad (4.41)$$

which consists of two stage phase lead compensators. As the proposed compensator has a phase lead characteristic, a comparison study is conducted with the phase lead repetitive controller $\mathrm{k_r z^m}$ [15]. Figure 4.9 shows the phase compensation of phase lead $\mathrm{k_r z^m}$. At a low frequency range [0.1,10] Hz, the compensated phase for $\mathrm{m}=2,3,4$ shown in Figure 4.3 is significantly small, very close to 0^0, compared to the compensated phase shown in Figure 4.9.

The frequency ranges inside the boundary $[-90^0,+90^0]$ as shown in Figure. 4.9 are also limited. In contrast, the proposed compensator gives a greatly wider frequency range as the compensated phases are still inside the stable range $[-90^0,+90^0]$ for almost all frequency components. Therefore, the proposed design provides a much better phase compensation, that results in a better tracking performance as shown in Figure 4.10.

For comparison, the $\mathrm{k_r z^m}$ compensator [15] is also simulated with $\mathrm{k_r}=2, m=4$. The value of m is chosen to give the largest stable bandwidth, while the gain $\mathrm{k_r}$ is chosen for fast convergence, and determined according to the design criterion as follows [15, 109]:

$$k_r M_{Gc}(\omega) < 2\cos(\theta_{Gc}(\omega) + m\omega) \tag{4.42}$$

where $M_{Gc}(\omega)$ and $\theta_{Gc}(\omega)$are the magnitude and the phase of $Gc(z)$, m is the chosen lead time

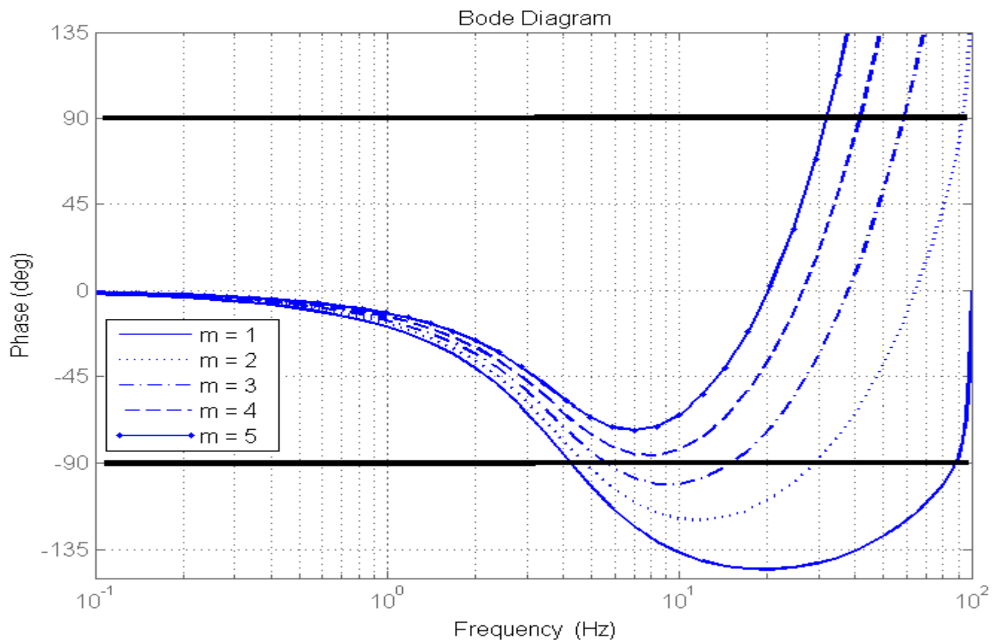

Figure 4.9 Phase response of $z^m G_c(z)$ for different m

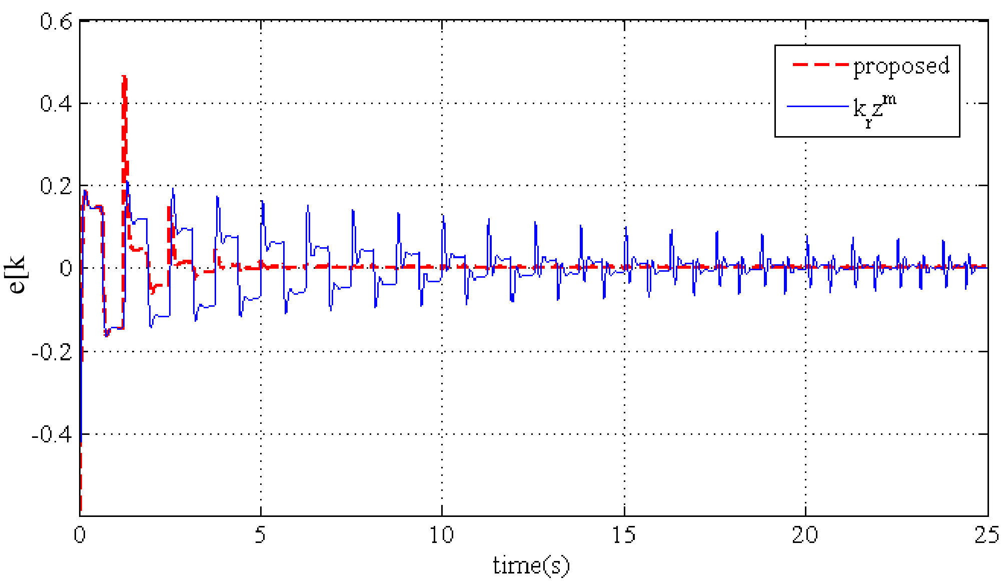

Figure 4.10 The tracking errors for the proposed (4.38) and phase lead $k_r z^m$ compensators

4.5.2 SIMULATION OF ROBUST RC COMPENSATOR

Suppose that the RC compensator is designed at the nominal sampling period $T_n = 0.005$ s as shown in (4.38)

A robust RC compensator is now designed to achieve a stable system when the sampling period varies in the range $T \in [0.0025, 0.0085]$s. The closed-loop transfer functions $G_c(z)$ at the lowest and highest sampling period are obtained as follows:

$$G_{cl}(z) = \frac{10^{-3}(0.1967z + 0.1907)}{z^2 - 1.9090z + 0.9128} \tag{4.43}$$

$$G_{cu}(z) = \frac{10^{-3}(0.2116z + 0.1904)}{z^2 - 1.7070z + 0.7472} \tag{4.44}$$

The chosen Q-filter, constant δ and τ are $Q(z) = 0.25z^{-1} + 0.5 + 0.25z$, 0.075 and 0.1 respectively. The robust compensator $F_r(z)$ can be obtained by solving the optimization problem (4.30).

$$F_r(z) = \frac{10^3(0.8022z^2 - 1.4423z + 0.6438)}{z^2 + 1.85z + 0.8556} \tag{4.45}$$

Let the nominal compensator at the lowest and highest sampling period be $F_{nl}(z)$ and $F_{nu}(z)$ respectively, that are obtained from the optimization (4.18):

$$F_{nl}(z) = \frac{10^4(0.7260z^2 - 1.3992z + 0.6755)}{z^2 + 1.85z + 0.8556} \tag{4.46}$$

$$F_{nu}(z) = \frac{10^3(0.7177z^2 - 1.2617z + 0.5711)}{z^2 + 1.85z + 0.8556} \tag{4.47}$$

The stability analysis of the designed RC systems is shown in Table 4.4. Column (1) indicates that all the eigenvalues of A_d are changing linearly with T. Column (2) shows how the compensated system meets the stability condition, where the nominal compensator $\mathrm{F_{nl}}(\mathrm{z})$ is stable in the lower sampling range $[0.0025, 0.003]$, $\mathrm{F_{nu}}(\mathrm{z})$ is stable in the high sampling range $[0.005, 0.0085]$, and $\mathrm{F_r}(\mathrm{z})$ is stable for the whole sampling range $[0.0025, 0.0085]$.

Table 4.4 Stability analysis for three compensators: $\mathrm{F_{nl}}(\mathrm{z})$, $\mathrm{F_{nu}}(\mathrm{z})$, and $\mathrm{F_r}(\mathrm{z})$

$T(s)$	**Stability Assessment**						
	(1). $\max\left\lvert \begin{matrix} Eig \\ of\ Ad \end{matrix} \right\rvert$	(2). $\left\lVert \left(1 - G_c(z)F(z)\right)Q(z) \right\rVert_\infty < 1 - \tau$					
		$\mathrm{F_{nl}}(\mathrm{z})$		$\mathrm{F_{nu}}(\mathrm{z})$		$\mathrm{F_r}(\mathrm{z})$	
0.0025	0.955	0.426	Stable	1.034	Unstable	0.899	Stable
0.003	0.947	0.573	Stable	0.989	Stable (very slow convergence)	0.838	Stable
0.004	0.931	1.117	Unstable	0.904	Stable (slow convergence)	0.716	Stable
0.005	0.915	2.017	Unstable	0.799	Stable	0.655	Stable
0.006	0.899	3.322	Unstable	0.676	Stable	0.656	Stable
0.007	0.885	4.848	Unstable	0.540	Stable	0.700	Stable
0.008	0.871	6.599	Unstable	0.416	Stable	0.808	Stable
0.0085	0.864	7.558	Unstable	0.409	Stable	0.899	Stable
Stable sampling period range		$[0.0025, 0.003]$		$[0.005, 0.0085]$		$[0.0025, 0.0085]$	

The simulated tracking errors for the three different compensators at $\mathrm{T} = 0.0025\ \mathrm{s}$, $\mathrm{T} = 0.005\ \mathrm{s}$ and $\mathrm{T} = 0.0085\ \mathrm{s}$ are shown in Figure 4.11, 4.12 and 4.13 respectively. The reference signal is a triangle waveform with amplitude $\pi/4$ and frequency 0.8 Hz. Figures 4.12(a) and 4.13(a) show that tracking errors using $\mathrm{F_{nl}}(\mathrm{z})$ become unstable at higher sampling period, while Figure 4.11(b) indicates that the tracking error when using $\mathrm{F_{nu}}(\mathrm{z})$ diverges at low sampling period. The tracking errors shown in Figure 4.11-13 (c) validate that the robust compensator is stable and works on the given sampling period range.

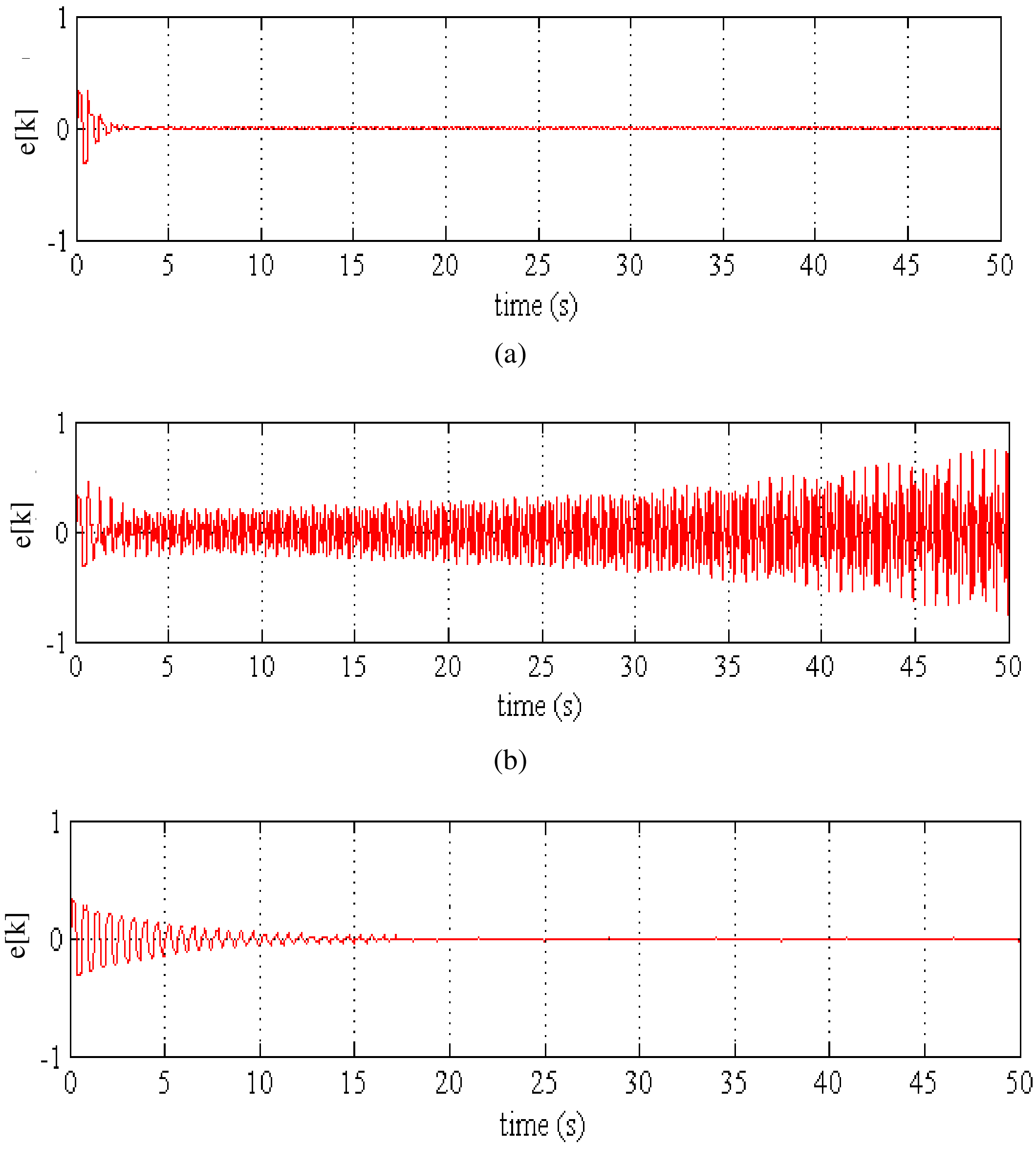

Figure 4.11 Tracking errors using three different RC compensators at $T = 0.0025$ s, (a) $F_{nl}(z)$, (b) $F_{nu}(z)$, and (c) $F_{r}(z)$

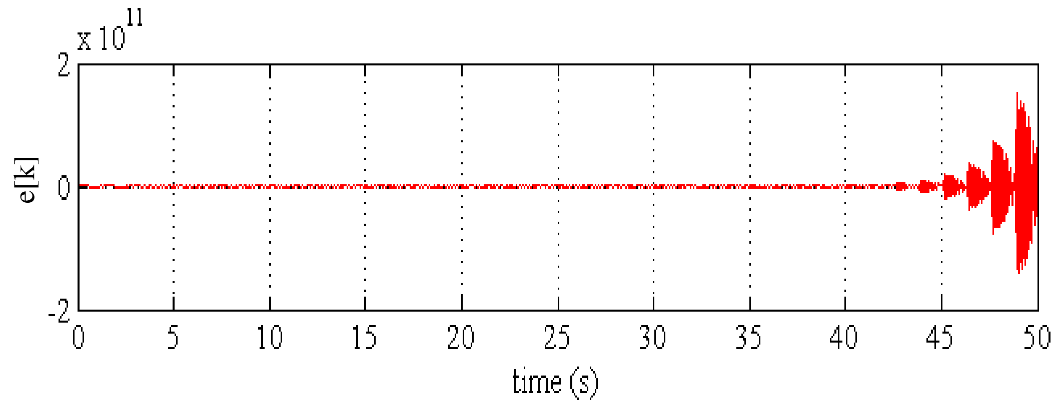

(a)

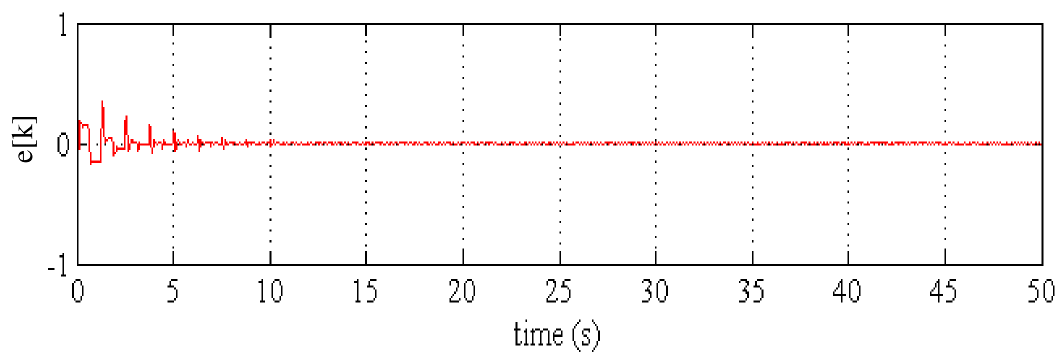

(b)

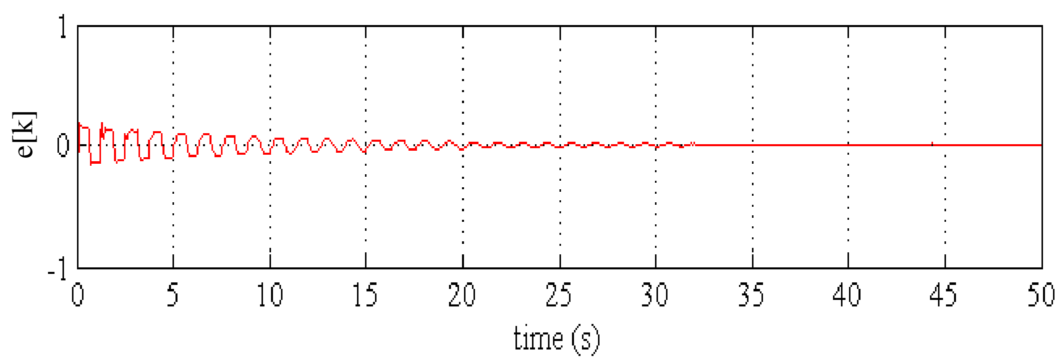

(c)

Figure 4.12 Tracking errors using three different RC compensators at $T = 0.005$ s, (a) $F_{nl}(z)$, (b) $F_{nu}(z)$, and (c) $F_r(z)$

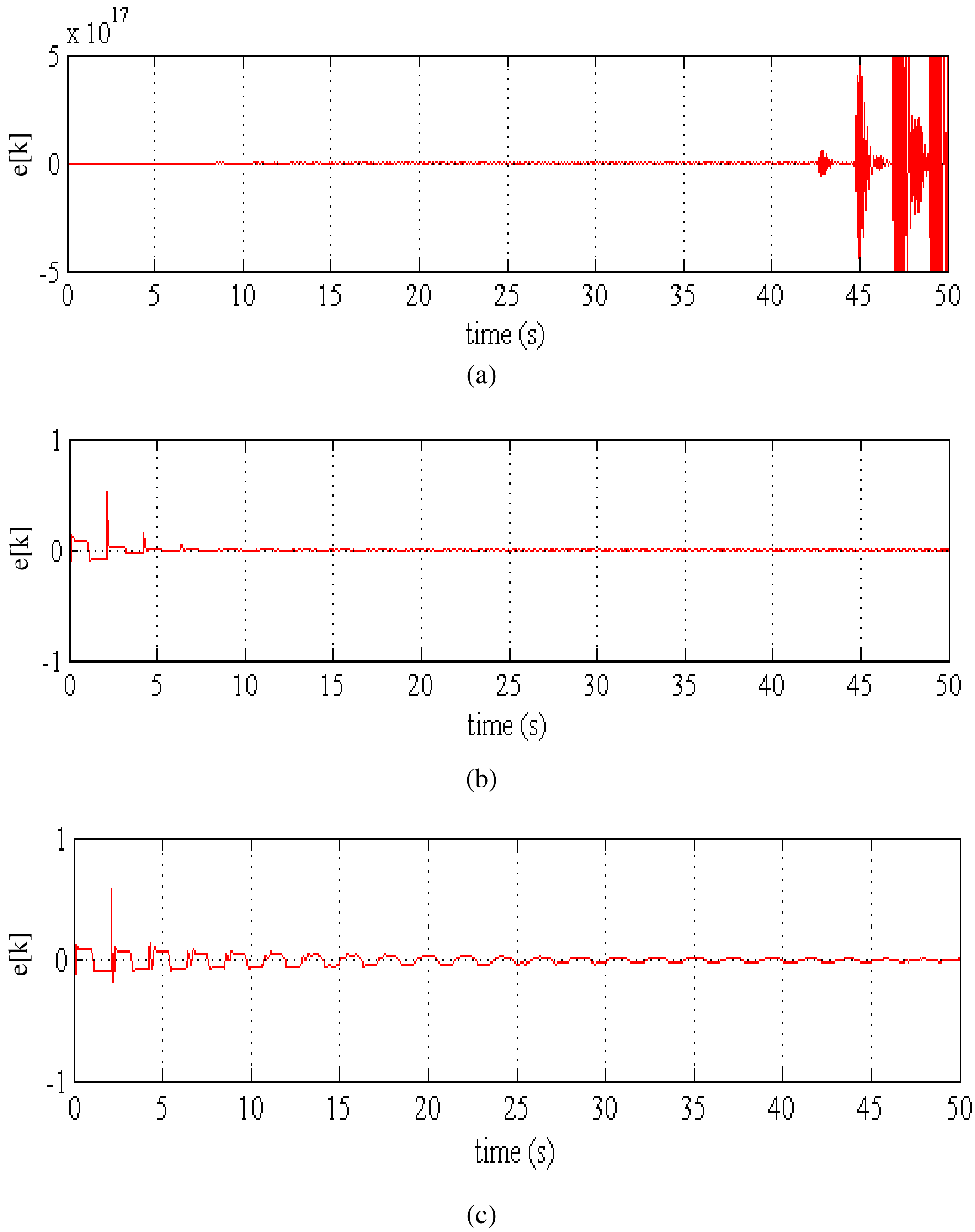

Figure 4.13 Tracking errors using three different RC compensators at $T = 0.0085$ s, (a) $F_{nl}(z)$, (b) $F_{nu}(z)$, and (c) $F_r(z)$

4.6 EXPERIMENTAL RESULTS

The real-time experiments were conducted to verify the effectiveness of the proposed design. The experiment aimed to control the angle position of the Quanser servomotor SRV02-E with no load, to exactly track the reference signal with amplitude $\pi/4$ rad (45 degrees).

4.6.1 EXPERIMENT OF NEW RC COMPENSATOR

The tracking performance for a triangle reference signal was tested. The proposed compensator in (4.38) was used. The tracking output and the tracking error of the system is shown in Figure 4.14(a) and Figure 4.14(c) respectively. For comparison, the $k_r z^m$ compensator [15] was also implemented with $k_r = 2, m = 4$. The tracking output and error are shown in Figure 4.14(b) and Figure 4.14 (c) respectively. Figure 4.14(c) indicates that the proposed compensator has a superior convergence rate.

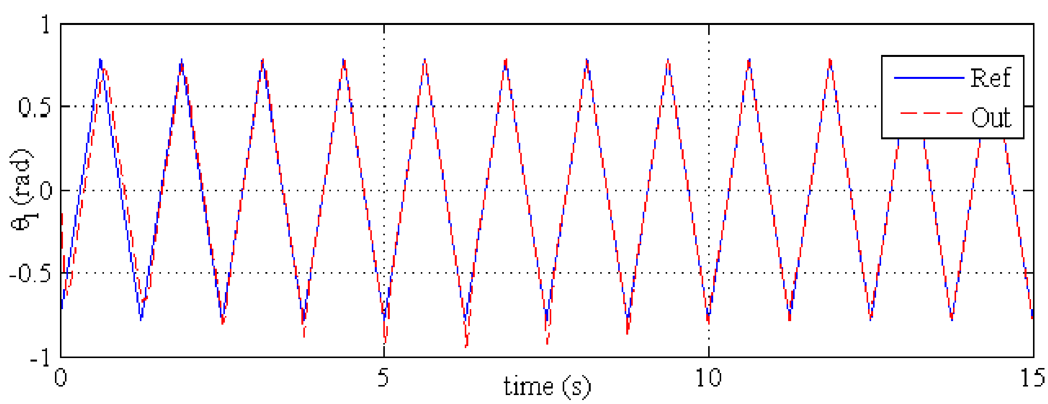

(a)

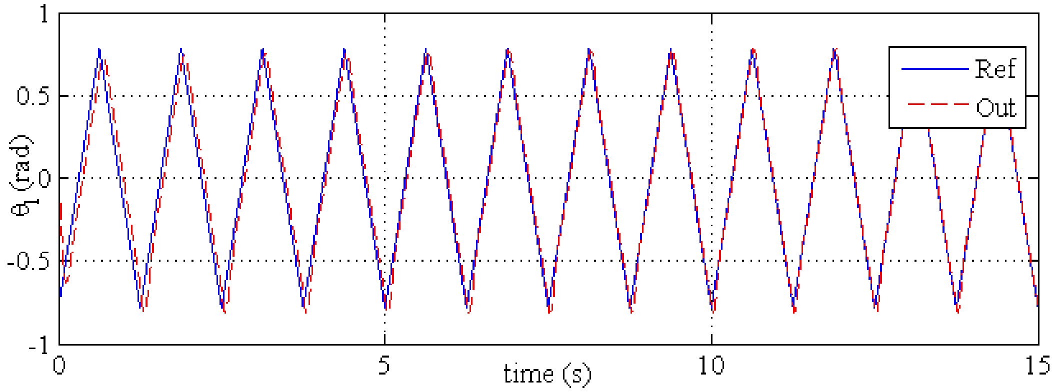

(b)

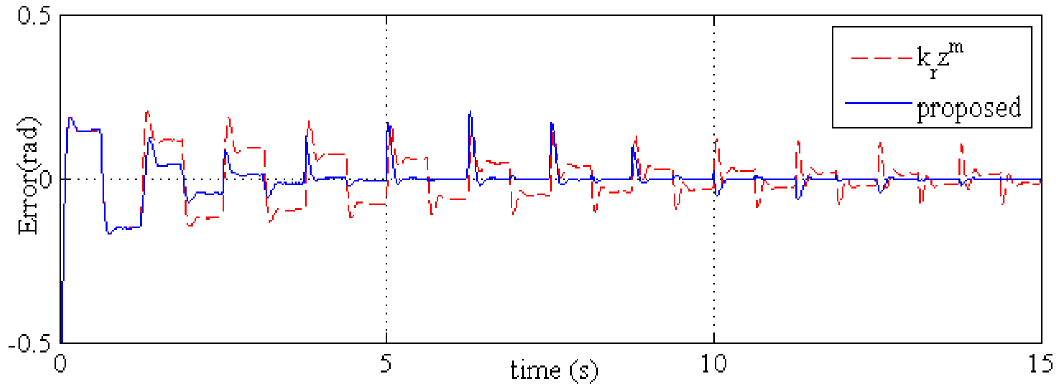

(c)

Figure 4.14 Tracking output and errors, (a) the proposed compensator, (b) the compensator $k_r z^m$, (c) the tracking errors for both compensators

4.6.2 Experiment of Robust RC Compensator

Given the triangle reference signal with amplitude $\pi/4$ rad (45 degrees), the tracking performance of the compensated RC system using robust compensator $F_r(z)$ in (4.45) at $T = 0.0025$ s, $T = 0.005$ s and $T = 0.0085$ s is shown in Figures 4.15, 4.16 and 4.17 respectively.

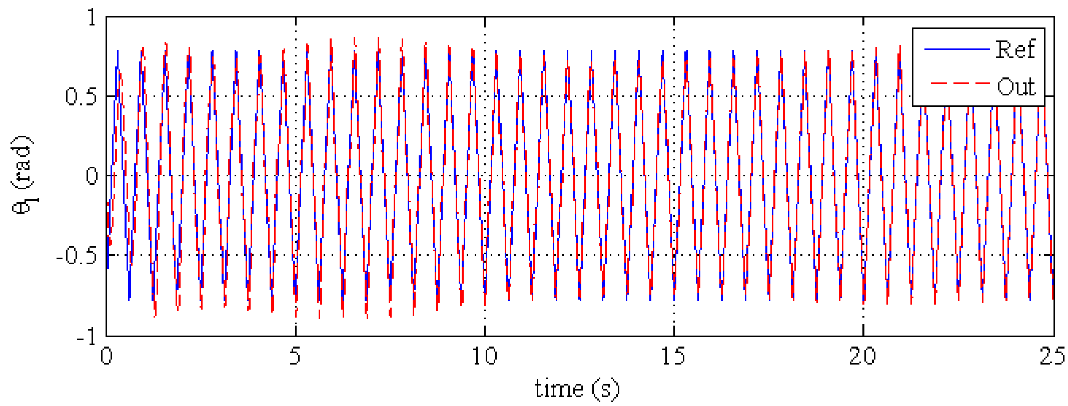

(a)

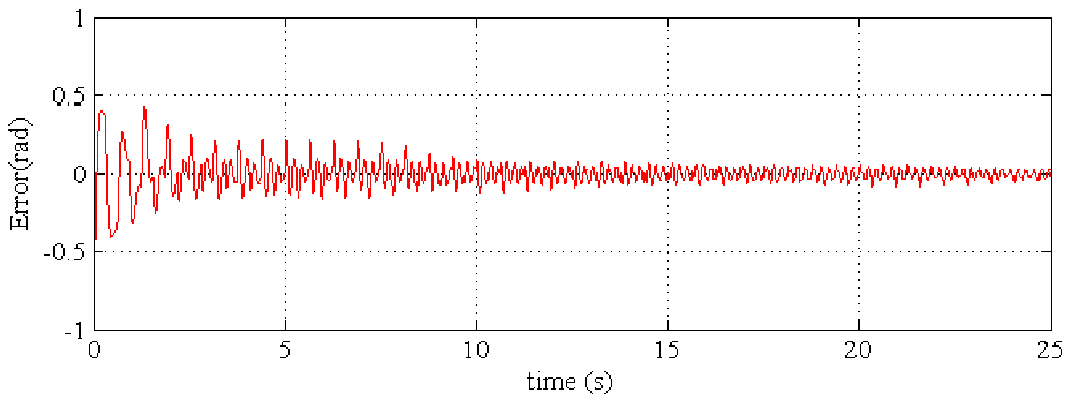

(b)

Figure 4.15 Tracking performance at T = 0.0025s, (a) tracking output,

(b) tracking error

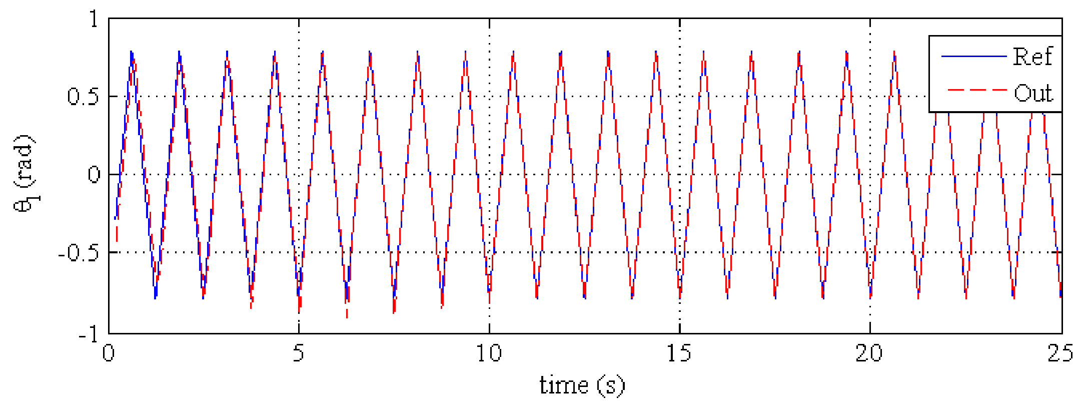

(a)

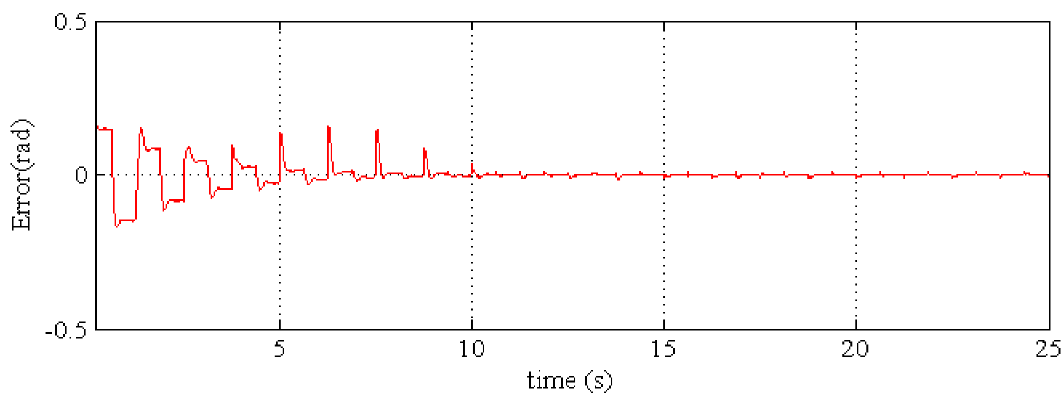

(b)

Figure 4.16 Tracking performance at T = 0.005s, (a) tracking output, (b) tracking error

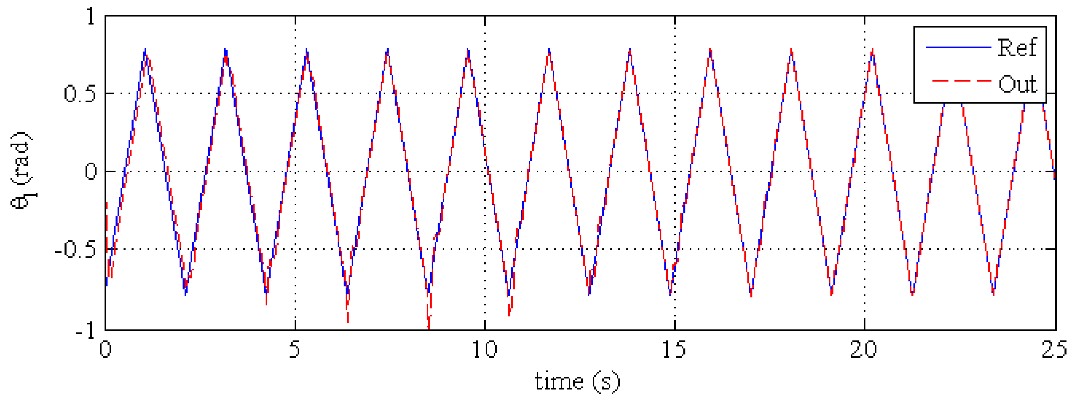

(a)

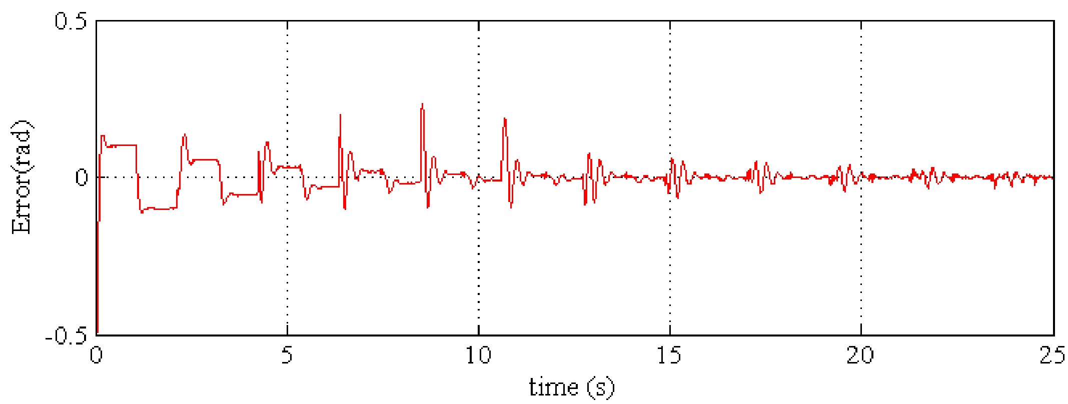

(b)

Figure 4.17 Tracking performance at T = 0.0085s, (a) tracking output, (b) tracking error

Figure 4.15 and Figure 4.17 show that the compensated system is stable at the lowest and highest sampling period. The above experimental results verify the effectiveness of the proposed robust compensator.

4.7 SUMMARY

This chapter has proposed two main ideas; a new design of RC compensator, and a robust RC design that works under a time-varying sampling period.

Firstly, an optimization problem based on the RC stability condition was formulated to obtain a low order, stable, and causal RC compensator. Since the compensator has a causal form, it was implemented independently without being merged to the IMP. This reduces the design complexity, as most existing repetitive compensators are either non-causal or unstable, which makes the implementation difficult. The design has worked for both minimum and non-minimum phase plant, where fast convergence and high tracking accuracy have been achieved. The compensator order should be equal or higher than the plant order to give good phase and magnitude compensation. The proposed compensator has been verified by simulation and real-time experiments, and shows better performance compared to the lead compensator as proposed by Zhang et al [15]. The proposed compensator here becomes a nominal compensator in the robust design.

A robust RC compensator closest to the nominal one was then designed to achieve a stable system when the sampling period varied in a defined range. The optimization problem in a robust design has more constraints compared to that in the nominal compensator design. These extra constraints are needed to examine the RC stability condition at the lowest and highest sampling period. Both simulation and experimental results have shown the effectiveness of the proposed robust design.

CHAPTER 5

DESIGN OF ADAPTIVE RC OF LINEAR SYSTEMS WITH TIME-VARYING PERIODIC DISTURBANCES

5.1 INTRODUCTION

A Robust RC design to deal with time-varying reference signal was discussed in Chapter 4. In this chapter, the problem of rejecting a class of time-varying periodic disturbances is addressed. As mentioned in Chapter 2, the discrete–time RC is usually designed by assuming a constant period of disturbance, which leads to the selection of a fixed sampling period. In practice, disturbance can be time-varying in period. If the sampling period is kept fixed while the period of disturbance changes, then the RC performance will significantly decay [24]. Cao and Narasimhulu [27] proposed a digital PLL-based RC, where the sampling period is locked to the period of the reference/disturbance signal to maintain a constant number of samples per period, which is required by RC. This sampling period adjustment results in a plant with time-varying coefficients, especially when the disturbance has a time varying period. By considering the direct adaptive control, it is possible to adapt the parameters of the controller to handle the time varying plant.

In this chapter, the design of an Adaptive RC (ARC) for unknown linear systems subject to time varying periodic disturbances is presented. It is also assumed that the sampling period will be locked to the period of disturbance signal to preserve a constant number of samples per disturbance period, as required by the RC. This ARC is proposed, based on direct adaptive control and the internal model principle. The internal model can reject the disturbance exactly, since the number of samples per period remains fixed. The time-varying plant parameters are handled by the direct adaptive control, as it tunes the controller parameters such that the closed-loop system is stable and the plant output tracks the reference.

The algorithm known as a Model Reference Repetitive Control (MRRC) is first proposed. The MRRC is designed for known plant subject to periodic disturbance with fixed frequency, where the MRRC becomes the foundation of the design of the Adaptive Repetitive Control (ARC). A digital design of ARC is then presented. A comparative study has been conducted, and the effectiveness of the ARC has been verified in simulations and experiments on a servo motor system.

This chapter is organized as follows. Section 2 presents the design of the MRRC, which simultaneously tracks the reference signal and rejects the periodic disturbance with fixed frequency. The matching equation, which obtains true controller parameters, and the stability proofing of the structure are discussed here. Section 3 proposes an ARC design to reject periodic disturbances with time-varying frequency, in which it also covers the stability analysis of the ARC. Simulation and experimental results are in Section 4 and 5 respectively. A comparison study is also given in Section 4. Section 6 summarizes the chapter.

5.2 MODEL REFERENCE REPETITIVE CONTROL (MRRC)

The MRRC algorithm is the foundation of the design of ARC in Section 5.3. Therefore, it is presented before the ARC. In MRRC, the plant is known and the disturbance frequency is fixed. The controller parameters are designed offline based on the known information of the plant and disturbance. The MRRC is designed to obtain a control law for the known plant $\mathrm{G(z)}$subject to fixed-period disturbance $d(k)$such that the closed-loop signals are stable and the plant output $\mathrm{y_p(k)}$ tracks the reference model output $\mathrm{y_m(k)}$. The structure of MRRC is shown in Figure 5.1, in which it consists of two parts of controller; Model Reference Control (MRC) and Repetitive Control (RC).

The plant output $y_p(k)$ is expressed in this following form:

$$y_p(k) = G(z)u_p(k) + d(k) \tag{5.1}$$

where

$$G(z) = k_p \frac{B(z)}{A(z)} \tag{5.2}$$

Let write $y_i(k)$ as the ideal plant output, is the output when the disturbance is not exist.

$$y_i(k) = G(z)u_p(k) \tag{5.3}$$

The reference model output $y_m(k)$ is generated from LTI model as follows:

$$y_m(k) = W_m(z)r(k) \tag{5.4}$$

where

$$W_m(z) = k_m \frac{N_m(z)}{D_m(z)} \tag{5.5}$$

Several assumptions are made to design MRRC control scheme here.

(A.1) $G(z)$ is minimum phase plant. $B(z)$, $A(z)$ are co-prime Monic Hurwitz polynomials.

(A.2) The degree of $A(z)$ is known. Let $\deg[A(z)] = n$.

(A.3) The sign of k_p is known

(A.4) The degree of $D_m(z)$ is less than the degree of $A(z)$.

$$\deg[D_m(z)] = m < \deg[A(z)] = n \tag{5.6}$$

(A.5) The relative degree $n^* = n - m$ is known

(A.6) The relative degree of the plant is equal to the relative degree of reference model

$$\deg[D_m(z)] - \deg[N_m(z)] = \deg[A(z)] - \deg[B(z)] \tag{5.7}$$

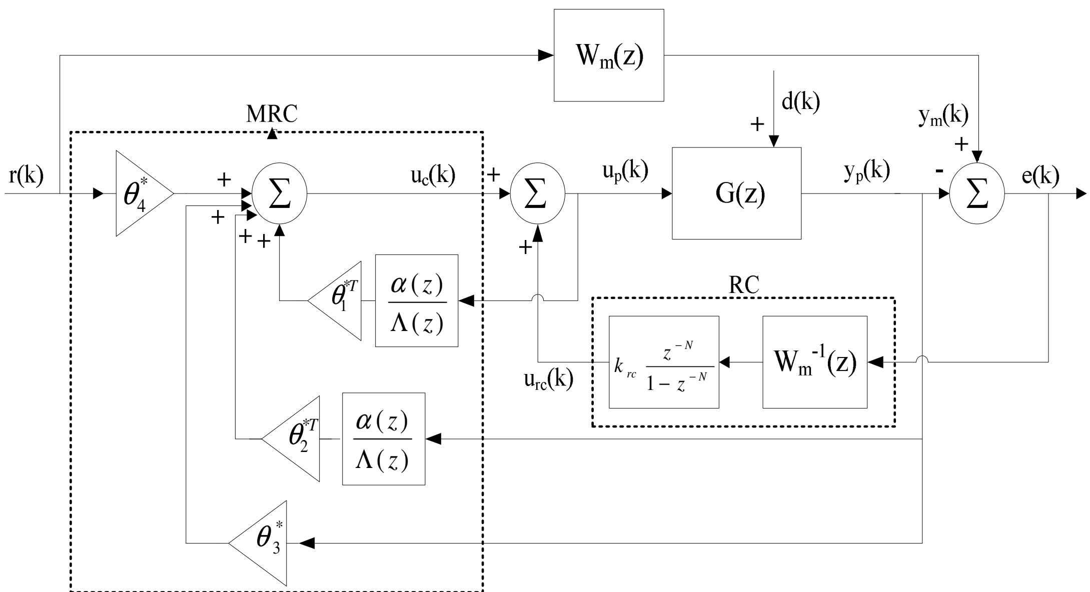

Figure 5.1 Block diagram of Model Reference Repetitive Control (MRRC)

Supposed $u_c(k)$ is the control law generated from MRC part:

$$u_c(k) = \theta_1^{*T} \frac{\alpha(z)}{\Lambda(z)} u_p(k) + \theta_2^{*T} \frac{\alpha(z)}{\Lambda(z)} y_p(k) + \theta_3^* y_p(k) + \theta_4^* r(k) \tag{5.8}$$

where

$$\alpha(z) = [z^{n-2}, z^{n-3}, z, 1]^T \quad \text{for } n \geq 2$$
$$\alpha(z) = 0 \qquad\qquad \text{for } n = 0 \tag{5.9}$$

$$\theta_1^*, \theta_2^* \in \mathcal{R}^{n-1}; \theta_3^*, \theta_4^* \in \mathcal{R}^1;\ \theta^* = [\theta_1^*, \theta_2^*, \theta_3^*, \theta_4^*]^T \tag{5.10}$$

$\Lambda(z)$ is monic hurwitz polynomial of degree $n-1$

$\theta^*$is a controller parameter vector to be designed so that the transfer function from $r(k)$ to $y_p(k)$ with no RC and disturbance, also meaning the transfer function from $r(k)$ to $y_i(k)$, is equal to $W_m(z)$. The controller parameters $\theta_1^*, \theta_2^*, \theta_3^*, \theta_4^*$ are chosen to satisfy the following transfer function matching:

$$\frac{G(z)\theta_4^*}{[1-\theta_1^{*T}\frac{\alpha(z)}{\Lambda(z)}-\theta_2^{*T}\frac{\alpha(z)G(z)}{\Lambda(z)}-\theta_3^*G(z)]} = W_m(z) \tag{5.11}$$

Choosing $\theta_4^* = \frac{k_m}{k_p}$, and $\Lambda(z) = \Lambda_0(z)N_m(z)$, the matching equation (5.11) becomes:

$$\begin{aligned}\left[\theta_1^*\alpha(z)A(z) + k_p\theta_2^*\alpha(z)B(z) + k_p\theta_3^*\Lambda(z)B(z)\right] = \\ \Lambda(z)A(z) - \Lambda_0(z)B(z)D_m(z)\end{aligned} \tag{5.12}$$

where $\Lambda_0(z)$is monic hurwitz polynomial of degree n_Λ, and $n_\Lambda = n-1-\deg[N_m(z)]$

The parameters θ_1^*, θ_2^*, and θ_3^* are the solution from the matching equation (5.12). As the plant parameters are known, the true parameter vector θ^* can be calculated directly.

The control law generated from the RC is given by

$$u_{rc}(k) = C_{rc}(z)e(k) \tag{5.13}$$

where $e(k)$ is the tracking error defined by

$$e(k) = y_m(k) - y_p(k) \tag{5.14}$$

, and $C_{rc}(z)$ is the digital RC.

The proposed digital RC has the following form:

$$C_{rc}(z) = I(z)F(z) = \left(\frac{\mathrm{z}^{-\mathrm{N}}}{1-\mathrm{z}^{-\mathrm{N}}}\right)\left(k_{rc}{W_m}^{-1}(z)\right) \tag{5.15}$$

where

$$N = \frac{T_d}{T} \in \mathbb{N} \tag{5.16}$$

with N being the number of samples per disturbance period, T_d being the disturbance period,T the sampling period, and k_{rc} is a RC gain.

The digital RC above consists of the internal model $I(z)$ and compensator $F(z)$. The internal model $I(z)$ behaves as generator of periodic signal which cancels the disturbance frequency and its harmonics, while compensator$F(z)$works to cancel the dynamic of reference model. The reference model is strictly proper that makes the compensator $F(z)$ improper. However, this compensator $F(z)$ is still realizable as it is merged with the internal model which has relative degree N. Therefore, this discrete-time RC is guaranteed to be in proper form.

The total control law coming to the plant is $u_p(k)$

$$u_p(k) = u_c(k) + u_{rc}(k) \tag{5.17}$$

The control law in (5.17) ensures that the tracking error (5.14) is $e(k) \in L^2$, which decays to zero in the finite k.

5.2.1 Stability Analysis of MRRC

In this section, we firstly derive the tracking error dynamic of MRRC. Then, stability proofing is presented.

Applying control law $u_p(k)$ to the plant $G(z)$ gives the plant output $y_p(k)$ as follows:

$$y_p(k) = G(z)\{\theta_1^{*T}\frac{\alpha(z)}{\Lambda(z)}u_p(k) + \theta_2^{*T}\frac{\alpha(z)}{\Lambda(z)}y_p(k) + \theta_3^{*}y_p(k) + \theta_4^{*}r(k) \\ +C_{rc}(z)e(k)\} + d(k) \tag{5.18}$$

Equation (5.1) can be rewritten as

$$\mathrm{u_p(k)} = \frac{1}{\mathrm{G(z)}}\left[\mathrm{y_p(k) - d(k)}\right] \tag{5.19}$$

Substituting (5.19) to (5.18) we obtain:

$$y_p(k) = G(z)\{\theta_1^{*T}\frac{\alpha(z)}{\Lambda(z)\mathrm{G(z)}}\left[\mathrm{y_p(k) - d(k)}\right] + \theta_2^{*T}\frac{\alpha(z)}{\Lambda(z)}y_p(k) + \theta_3^{*}y_p(k) \\ +\theta_4^{*}r(k) + C_{rc}(z)e(k)\}d(k) \tag{5.20}$$

Rearranging (5.20), thus we obtain:

$$y_p(k) = \frac{G(z)\theta_4^*}{\left[1 - \theta_1^{*T}\frac{\alpha(z)}{\Lambda(z)} - \theta_2^{*T}\frac{\alpha(z)G(z)}{\Lambda(z)} - \theta_3^{*}G(z)\right]}r(k) + \\ \frac{G(z)C_{rc}(z)}{\left[1 - \theta_1^{*T}\frac{\alpha(z)}{\Lambda(z)} - \theta_2^{*T}\frac{\alpha(z)G(z)}{\Lambda(z)} - \theta_3^{*}G(z)\right]}e(k) - \tag{5.21}$$

$$\frac{1}{\left[1-\theta_1^{*T}\frac{\alpha(z)}{\Lambda(z)}-\theta_2^{*T}\frac{\alpha(z)G(z)}{\Lambda(z)}-\theta_3^{*}G(z)\right]}\left[\theta_1^{*T}\frac{\alpha(z)}{\Lambda(z)}+1\right]d(k)$$

Substituting (5.11) to (5.21), we have:

$$y_p(k)=W_m(z)\,r(k)-\frac{k_{rc}}{\theta_4^*}\frac{\mathrm{z}^{-\mathrm{N}}}{1-\mathrm{z}^{-\mathrm{N}}}e(k)+\frac{W_m(z)}{G(z)\theta_4^*}\left[\theta_1^{*T}\frac{\alpha(z)}{\Lambda(z)}+1\right]d(k) \qquad (5.22)$$

Denote $\psi(z)$ is equal to

$$\psi(z)=\frac{A(z)W_m(z)}{k_pB(z)\theta_4^*}\left[\theta_1^{*T}\frac{\alpha(z)}{\Lambda(z)}+1\right] \qquad (5.23)$$

The facts that $B(z), A(z)$ are co-prime and both $B(z)$ and $\Lambda(z)$ are monic hurwitz polynomials, ensure that $\psi(z)$ is a stable transfer function. In addition, Assumption (A.6) guarantees the properness of $\psi(z)$. Equation (5.21) shows that the plant output is a function of three different input signals; $r(k)$, $e(k)$, and $d(k)$. Each signal is filtered by a stable LTI system. Thus, if $r(k)$, $e(k)$, and $d(k)$ are bounded signals, then $y_p(k)$ will be a bounded signal.

Let write $d_1(k)$ as the filtered $d(k)$, where the periodic property of $d(k)$ appears on $d_1(k)$, but the magnitude and phase of $d(k)$may change.

$$d_1(k)=\psi(z)d(k) \qquad (5.24)$$

Substituting (5.22) - (5.23) to (5.14) and using $\theta_4^*=\frac{k_m}{k_p}$, the error dynamic $e(k)$ can be formulated as follows:

$$e(k)=d_1(k)-K\frac{\mathrm{z}^{-\mathrm{N}}}{1-\mathrm{z}^{-\mathrm{N}}}e(k) \qquad (5.25)$$

where

$$K = \frac{k_p k_{rc}}{k_m} \tag{5.26}$$

Denote $\hat{d}_1(k)$ is equal to

$$\hat{d}_1(k) = K \frac{\mathrm{z}^{-\mathrm{N}}}{1 - \mathrm{z}^{-\mathrm{N}}} e(k) \tag{5.27}$$

Thus, (5.25) can be rewritten as

$$e(k) = d_1(k) - \hat{d}_1(k) \tag{5.28}$$

Signal $\hat{d}_1(k)$ can be viewed as the estimation of $d_1(k)$ which has an updating rule as follows:

$$\hat{d}_1(k) = \hat{d}_1(k - N) + Ke(k - N) \tag{5.29}$$

Based on the error dynamic (5.25), we can prove the system stability.

Theorem 5.1: The control law in (5.17) ensures that the tracking error of MRRC structure shown in Figure 5.1 is $e(k) \in L^2$ which converges to zero in the finite time k

Proof:
Given a positive definite function $V\big(e(k)\big)$

$$V\big(e(k)\big) = \frac{1}{2K} \sum_{\tau = k - N}^{k-1} e^2(\tau) \tag{5.30}$$

The time increment of $V\big(e(k)\big)$ is

$$V\big(e(k+1)\big) - V\big(e(k)\big) = \frac{1}{2K}\sum_{\tau=k-N+1}^{k} e^2(\tau) - \frac{1}{2K}\sum_{\tau=k-N}^{k-1} e^2(\tau) \tag{5.31}$$

$$= \frac{1}{2K}\left\{\left[d_1(k) - \hat{d}_1(k)\right]^2 - \left[d_1(k-N) - \hat{d}_1(k-N)\right]^2\right\} \tag{5.32}$$

Applying two important properties;

1. $d(k) = d(k-N) \rightarrow\ d_1(k) = d_1(k-N)$
2. $\hat{d}_1(k) - \hat{d}_1(k-N) = Ke(k-N)$

Equation (5.32) can be further derived as

$$= \frac{1}{2K}[\hat{d}_1{}^2(k) - \hat{d}_1{}^2(k-N) - 2d_1(k)\hat{d}_1(k)$$
$$+ 2d_1(k-N)\hat{d}_1(k-N)]$$

$$= \frac{1}{2K}\left[\hat{d}_1(k) - \hat{d}_1(k-N)\right]\left[\hat{d}_1(k) + \hat{d}_1(k-N) - 2d_1(k)\right]$$

$$= \frac{1}{2}e(k-N)\left[-2e(k-N) + \hat{d}_1(k) - \hat{d}_1(k-N)\right]$$

$$= \frac{1}{2}e(k-N)[-2e(k-N) + Ke(k-N)]$$

$$= -\left[1 - \frac{K}{2}\right]e^2(k-N) \tag{5.33}$$

Equation (5.33) implies that for $\left[1 - \frac{K}{2}\right] > 0$, $e(k) \in L^2$, and for finite k, the tracking error $e(k)$ converges to zero. This also gives a range of RC gain to be $0 < k_{rc} < 2\left|\frac{k_m}{k_p}\right|$.

5.3 Adaptive Repetitive Control (ARC)

This section covers the digital design of Adaptive Repetitive Control (ARC) for unknown linear systems subject to time-varying periodic disturbances. The structure of

ARC as shown in Figure 5.2 consists of two main controllers: Model Reference Adaptive Control (MRAC), and RC, in which the structure is almost similar to MRRC. The different is that the controller parameters of MRRC are fixed, and designed offline, while the controller parameters of ARC are evolved, and updated each sampling time.

Assume that a linear discrete-time plant is represented by the following transfer function at the sampling period T :

$$G(z,T) \quad = k_p \frac{B(z)}{A(z)} = k_p(T) \frac{z^{n-1} + b_1(T)z^{n-2} + \cdots + b_{(n-1)}(T)}{z^n + a_1(T)z^{n-1} + \cdots + a_n(T)} \tag{5.34}$$

where parameters $a_i(T)$and $b_i(T)$are functions of the sampling period T.

Due to the presence of the periodic disturbance with time-varying period $d_t(k)$, the sampling period T is changed to keep a fixed integer number of samples per period N. As a result of the time-varying sampling period, the discrete-time plant model $G(z,T)$ becomes a special class of time-varying plant in which the parameters k_p, a_i and b_i are bounded and jump to the new constant values when the sampling period T changes.

The objective is to design control signal $u_p(k)$ for the time-varying plant $G(z,T)$ shown in (6.34) subject to periodic disturbance $d_t(k)$ such that the plant output $y_p(k)$ tracks the reference model output $y_m(k)$.

Now we propose an ARC based on the MRAC and IMP, which is shown in Figure. 6.2.

The reference model output $y_m(k)$ is generated from the LTI model as shown in (5.4). Several assumptions are also made to design the ARC scheme here:

(A.1) $G(z,T)$ is a stable and minimum phase plant for a sampling period T . $B(z)$and$A(z)$ are co-prime Monic Hurwitz polynomials.

(A.2) The minimum time between sampling period changes is sufficient interval.

(A.3) The degree of $A(z)$ is known. Let $\deg[A(z)] = n$.

(A.4) The sign of k_p is known.

(A.5) The degree of $D_m(z)$ is less than the degree of $A(z)$.

(A.6) The relative degree $n^* = n - m$ is known

(A.7) The relative degree of the plant is equal to the relative degree of reference model

(A.8) The disturbance period is unknown, but the sampling period is updated to obtain N samples per period by using algorithms such as PLL (Phase Locked Loop) [27, 93, 110].

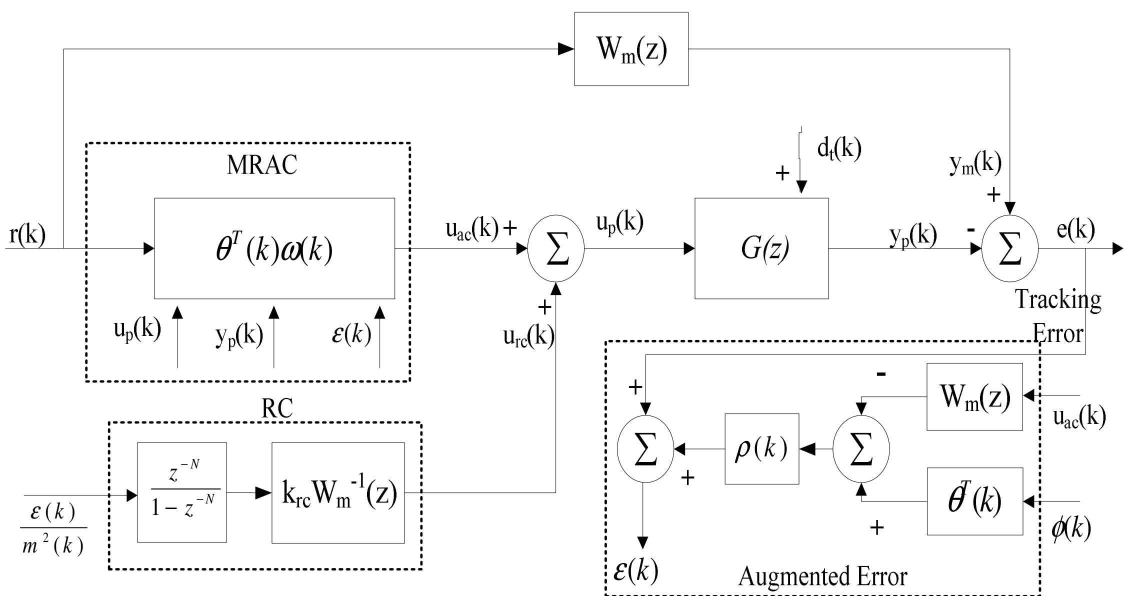

Figure 5.2 Block diagram of Adaptive Repetitive Control (ARC)

The plant output $y_p(k)$ is expressed in the following form

$$y_p(k) = G(z,T)u_p(k) + d_t(k) \tag{5.35}$$

The control signal fed to the plant is formulated as follows:

$$u_p(k) = u_{ac}(k) + u_{rc}(k) \tag{5.36}$$

A control signal $u_{ac}(k)$ is generated from the MRAC block

$$u_{ac}(k) = \theta^T(k)\omega(k)$$
$$= \theta_1^T(k)\omega_1(k) + \theta_2^T(k)\omega_2(k) + \theta_3(k)y_p(k) + \theta_4(k)r(k) \quad (5.37)$$

where

$$\theta(k) = [\theta_1^T(\mathrm{k}), \theta_2^T(\mathrm{k}), \theta_3(\mathrm{k}), \theta_4(\mathrm{k})]^T; \theta_3, \theta_4 \in \mathcal{R}^1; \theta_1, \theta_2 \in \mathcal{R}^{n-1} \quad (5.38)$$

$$\omega(k) = [\omega_1(k), \omega_2(k), y(k), r(k)]^T$$
$$= \left[\frac{\alpha(z)}{\Lambda(z)}u_p(k), \frac{\alpha(z)}{\Lambda(z)}y_p(k), y_p(k), r(k)\right]^T; \omega_1, \omega_2 \in \mathcal{R}^{n-1} \quad (5.39)$$

$\Lambda(z)$is a Monic Hurwitz polynomial of degree $n-1$, $\alpha(z)$ is similar to (5.9), and $\theta(k)$is the estimation of θ^*, which is the true parameters vector at a sampling period T.

For each sampling period T, the plant parameters $\mathrm{k_p}, \mathrm{a_i}$, and $\mathrm{b_i}$ are unknown. We choose gradient adaptive law with parameter projection [111] for updating $\theta(k)$ and $\rho(k)$

$$\theta(k+1) = \theta(k) + \frac{\text{sign }[k_p]\Gamma\phi(k)\varepsilon(k)}{m^2(k)} + f_\theta \quad (5.40)$$

$$\rho(k+1) = \rho(k) + \frac{\gamma\eta(k)\varepsilon(k)}{m^2(k)} + f_\rho \quad (5.41)$$

where

$$\Gamma = \Gamma^{\mathrm{T}} > 0, \Gamma \in \mathcal{R}^{2\mathrm{nx}2\mathrm{n}} \quad (5.42)$$

$$\gamma > 0 \ \gamma \in \mathcal{R} \quad (5.43)$$

$$m^2(k) = 1 + \phi^T(k)\Gamma\phi(k) \tag{5.44}$$

$$\phi(k) = W_m(z)\omega(k) \tag{5.45}$$

$$\eta(k) = W_m(z)[\theta^T(k)\omega(k)] - \theta^T(k)\phi(k) \tag{5.46}$$

$$\varepsilon(k) = y_m(k) - y_p(k) + \rho(k)\eta(k) \tag{5.47}$$

$$f_{\theta_i}(k) = \begin{cases} 0 & \text{if } \theta_i - g_{\theta_i} \in [\theta_i^l, \theta_i^u] \\ \theta_i^u - \theta_i - g_{\theta_i} & \text{if } \theta_i - g_{\theta_i} > \theta_i^u \\ \theta_i^l - \theta_i - g_{\theta_i} & \text{if } \theta_i - g_{\theta_i} < \theta_i^l \end{cases} \tag{5.48}$$

$$f_\rho(k) = \begin{cases} 0 & \text{if } \rho - g_\rho \in [\rho^l, \rho^u] \\ \rho^u - \rho - g_\rho & \text{if } \rho - g_\rho > \rho^u \\ \rho^l - \rho - g_\rho & \text{if } \rho - g_\rho < \rho^l \end{cases} \tag{5.49}$$

$$g_\theta(k) = \frac{\Gamma\phi(k)\varepsilon(k)}{m^2(k)} \tag{5.50}$$

$$g_\rho(k) = \frac{\gamma\eta(k)\varepsilon(k)}{m^2(k)} \tag{5.51}$$

$\theta_i(k)$and $g_{\theta_i}(k)$ is i-th component of $\theta(k)$ and $g_\theta(k)$ respectively,

i=1,..,2n

θ_i^l, θ_i^u are the lower and upper bound of $\theta_i(k)$

ρ^l, ρ^u are the lower and upper bound of $\rho(k)$

$\theta^* \in [\theta^l, \theta^u]$,$\rho^* \in [\rho^l, \rho^u]$

The control law generated from the RC is given by

$$u_{rc}(k) = C_{rc}(z)\frac{\varepsilon(k)}{m^2(k)} \tag{5.52}$$

where $C_{rc}(z)$ has similar form as shown in (5.15)

The control law in (5.36) with adaptation law (5.40)-(5.41) ensures that $\theta(k), \rho(k),$ and $\varepsilon(k) \in L^{\infty}$ which are bounded signals, and also ensures that $\varepsilon(k) \in L^{2}$ which decays to zero.

5.3.1 STABILITY ANALYSIS OF ARC

To prove the stability, we firstly need to derive the system error dynamics for the proposed ARC. For each sampling period T, there exists unique solution θ^{*} so that the transfer function from $r(k)$ to $y_{p}(k)$ with no RC and disturbance, is equal to $W_{m}(z)$

$$\frac{G(z,T)\theta_4^*}{[1-\theta_1^{*T}\frac{\alpha(z)}{\Lambda(z)}-\theta_2^{*T}\frac{\alpha(z)G(z)}{\Lambda(z)}-\theta_3^*G(z,T)]}=W_m(z) \tag{5.53}$$

Choosing $\theta_4^* = k_m/k_p$, and $\Lambda(z) = \Lambda_0(z)N_m(z)$, the matching equation becomes

$$\theta_1^*\alpha(z)A(z)-k_pB(z)\big(\theta_2^*\alpha(z)+\theta_3^*\Lambda(z)\big)=\Lambda(z)A(z)-\Lambda_0(z)B(z)D_m(z) \tag{5.54}$$

Rearranging (5.54), we obtain

$$[\theta_1^*\alpha(z)-\Lambda(z)]A(z)+\big[\Lambda_0(z)D_m(z)+k_p\theta_2^*\alpha(z)+k_p\theta_3^*\Lambda(z)\big]B(z)=0 \tag{5.55}$$

The polynomial $A(z)$and$B(z)$ are co-prime, so there is a polynomial $M(z)$ such

$$[\theta_1^*\alpha(z)-\Lambda(z)]=M(z)B(z) \tag{5.56}$$

$$\big[\Lambda_0(z)D_m(z)+k_p\theta_2^*\alpha(z)+k_p\theta_3^*\Lambda(z)\big]=-M(z)A(z) \tag{5.57}$$

Multiplying both sides of (6.57) by $y_p(k)$ and rearrange, we get

$$M(z)A(z)y_p(k)+k_p\theta_2^*\alpha(z)y_p(k)+k_p\theta_3^*\Lambda(z)y_p(k)=-\Lambda_0(z)D_m(z)y_p(k) \tag{5.58}$$

Equation (5.35) can be rewritten as follows:

$$y_p(k)A(z) = k_pB(z)u_p(k) + A(z)d_t(k) \tag{5.59}$$

Substituting (5.59) and (5.57) to (5.58), we have

$$\begin{aligned} k_p\left[\theta_1^*\alpha(z)u_p(k) + \theta_2^*\alpha(z)y_p(k) + \theta_3^*\Lambda(z)y_p(k)\right] + M(z)A(z)d_t(k) \\ -k_p\Lambda(z)u_p(k) = -\Lambda_0(z)D_m(z)y_p(k) \end{aligned} \tag{5.60}$$

Dividing both sides of (5.60) by $k_p\Lambda(z)$and rearrange, we get

$$\begin{aligned} \theta_1^*\frac{\alpha(z)}{\Lambda(z)}u_p(k) + \theta_2^*\frac{\alpha(z)}{\Lambda(z)}y_p(k) + \theta_3^*y_p(k) \\ +\frac{1}{k_p}M(z)A(z)d_t(k) = u_p(k) - \frac{1}{k_p}\frac{N_m(z)}{D_m(z)}y_p(k) \end{aligned} \tag{5.61}$$

Using (5.36)-(5.37), (5.61) can be rewritten as:

$$\begin{aligned} \theta_1^{*T}\omega_1(k) + \theta_2^{*T}\omega_2(k) + \theta_3^*y_p(k) + \theta_4^*r(k) = \theta_1^T\omega_1(k) + \theta_2^T\omega_2(k) \\ +\theta_3y_p(k) + \theta_4r(k) + \theta_4^*r(k) - \theta_4^*{W_m}^{-1}(z)y_p(k) \\ +\mathrm{u_{rc}(k)} - \frac{1}{k_p}M(z)A(z)d_t(k) \end{aligned} \tag{5.62}$$

We need to define parameter error $\widetilde{\theta}(k)$as the difference between the estimation $\theta(k)$and true parameter θ^*.

$$\tilde{\theta}(k) = \theta(k) - \theta^* \tag{5.63}$$

Using (5.63), we can rewrite (5.62) as

$$-\tilde{\theta}(k)\omega(\mathrm{k}) = \theta_4^*r(k) - \theta_4^*{W_m}^{-1}(z)y_p(k) + \mathrm{u_{rc}(k)} - \frac{1}{k_p}M(z)A(z)d_t(k) \tag{5.64}$$

Multiplying both sides of (5.64) by $\frac{W_m(z)}{\theta_4^*}$, we obtain

$$-\frac{W_m(z)}{\theta_4^*}\left[\tilde{\theta}(k)\omega(\mathrm{k})\right] = y_m(k) - y_p(k) + \frac{1}{\theta_4^*}W_m(z)\mathrm{u_{rc}}(\mathrm{k}) - \frac{1}{k_m}W_m(z)M(z)A(z)d_t(k) \tag{5.65}$$

Denote $d_1(k)$as

$$d_1(k) = \frac{1}{k_m}W_m(z)M(z)A(z)d_t(k) \tag{5.66}$$

Using equality (5.57), $d_1(k)$ can be rewritten as follows

$$d_1(k) = -\left[\Lambda(z)+\frac{1}{\theta_4^*}[\theta_2^{*T}\alpha(z)]W_m(z) \; + \frac{1}{\theta_4^*}\theta_3^*\Lambda(z)W_m(z)\right]d_t(k) \tag{5.67}$$

The facts that $\Lambda(z)$and $W_m(z)$ are a monic hurwitz polynomial and a stable transfer function respectively, ensures that $d_1(k)$ is a bounded signal. Signal $d_1(k)$ is simply the filtered $d_t(k)$ where the periodic property of $d_t(k)$ remains, but the magnitude and phase of $d_t(k)$ may change. Therefore, $d_1(k)$ has the following property:

$$d_1(k) = d_1(k+N) = d_1(k-N) \tag{5.68}$$

Let write $\hat{\mathrm{d}}_1(\mathrm{k})$ as

$$\hat{\mathrm{d}}_1(\mathrm{k}) = \frac{1}{\theta_4^*}\mathrm{W_m(z)u_{rc}(k)} \tag{5.69}$$

Since $\mathrm{u_{rc}(k)}$is a control signal generated from the RC as formulated in (5.52), $\hat{\mathrm{d}}_1(\mathrm{k})$ can be expressed as follows:

$$\hat{d}_1(k) = K\frac{1}{z^N - 1}\frac{\varepsilon(\mathrm{k})}{m^2(k)} \tag{5.70}$$

where $\mathrm{K} = \frac{\mathrm{k_{rc}}}{\theta_4^*}$

Signal $\hat{d}_1(k)$ also can be considered as the estimation of $d_1(k)$ which has the following updating rule:

$$\hat{d}_1(k+N) = \hat{d}_1(k) + K\frac{\varepsilon(\mathrm{k})}{m^2(k)} \tag{5.71}$$

Equation (6.65) can be rewritten as follows:

$$-\frac{W_m(z)}{\theta_4^*}\left[\tilde{\theta}(k)\omega(\mathrm{k})\right] = y_m(k) - y_p(k) + \hat{d}_1(k) - d_1(k) \tag{5.72}$$

From (5.72), the tracking error $e(k)$ can be formulated as follows:

$$e(k) = y_m(k) - y_p(k) = -\rho^* W_m(z)\left[\tilde{\theta}(k)\omega(\mathrm{k})\right] + \varepsilon_{\boldsymbol{d}}(k) \tag{5.73}$$

where $\rho^* = \frac{1}{\theta_4^*}$ and $\varepsilon_{\boldsymbol{d}}(k) = d_1(k) - \hat{d}_1(k)$.

Substituting (5.46) and (5.73) to (5.47), we obtain

$$\varepsilon(k) = -\rho^*\tilde{\theta}(k)\phi(k) - \tilde{\rho}(k)\eta(\mathrm{k}) + \varepsilon_d(k) \tag{5.74}$$

where $\widetilde{\rho}(k) = \rho(\mathrm{k}) - \rho^*$

Finally, we obtain the augmented error $\varepsilon(k)$ which consists of three different errors: parameter error $\tilde{\theta}(k)$, parameter error $\tilde{\rho}(k)$, and repetitive error $\varepsilon_d(k)$.

Now, we prove the system stability.

Theorem 5.2: For each sampling period T, the control law in (5.36) with adaptation law (6.40)-(6.41) ensures that $\theta(\mathrm{k}), \rho(\mathrm{k}), \varepsilon(\mathrm{k}) \in \mathrm{L}^\infty$ which are bounded, and $\varepsilon(\mathrm{k}) \in \mathrm{L}^2$ which converges to zero.

Proof:

Let us choose a Lyapunov function $\mathrm{V}(\tilde{\theta}, \tilde{\rho}, \varepsilon_\mathrm{d})$ as follows

$$V\left(\tilde{\theta}, \tilde{\rho}, \varepsilon_d\right) = V_1\left(\tilde{\theta}\right) + V_2(\tilde{\rho}) + V_3(\varepsilon_{\boldsymbol{d}}) \tag{5.75}$$

where

$$V_1\left(\tilde{\theta}\right) = \rho^* \tilde{\theta}^T(k) \Gamma^{-1} \tilde{\theta}(k) \tag{5.76}$$

$$V_2(\tilde{\rho}) = \frac{\tilde{\rho}^2(k)}{\gamma} \tag{5.77}$$

$$V_3(\varepsilon_{\boldsymbol{d}}) = \frac{1}{K} \sum_{\tau=k}^{k-1+N} \varepsilon_{\boldsymbol{d}}{}^{\boldsymbol{2}}(\tau) \tag{5.78}$$

The time difference of Lyapunov function $V_1\left(\tilde{\theta}\right)$ is

$$V_1\left(\tilde{\theta}(k+1)\right) - V_1\left(\tilde{\theta}(k)\right) = \rho^* \tilde{\theta}^{\mathrm{T}}(\mathrm{k}+1) \Gamma^{-1} \tilde{\theta}(\mathrm{k}+1) - \rho^* \tilde{\theta}^{\mathrm{T}}(\mathrm{k}) \Gamma^{-1} \tilde{\theta}(\mathrm{k}) \tag{5.79}$$

$$= \rho^* \Gamma^{-1} \left\{ \left[\tilde{\theta}^T(k+1) - \tilde{\theta}^T(k)\right] \tilde{\theta}(k+1) - \left[\tilde{\theta}^T(k+1) - \tilde{\theta}^T(k)\right] \tilde{\theta}(k) \right\}$$

$$= \rho^* \left[\frac{\phi^T(k) \Gamma \varepsilon(k)}{m^2(k)} + f_\theta^T\right] \left[\frac{\phi(k) \varepsilon(k)}{m^2(k)} + \Gamma^{-1} f_\theta + 2\Gamma^{-1} \tilde{\theta}(k)\right]$$

$$= \rho^* \frac{\phi^T(k) \Gamma \phi(k) \varepsilon^2(k)}{m^4(k)} + 2\rho^* \frac{\phi^T(k) \tilde{\theta}(k) \varepsilon(k)}{m^2(k)} + \rho^* f_\theta^T \Gamma^{-1} f_\theta$$
$$+ 2\rho^* f_\theta^T \Gamma^{-1} g_\theta + 2\rho^* f_\theta^T \Gamma^{-1} \tilde{\theta}(k)$$

$$\leq \rho^* \frac{\phi^T(k) \Gamma \phi(k) \varepsilon^2(k)}{m^4(k)} + 2\rho^* \frac{\phi^T(k) \tilde{\theta}(k) \varepsilon(k)}{m^2(k)}$$
$$+ 2\rho^* f_\theta^T \Gamma^{-1} \left[f_\theta + g_\theta + \tilde{\theta}(k)\right] \tag{5.80}$$

The time difference of Lyapunov function $V_2(\tilde{\rho})$ is

$$V_2(\tilde{\rho}(k+1)) - V_2(\tilde{\rho}(k)) = \frac{\tilde{\rho}^2(k+1)}{\gamma} - \frac{\tilde{\rho}^2(k)}{\gamma} \tag{5.81}$$

$$= \gamma^{-1} [\tilde{\rho}(k+1) - \tilde{\rho}(k)] \tilde{\rho}(k+1) - \gamma^{-1} [\tilde{\rho}(k+1) - \tilde{\rho}(k)] \tilde{\rho}(k)$$

$$= \left[\frac{\eta(k)\varepsilon(k)}{m^2(k)} + \gamma^{-1} f_\rho\right]\left[\frac{\gamma\eta(k)\varepsilon(k)}{m^2(k)} + f_\rho + 2\tilde{\rho}(k)\right]$$

$$= \frac{\gamma\eta^2(k)\varepsilon^2(k)}{m^4(k)} + 2\frac{\eta(k)\tilde{\rho}(k)\varepsilon(k)}{m^2(k)} + 2\gamma^{-1} f_\rho g_\rho + \gamma^{-1} {f_\rho}^2 + 2\gamma^{-1} f_\rho \tilde{\rho}(k)$$

$$\leq \frac{\gamma\eta^2(k)\varepsilon^2(k)}{m^4(k)} + 2\frac{\eta(k)\tilde{\rho}(k)\varepsilon(k)}{m^2(k)} + 2\gamma^{-1} f_\rho\left[f_\rho + g_\rho + \tilde{\rho}(k)\right] \tag{5.82}$$

The time difference of Lyapunov function $V_3(\varepsilon_{\boldsymbol{d}})$ is

$$V_3(\varepsilon_d(k+1)) - V_3(\varepsilon_d(k)) = \frac{1}{K}\sum_{\tau=k+1}^{k+N} {\varepsilon_d}^2(\tau) - \frac{1}{K}\sum_{\tau=k}^{k-1+N} {\varepsilon_{\boldsymbol{d}}}^{\boldsymbol{2}}(\tau) \tag{5.83}$$

$$= \frac{1}{K}\left\{\left[\hat{d}_1(k+N) - d_1(k+N)\right]^2 - \left[\hat{d}_1(k) - d_1(k)\right]^2\right\}$$

$$= \frac{1}{K}\left[\hat{d}_1(k+N) - \hat{d}_1(k)\right]\left[\hat{d}_1(k+N) - \hat{d}_1(k) - 2\varepsilon_{\boldsymbol{d}}(k)\right]$$

$$= \frac{\varepsilon(k)}{m^2(k)}\left[\frac{K\varepsilon(k)}{m^2(k)} - 2\varepsilon_{\boldsymbol{d}}(k)\right] \tag{5.84}$$

We obtain the increment of Lyapunov function $V(\tilde{\theta}, \tilde{\rho}, \varepsilon_{\boldsymbol{d}})$ as the sum of (5.80), (5.82), and (5.84):

$$\begin{aligned}
&V\left(\tilde{\theta}(k+1), \tilde{\rho}(k+1), \varepsilon_{\boldsymbol{d}}(k+1)\right) - V\left(\tilde{\theta}(k), \tilde{\rho}(k), \varepsilon_{\boldsymbol{d}}(k)\right) \\
&\leq \rho^* \frac{\phi^T(k)\Gamma\phi(k)\varepsilon^2(k)}{m^4(k)} + \frac{\gamma\eta^2(k)\varepsilon^2(k)}{m^4(k)} \\
&\quad +2\left[\rho^*\phi^T(k)\tilde{\theta}(k) + \eta(k)\tilde{\rho}(k)\right]\frac{\varepsilon(k)}{m^2(k)} + 2\rho^* f_\theta^T \Gamma^{-1}\left[f_\theta + g_\theta + \tilde{\theta}(k)\right] \\
&\qquad\qquad +2\gamma^{-1} f_\rho\left[f_\rho + g_\rho + \tilde{\rho}(k)\right] + \frac{\varepsilon(k)}{m^2(k)}\left[\frac{K\varepsilon(k)}{m^2(k)} - 2\varepsilon_d(k)\right]
\end{aligned} \tag{5.85}$$

Using parameter projection properties (5.48)-(5.49) implies that

$$2\rho^* f_\theta^T \Gamma^{-1}\left[f_\theta + g_\theta + \tilde{\theta}(k)\right] \leq 0 \tag{5.86}$$

$$2\gamma^{-1} f_\rho\left[f_\rho + g_\rho + \tilde{\rho}(k)\right] \leq 0 \tag{5.87}$$

The parameter projection algorithm (5.48)-(5.49) also ensures $\theta(k)$ and $\rho(k)$ to be bounded signals.

Hence, we can rewrite (5.85) as follows:

$$V\left(\tilde{\theta}(k+1), \tilde{\rho}(k+1), \varepsilon_{\boldsymbol{d}}(k+1)\right) - V\left(\tilde{\theta}(k), \tilde{\rho}(k), \varepsilon_{\boldsymbol{d}}(k)\right)$$

$$\leq \rho^* \frac{\phi^T(k)\Gamma\phi(k)\varepsilon^2(k)}{m^4(k)} + \frac{\gamma\eta^2(k)\varepsilon^2(k)}{m^4(k)} + 2[-\varepsilon(k) + \varepsilon_d(k)]\frac{\varepsilon(k)}{m^2(k)} + \frac{\varepsilon(k)}{m^2(k)}\left[\frac{K\varepsilon(k)}{m^2(k)} - 2\varepsilon_d(k)\right]$$

$$\leq -\left(2 - \frac{\rho^*\phi^T(k)\Gamma\phi(k)}{m^2(k)} - \frac{\gamma\eta^2(k)}{m^2(k)} - \frac{K}{m^2(k)}\right)\frac{\varepsilon^2(k)}{m^2(k)}$$

$$\leq -\delta\frac{\varepsilon^2(k)}{m^2(k)} \tag{5.88}$$

where

$$\delta = \left(2 - \frac{\rho^*\phi^T(k)\Gamma\phi(k)}{m^2(k)} - \frac{\gamma\eta^2(k)}{m^2(k)} - \frac{K}{m^2(k)}\right) \tag{5.89}$$

Equation (5.89) implies that for $\delta > 0$, $\theta(k), \rho(k) \in L^\infty$ and $\varepsilon(k) \in L^\infty \cap L^2$. This means that $\theta(k)$ and $\rho(k)$ are bounded signals, and $\varepsilon(k)$ is both bounded and decaying signal.

5.4 Simulation Results

We now perform simulations to verify both the MRRC and ARC designs proposed in Section 2 and 3 respectively. The open-loop plant model has a continuous transfer function as follows

$$G(s) = \frac{1.74}{0.0275s^2 + s} \tag{5.90}$$

which represents Quanser servomotor SRV02-E with bar load as described in Chapter 3.

5.4.1 SIMULATION OF MRRC

The proportional controller with gain 4 is used to stabilize the open-loop model. Hence, we have a second order closed-loop model. With the fixed sampling period $T = 0.05\ s$, we obtain a second order discrete model with a relative degree 1 as follows:

$$G_c(z) = 0.1877\frac{z + 0.5530}{z^2 - 0.9747z + 0.2662} \tag{5.91}$$

The reference model $\mathrm{W_m(z)}$ is chosen to satisfy (A.4) and (A.6) described in section 2. The transfer function $\mathrm{W_m(z)}$and polynomial $\Lambda(\mathrm{z})$are chosen respectively as follow:

$$W_m(z) = \frac{1}{z}, \Lambda(\mathrm{z}) = \mathrm{z} \tag{5.92}$$

As we have a second order plant model, then we need a controller parameter vector as follows:

$$\theta^* = [\theta_1^*, \theta_2^*, \theta_3^*, \theta_4^*]^{\mathrm{T}} \tag{5.93}$$

where $\theta_1^*, \theta_2^*, \theta_3^*, \theta_4^* \in \mathcal{R}^1$

Firstly, θ_4^* is obtained from

$$\theta_4^* = \frac{k_m}{k_p} = 5.328 \tag{5.94}$$

Then, θ_1^*, θ_2^*, and , θ_3^* are obtained by solving the matching equation (5.12).Thus, we get the true parameter vector θ^*as follows:

$$\theta^* = \begin{bmatrix} \theta_1^* \\ \theta_2^* \\ \theta_3^* \\ \theta_4^* \end{bmatrix} = \begin{bmatrix} -0.553 \\ 1.418 \\ -5.194 \\ 5.328 \end{bmatrix} \tag{5.95}$$

Suppose a disturbance $d(k)$ with fixed period $1\ s$ illustrated in Figure 5.3(c) corrupts the plant output. Thus, the number of samples per disturbance period N is 20.Let the repetitive controller gain $k_{rc} = 2$ that satisfies $\left[1 - \frac{k_{rc}}{2\theta_4^*}\right] > 0$ is chosen. Larger RC gain can be chosen for fast convergence rate. The repetitive controller $C_{rc}(z)$ can be formulated as follows.

$$C_{rc}(z) = \left(2\frac{z^{-19}}{1 - z^{-20}}\right) \tag{5.96}$$

We consider two types of references: a triangle signal with a period $10\ s$ shown in Figure 5.3(a) and a constant input with a magnitude of $\pi/4$ rad shown in Figure 5.3(b).

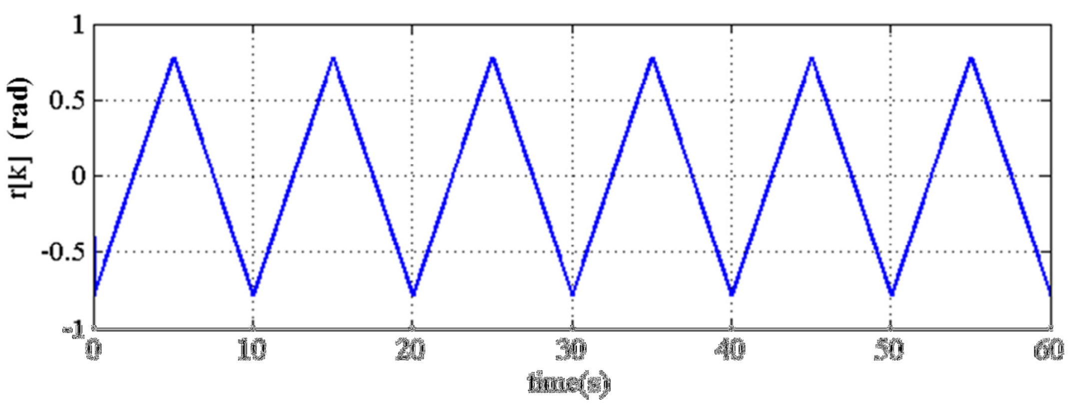

(a)

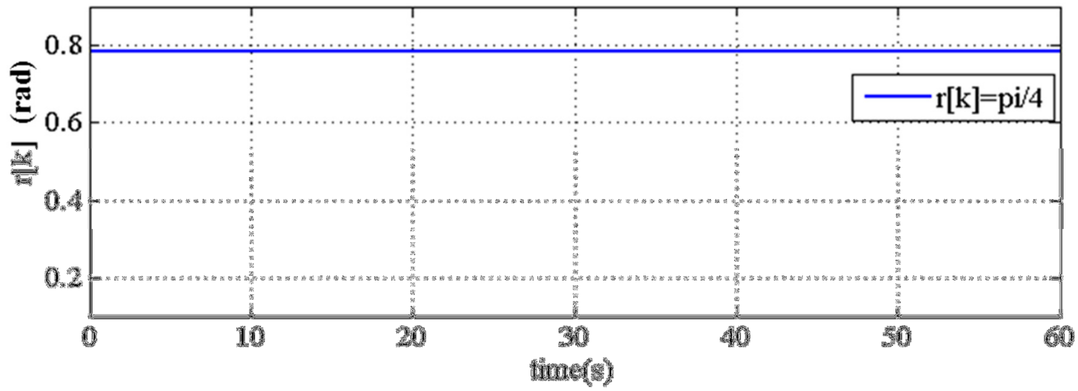

(b)

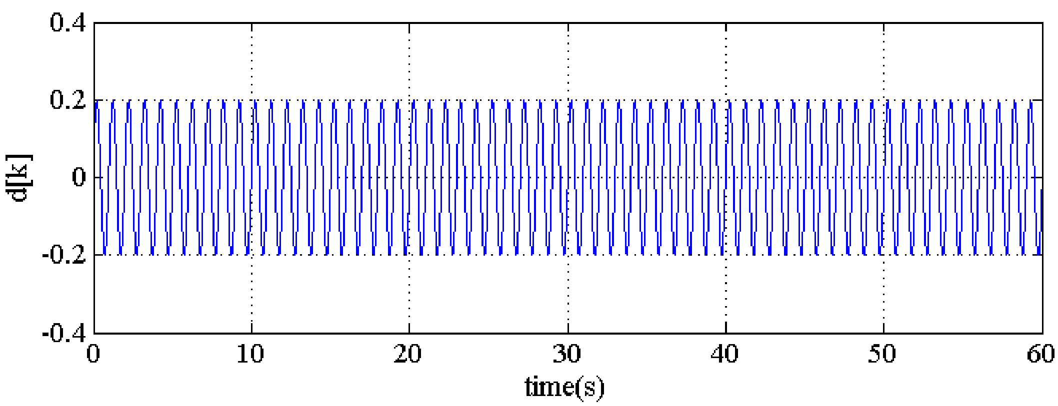

(c)

Figure 5.3 (a) a triangle reference signal (b) a constant reference signal (c)a periodic disturbance

The tracking outputs and tracking errors for two reference signals are shown in Figure 5.4 and Figure 5.5 respectively. Figure 5.4 and 5.5 show that the proposed MRRC can simultaneously track the reference signal $r(k)$ and reject the disturbance $d(k)$. Figure 5.4 (a) and 5.5 (a) also indicate perfect tracking performance for two types reference signals. Figure 5.6 shows the tracking error of the system when only MRC is used. The periodic signal with smaller amplitude appears as an error. When RC is not applied or $u_{rc}(k)$ is zero, the error equation $e(k)$ (5.28) is equal to $d_1(k)$. Hence, the error signal is only the filtered $d(k)$, where the periodic property of $d(k)$ remains, but both the magnitude and phase of $d(k)$ change.

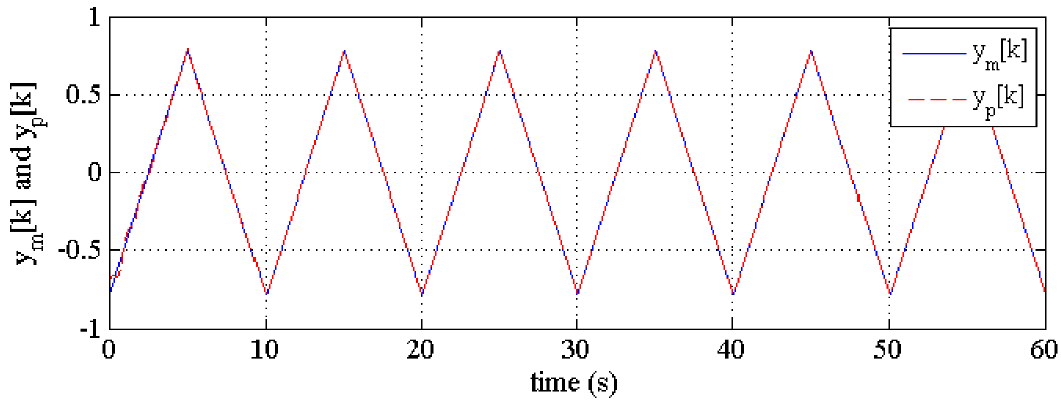

(a)

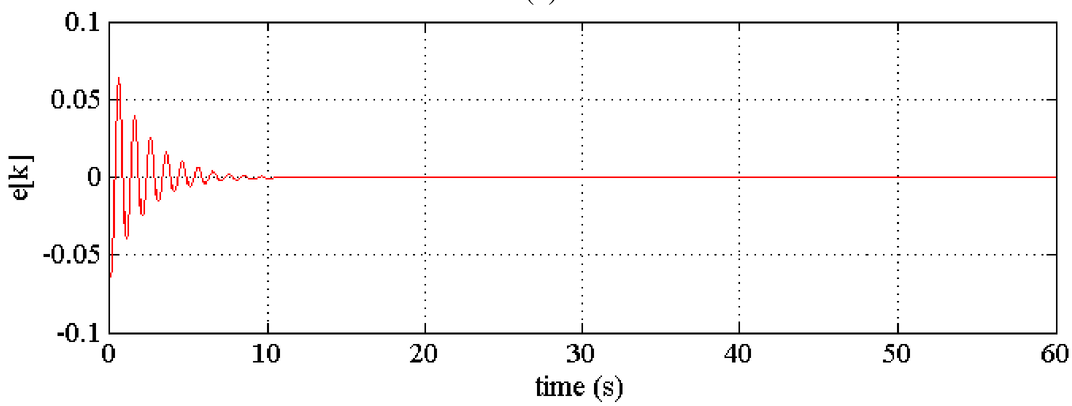

(b)

Figure 5.4 (a) Tracking output $y_p(k)$,(b) tracking error $e(k)$of MRRC for triangle reference signal

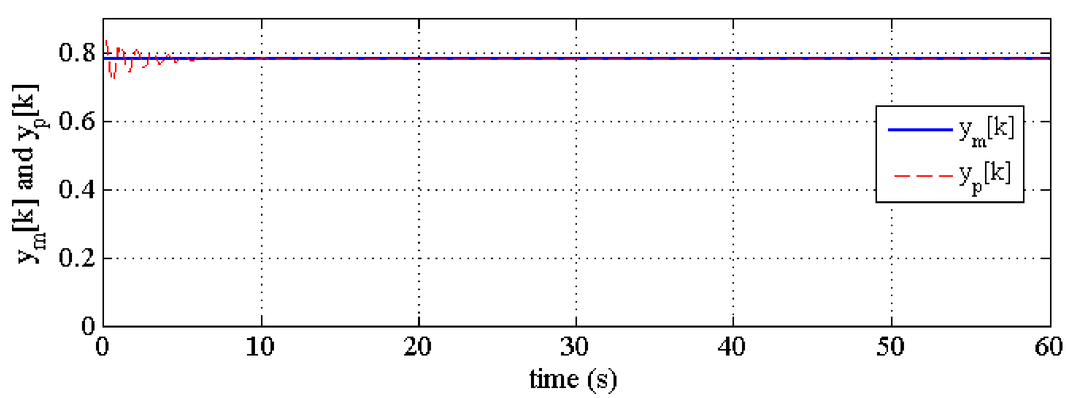

(a)

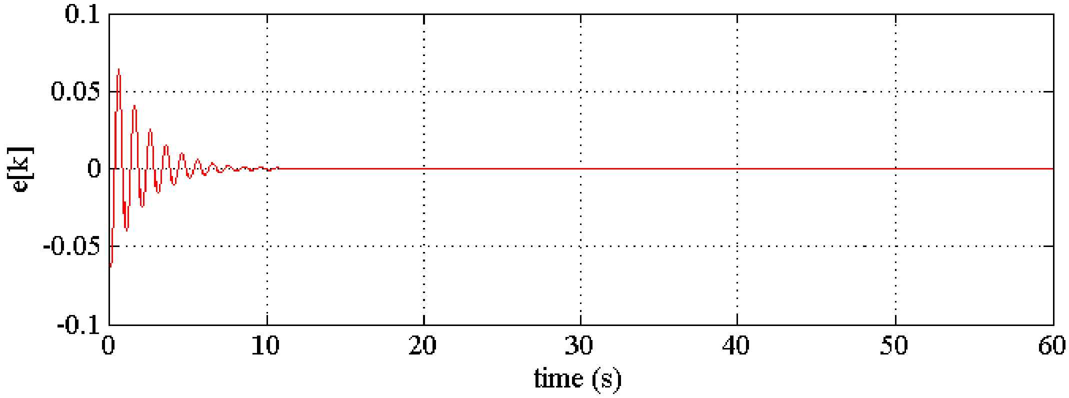

(b)

Figure 5.5 (a) Tracking output$y_p(k)$,(b) tracking error $e(k)$of MRRC for constant reference signal

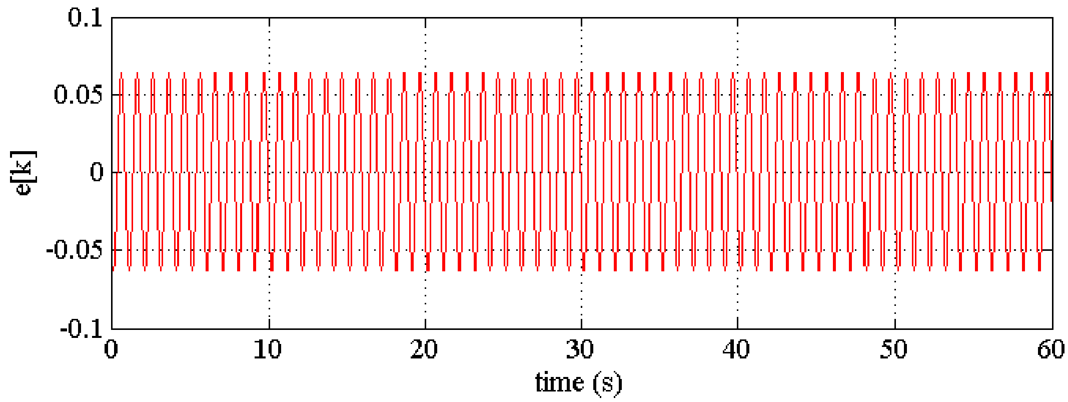

Figure 5.6 Tracking error $e(k)$of MRC for constant reference signal

5.4.2 SIMULATION OF ARC

We now perform simulations to verify the ARC design proposed in Section 3. The same continuous plant model is used here. The discrete plant model is a second order plant with a relative degree 1. The transfer function $W_m(z)$, a polynomial $\Lambda(z)$,an initial controller parameters θ_0, and a RC gain k_{rc} are chosen respectively as follow:

$$W_m(z) = \frac{1}{z}, \Lambda(z) = z, \theta_0 = [0\ 0\ 0\ 0]^T, k_{rc} = 2 \tag{5.97}$$

If we choose the desired number of samples N as 20, then the repetitive controller $C_{rc}(z)$ has the same formula as shown in (5.96).

The disturbance is illustrated in Figure 5.7, in which the period is 1 s, 1.5 s and 0.8 s at 0 s, 20 s and 40 s respectively. The sampling period is 0.05 s, 0.075 s and 0.04 s to obtain 20 samples per disturbance period. At 40 s, the period drops to nearly half of the previous representing a large period change.

Now we also consider two types of references: a triangle signal with a period 10s shown in Figure 5.3(a) and a constant input with a magnitude of $\pi/4$ rad shown in Figure 5.3(b).

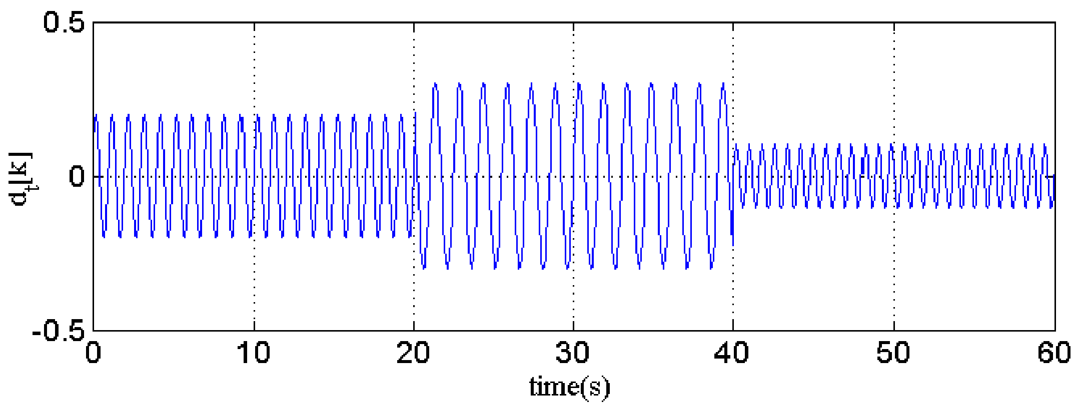

Figure 5.7 Time-varying periodic disturbance $d_t(k)$ with a large period change

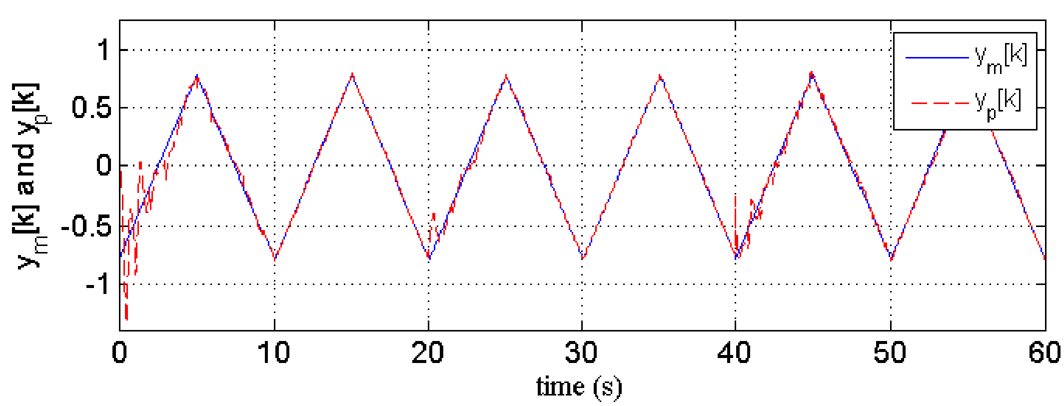

(a)

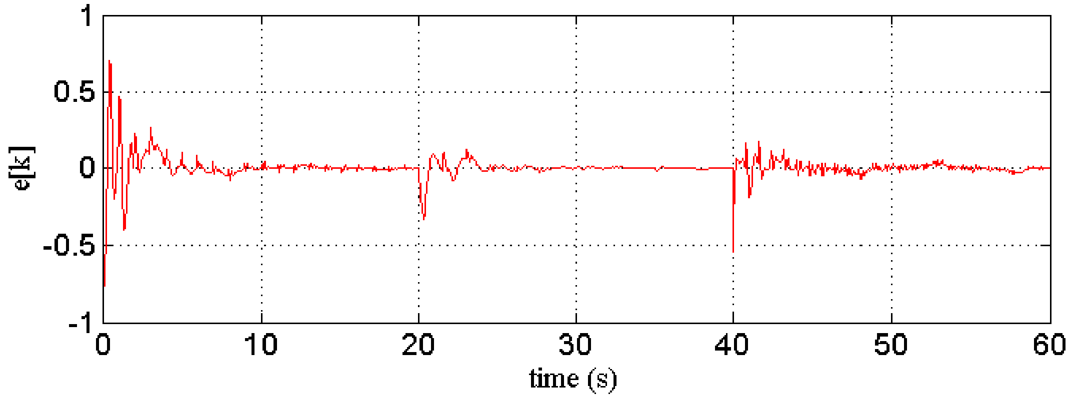

(b)

Figure 5.8 The proposed ARC performance tracking a periodic reference (a) the system output (b) the output error

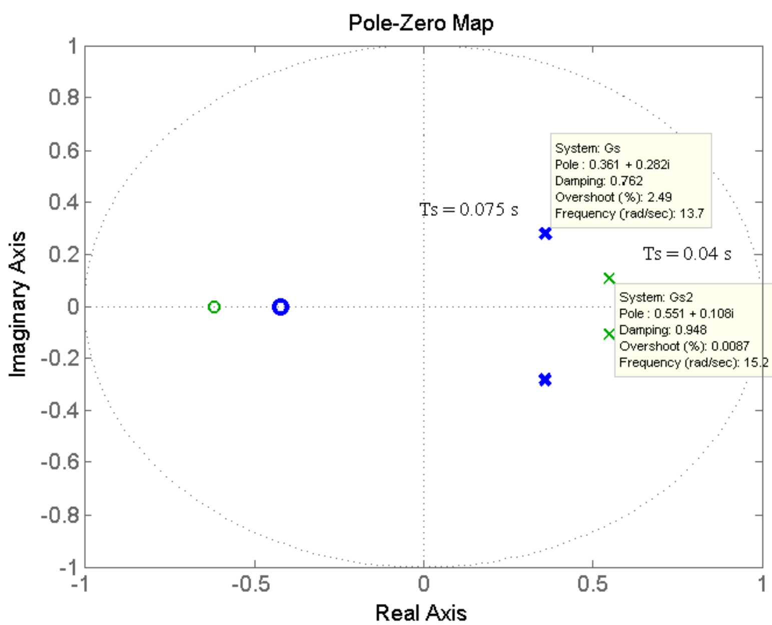

Figure 5.9 Pole-zero map of $G(z)$ when $T = 0.075$ s and 0.04 s

Figure 5.8 shows the proposed ARC tracking and rejecting periodic signals at the same time. The reference period is not necessarily the same or multiple of the disturbance period. Figure 5.8(b) shows that the first transient error reaches 5% settling time around 8.3 s, which is about 8 cycles of disturbance signal. When the sampling period change to 0.075s (disturbance period increases from the previous), the new transient error occurs. This is due to the adaptive controller needs to adapt to the new correct values. In the middle transient, the error dies down around 4 s, which is 2.6

cycles of the disturbance. The last transient error takes 9 s to reach 5% settling, which is about 11 cycles of the disturbance. In the last transient, the period drops to nearly half of the previous one, representing a large period variation and significant changes of the plant coefficients as indicated from poles and zeros displacement shown in Figure 5.9.

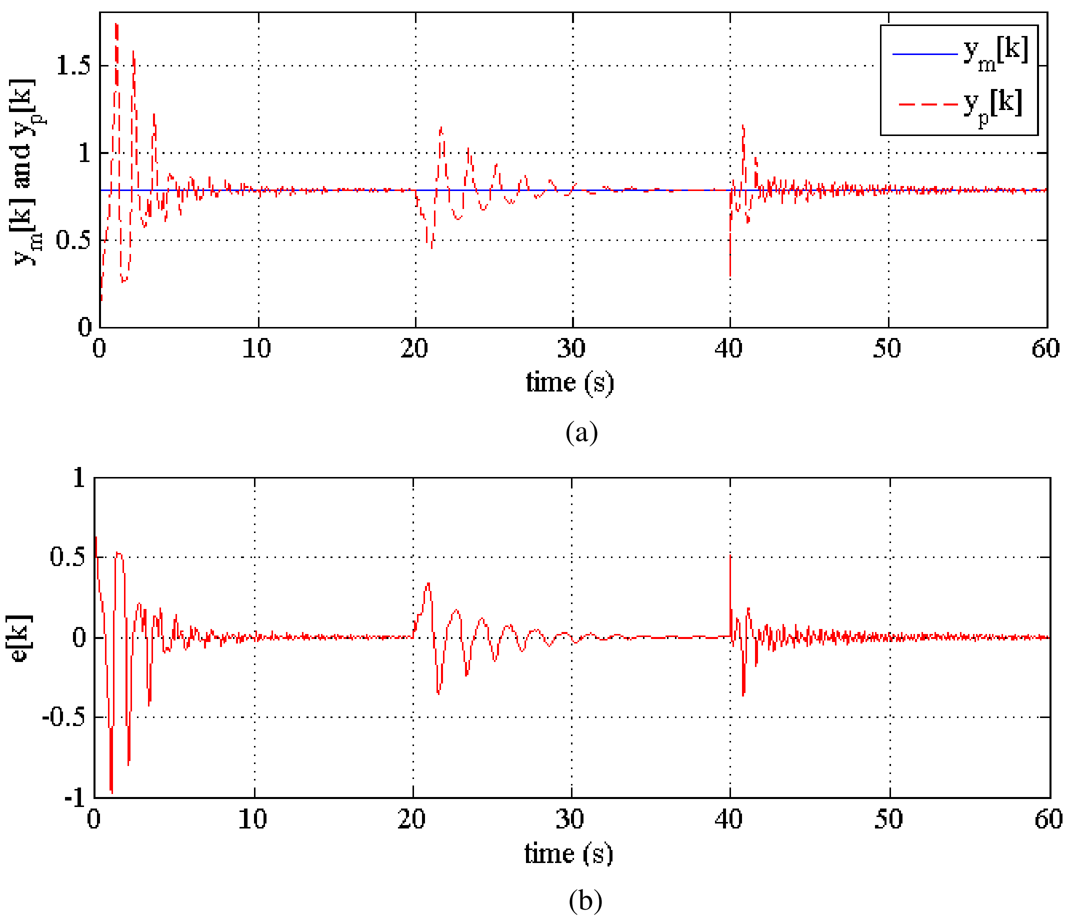

Figure 5.10 The proposed ARC performance tracking a constant reference (a) the system output (b) the output error

Figure 5.10 shows tracking a constant reference and rejecting a time varying periodic disturbance, in which all transient errors decay to zero. Similar performance has been achieved.

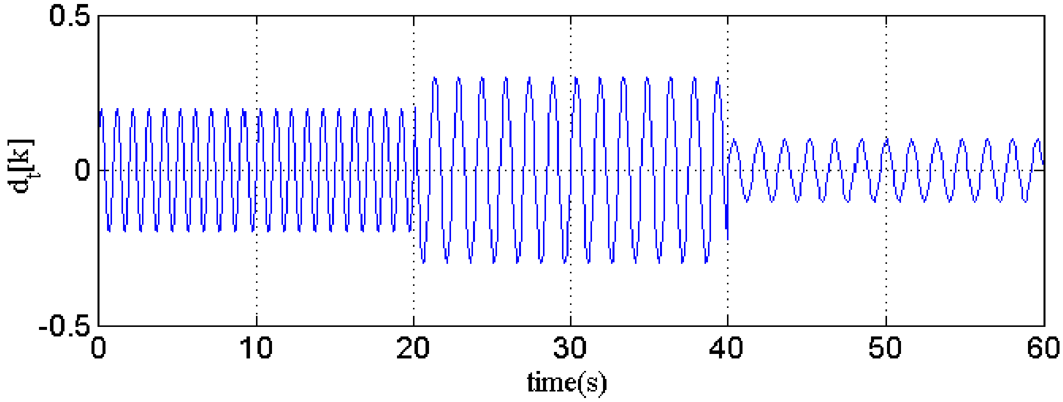

(a)

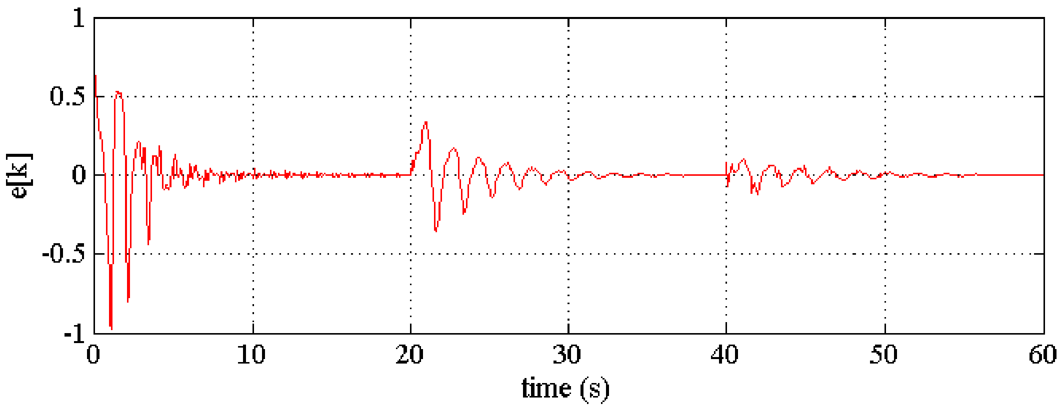

(b)

Figure 5.11 The proposed ARC tracking a constant reference with a graduate time varying disturbance (a) disturbance (b) the output error

Tracking a constant reference with a less time-varying disturbance is also simulated, in which the sampling period adapted as 0.05s, 0.075s and 0.08s. Figure 5.11(a) shows the disturbance and Figure 5.11(b) shows the error, in which the error is much smaller at the last transient compared with Figure 5.10(c).

5.4.3 A Comparison Study of ARC

This subsection presents the comparison study to show the significance of ARC design. The proposed ARC is compared with various existing controllers. Figure 5.12 shows the output error of the MRAC and prototype RC (PRC) [10] when the sampling period is fixed and a constant reference is used. In Figure 5.12 (a), the periodic disturbance exists in the MRAC output consistently, although the transient errors are smaller because of the constant sampling period and no change in the plant coefficients. Figure 5.12(b) shows the output error of the PRC does not converge to zero, when the sampling period is adapted to the disturbance period.

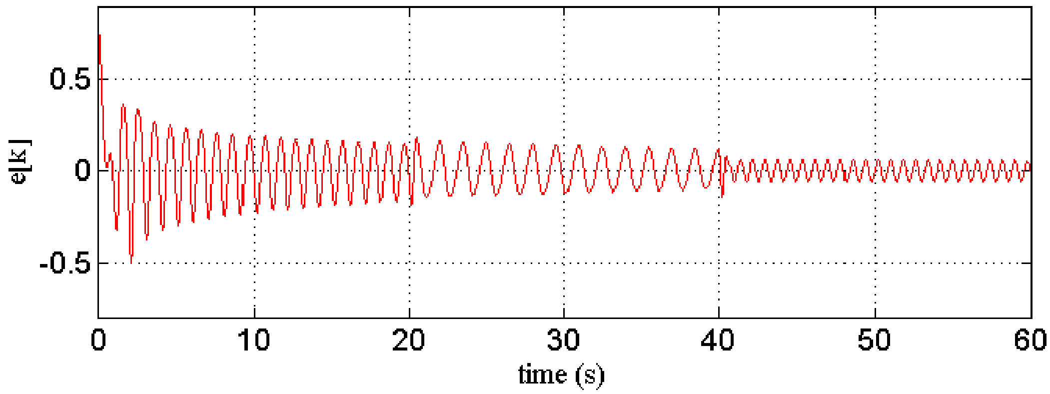

(a)

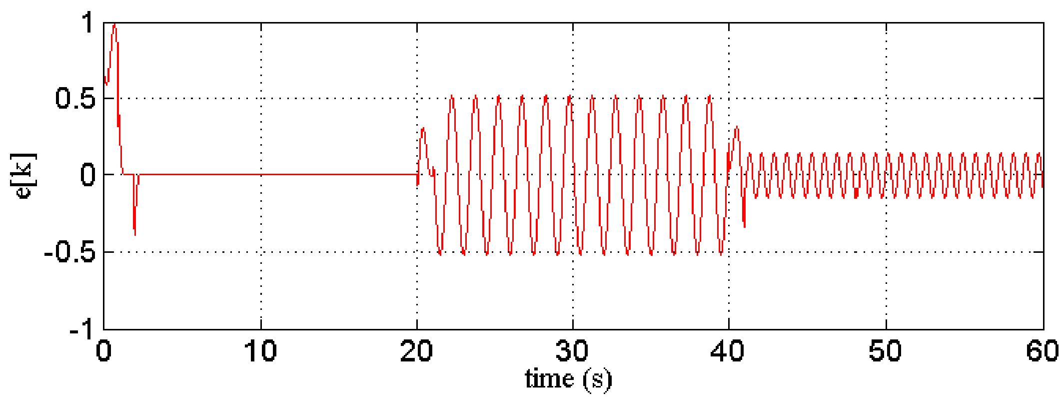

(b)

Figure 5.12 The output error with a fixed sampling period (a) using MRAC (b) using PRC.

Figure 5.13 shows the output errors when the sampling period is updated to keep a constant N samples per disturbance period. The output error of the MRAC exists persistently in Figure 5.13(a), while the output error of the ARC converges to zero in Figure 5.10(b). The magnitudes of the transient errors are similar in both cases, since the sampling period and plant coefficients are changing. Figure 5.13(b) shows the output error when the fixed PRC [10] based on zero phase error tracking controller (ZPETC) [11] is used, in which the system is unstable in the second transient, since the sampling period is varying and the system does not meet the stability condition [10], especially condition no. 2:

1. $G(z)$ is stable (5.98)

2. $|1 - F_{rc}(z)G(z)|_{\infty} < 1$ (5.99)

where $F_{rc}(z)$ is a ZPETC as proposed in (2.11)-(2.12).

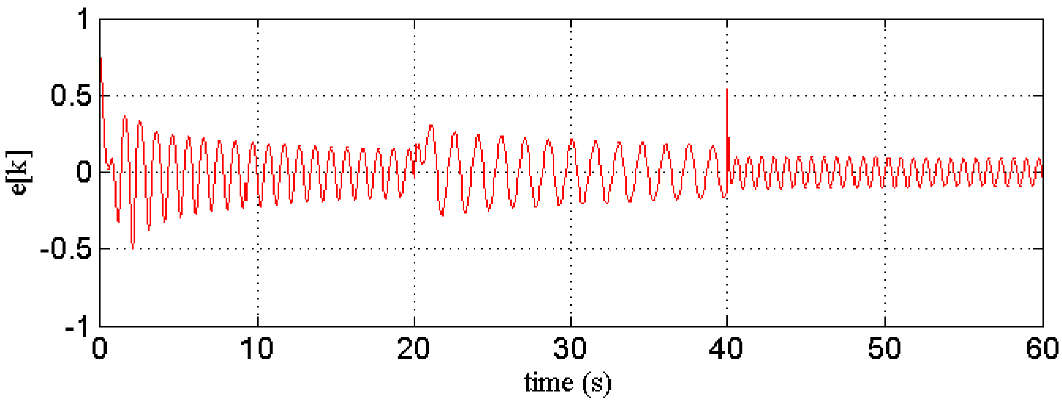

(a)

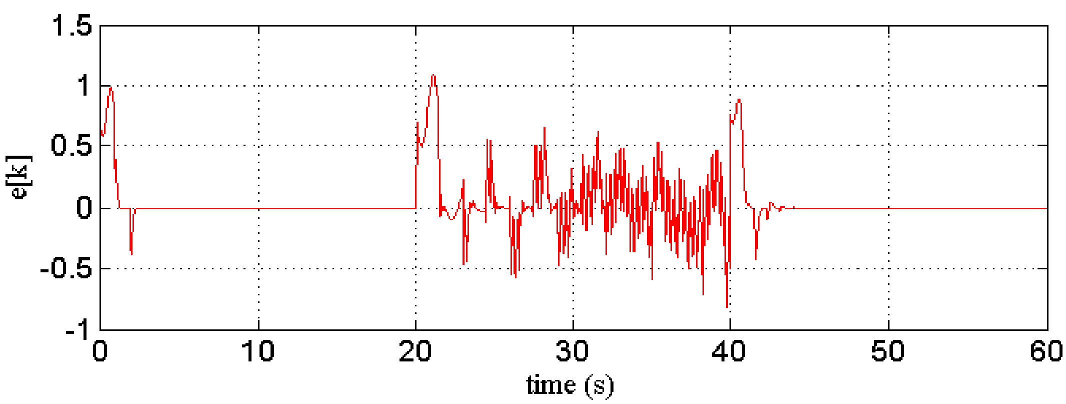

(b)

Figure 5.13 The output error with a time varying sampling period (a) using MRAC (b) using PRC.

5.5 EXPERIMENTAL RESULTS

This section presents the experimental results of using ARC. The real-time experiments were conducted on a Quanser servo motor SRV02-E with bar load. The aim of the system is to control the angle position of the servomotor to follow the triangle signal with a period of 10 s and a constant reference of $\pi/4$ rad (45 degrees). The plant input is corrupted by adding a disturbance, which is generated by computer.

The same disturbance shown in Figure 5.7 is used here. Figure 5.14 shows the control signal, servo output, and output error when the ARC is used to track a triangle signal. Figure 5.15 shows the control signal, servo output, and output error when the ARC is tracking a constant reference. In both cases, a similar performance has been achieved to the simulations.

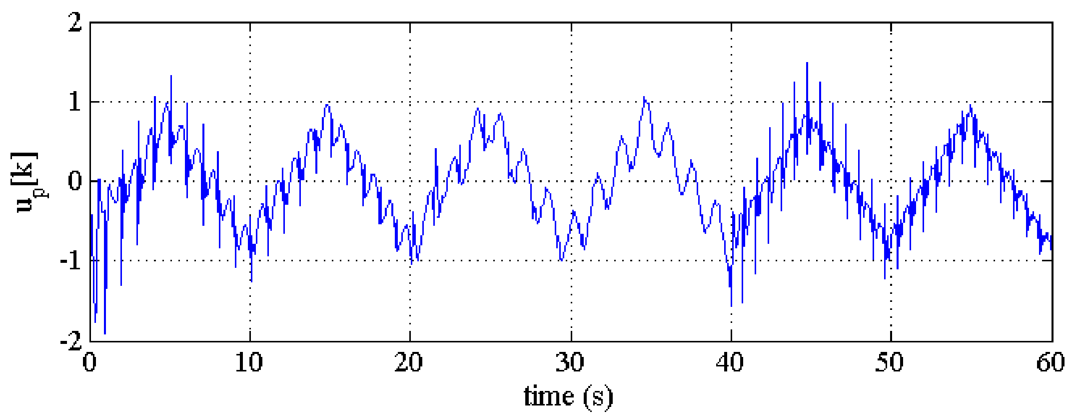

(a)

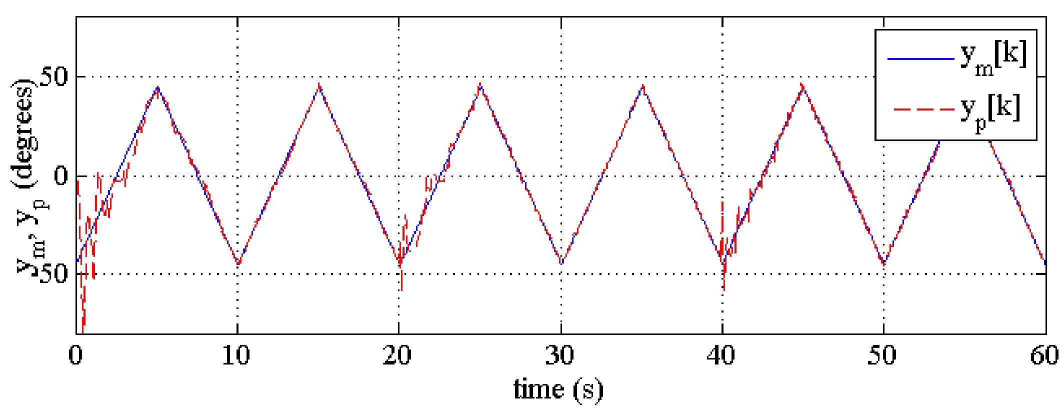

(b)

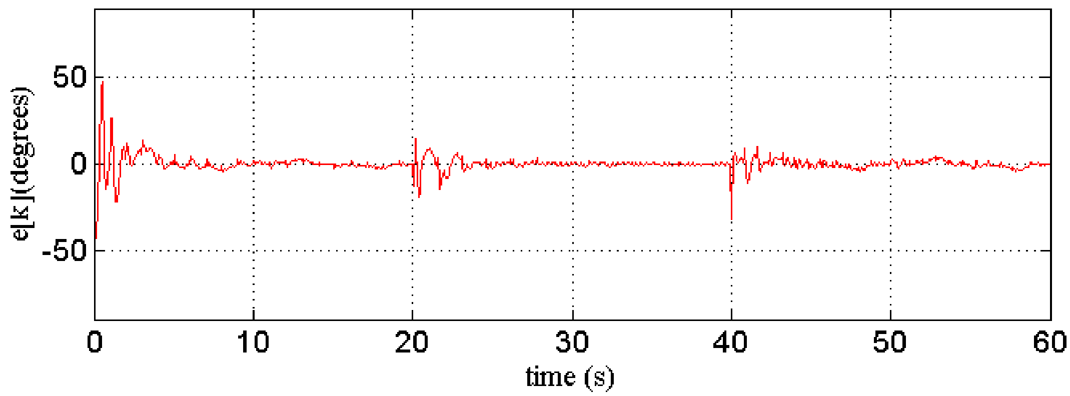

(c)

Figure 5.14 The proposed ARC with triangle reference signal (a) the control values (b) the system output (c) the output error

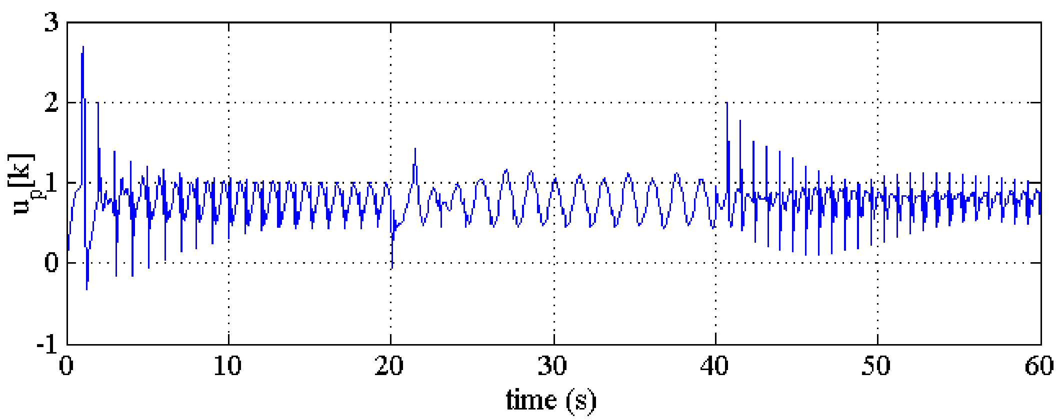

(a)

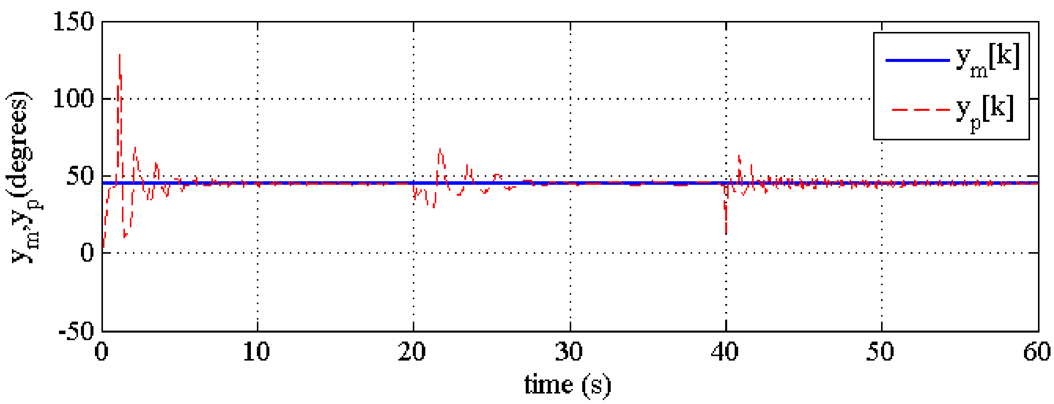

(b)

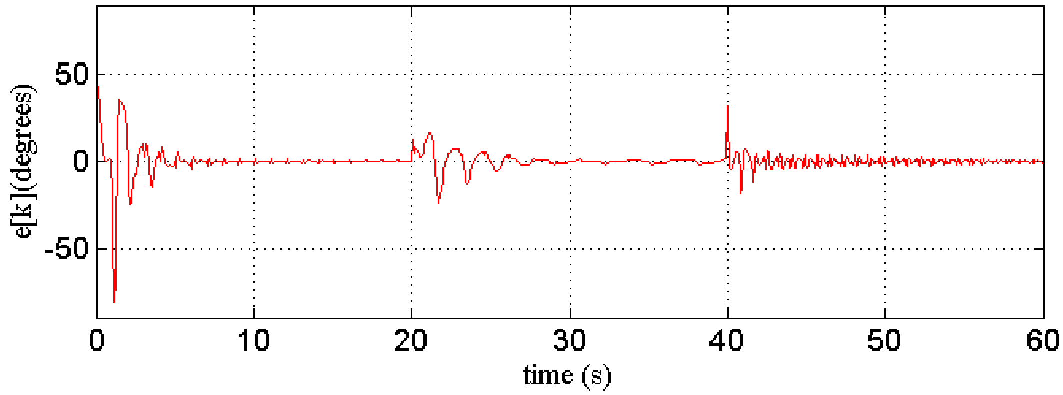

(b)

Figure 5.15 The proposed ARC with constant reference signal (a) the control values (b) the system output (c) the output error

The proposed ARC is compared with the PRC with: (a) a fixed sampling period (b) a time-varying sampling period. Figure 5.15 (a) shows the tracking error when the sampling period is kept fixed $T = 0.05\ s$. On the second and third interval, the perfect tracking is not achieved due to the number of samples per disturbance period is no longer N. Figure 5.15 (b) shows the tracking error when the sampling period is changed to keep N samples per period. On the second transient, the tracking error keeps increasing and becomes unstable. This is due to the change of plant parameters, which makes the closed-loop RC system is unstable.

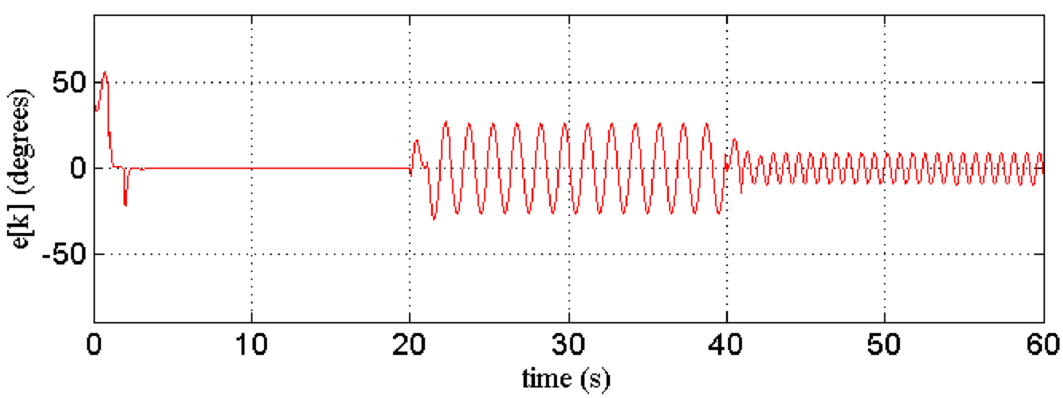

(a)

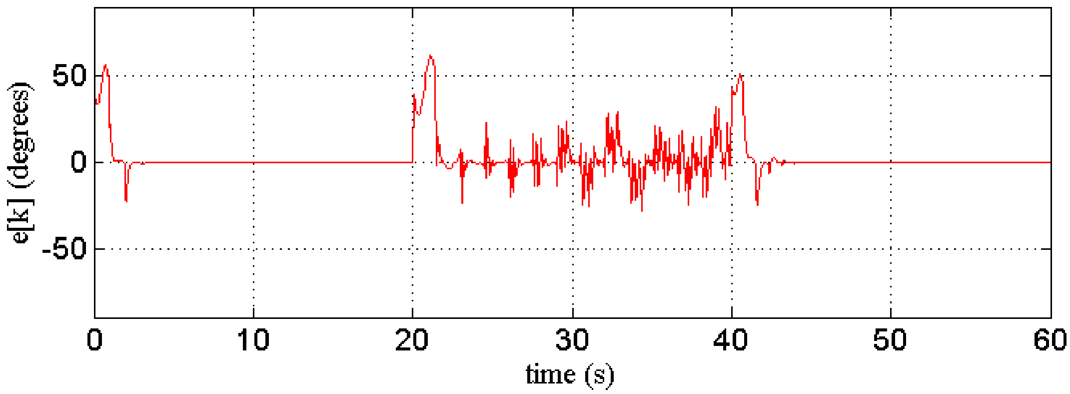

(b)

Figure 5.16 The output error $e(k)$ of the general RC with (a) fixed sampling period, (b) time-varying sampling period.

5.6 SUMMARY

This chapter has proposed an MRRC and ARC design method. Both MRRC and ARC can simultaneously track the periodic reference signal and reject the periodic disturbance, where the reference period is not necessarily the same or multiple of the disturbance period.

The MRRC scheme has successfully worked for known plant subject to periodic disturbance with fixed frequency. ARC has been proposed for an unknown linear system subject to periodic disturbances with time-varying frequency. The designed ARC can perfectly reject the disturbance since the number of samples per period remains fixed. The time-varying plant parameters have been handled by the MRAC which tunes the controller parameters such that the closed-loop system is stable and the plant output tracks the reference model output. Both simulations and experiments results have been presented to verify the effectiveness of the proposed design.

CHAPTER 6

DESIGN OF DECENTRALIZED RC OF LINEAR MIMO SYSTEMS

6.1 INTRODUCTION

In Chapters 4 and 5, RC designs were proposed for SISO systems. An RC design for MIMO systems will now be addressed in this chapter. Most of the designs for RC MIMO systems are based on the full MIMO approach, resulting in a controller with the same dimension as the plant. This implies that if we have an mxm MIMO system (m^2 transfer functions), then we need to design m^2 RC compensators. Moreover, the designs also end up with a non-causal compensator that needs to be merged with the internal model to make it realizable. This gives rise to complexity in the implementation, especially when the order of the internal model is very large.

The fact that most of MIMO control problems can be treated on decentralized basis [101] gives a motivation to design RC based on decentralized control, called as decentralized RC (DRC). Decentralized control means that the MIMO system is considered to be a set of SISO systems. In addition, the decentralized control design is considered to be easier as it can apply simpler SISO theories [101]. A further advantage of decentralized control here is only m RC compensators are required.

This chapter presents two approaches to decentralized RC (DRC) ; DRC-1 and DRC-2. Both approaches result in a low order, stable and causal compensators.

Moreover, there are only m compensators to be obtained from the proposed algorithms. A complete series of simulation and experiments is carried out to demonstrate the effectiveness of the proposed algorithms.

This chapter is organized as follows. Section 2 presents the design of DRC-1, which covers the RGA and robustness analysis, the decentralized stabilizing controller design, the compensator design, and the RC MIMO stability analysis. Section 3 discusses the design of DRC-2, which is more straightforward than the DRC-1 design. Simulation results and details of a comparison study conducted to PCI are also given in Section 4. Experimental results of the 2 DOF robot plant are presented in Section 5. Section 6 concludes the chapter.

6.2 DECENTRALIZED RC: APPROACH 1 (DRC-1)

Let a mxm MIMO system $\mathrm{G(s)}$ be represented by the following transfer functions

$$G(s) = \begin{bmatrix} g_{11}(s) & \cdots & g_{1m}(s) \\ \vdots & \ddots & \vdots \\ g_{m1}(s) & \cdots & g_{mm}(s) \end{bmatrix} \tag{6.1}$$

The plant model $\mathrm{G(s)}$ has m inputs and outputs, where the relation between inputs and outputs can be formulated as follows:

$$\begin{bmatrix} y_1(t) \\ y_2(t) \\ \vdots \\ y_m(t) \end{bmatrix} = \begin{bmatrix} g_{11}(s)u_1(t) + \cdots + g_{1m}(s)u_m(t) \\ g_{21}(s)u_1(t) + g_{22}(s)u_2(t)..+g_{2m}(s)u_m(t) \\ \vdots \\ g_{m1}(s)u_1(t)+..+g_{mm}(s)u_m(t) \end{bmatrix} \tag{6.2}$$

where$\mathrm{y_1(t), \dots, y_m(t)}$ and $\mathrm{u_1(t), \dots, u_m(t)}$ are plant outputs and inputs respectively.

Decentralized control aims to approximate the MIMO system into a set of independent SISO systems. This is different to decoupling control which tries to convert the full MIMO model into a perfect set of independent SISO models. The assumption in the design of decentralized control is to ignore dynamics that result in weak interactions. Each of the system outputs is approximated from the input response that makes the dominant contribution. Therefore, the degree of interaction needs to be quantified in the decentralized control. The Relative Gain Array (RGA) introduced by Bristol [112] is one of the techniques termed as dominant interaction control method that can be used to determine the best input output pairings for multivariable control [113].

RGA is defined as matrix Λ which is formulated as follows:

$$\Lambda = G(0).* [G^{-1}(0)]^T \tag{6.3}$$

where $\mathrm{G}(0)$ and $\mathrm{G}^{-1}(0)$ are the system dc gain matrix and its inverse, Notation $.*$ and T operate as element wise multiplication and transpose of the matrix respectively.

In particular, the best pairings are chosen from the entries of Λ which are large. Suppose the diagonal entries of Λ have larger values than the non-diagonal entries, then the best pairings are $[u_i, y_i]$ pairings, where $= 1, \dots, m$. This also means that we need to consider the transfer functions $g_{ii}(s)$ as the strong dynamics that give dominant contribution to the plant outputs.

Now, we need to choose the nominal complimentary sensitivity function $\mathrm{T(s)}$ as the desired stabilized closed-loop model of $\mathrm{g_{ii}(s)}$.

$$\mathrm{T(s) = diag[t_1(s), \dots, t_m(s)]} \tag{6.4}$$

With decentralized control, robustness analysis is needed to check the impact of the neglected dynamics [101]. To perform robustness analysis, the $\mathrm{G(s)}$ is first represented as the nominal model $\mathrm{G_n(s)}$ with additive uncertainty $\mathrm{G_\Delta(s)}$ [101].

$$\mathrm{G(s) = G_n(s)[I + G_\Delta(s)]} \tag{6.5}$$

where

$$\mathrm{G_n(s)} = \begin{bmatrix} \mathrm{g_{11}(s)} & 0 & 0 \\ 0 & \ddots & 0 \\ 0 & 0 & \mathrm{g_{mm}(s)} \end{bmatrix} \tag{6.6}$$

$$G_\Delta(s) = [G(s) - G_n(s)][G_n^{-1}(s)] \quad (6.7)$$

and I is a mxm identity matrix

Then, the robustness check is given by the stability condition as follows [101]:

$$\overline{\sigma}[G_\Delta(j\omega)T(j\omega)] < 1 \forall\ \omega \in \mathbb{R} \quad (6.8)$$

Equation (6.8) states that the maximum singular value of $[G_\Delta(j\omega)Gs(j\omega)]$ has to be less than one.

Once the robustness check has been performed, then the decentralized stabilizing controller $C(s)$ can be designed to match the chosen complimentary sensitivity function $T(s)$.

$$C(s) = \mathrm{diag}[c_1(s), \ldots, c_m(s)] \quad (6.9)$$

where $c_i(s), i = 1, \ldots, m$ are obtained to satisfy the following equality

$$\frac{c_i(s)g_{ii}(s)}{1 + c_i(s)g_{ii}(s)} = t_i(s) \quad (6.10)$$

Let $c_i(s)$, $g_{ii}(s)$, and $t_i(s)$ be expressed in the form of numerator and denumerator as follows:

$$c_i(s) = \frac{nc_i(s)}{dc_i(s)}, g_{ii}(s) = \frac{ng_{ii}(s)}{dg_{ii}(s)}, t_i(s) = \frac{nt_i(s)}{dt_i(s)} \quad (6.11)$$

The polynomials $nc_i(s)$ and $dc_i(s)$ can be obtained by solving the following Diophantine Equation

$$nc_i(s)[ng_{ii}(s)nt_i(s) - ng_{ii}(s)dt_i[s] + dc_i(s)[dg_{ii}(s)nt_i(s)] = 0 \quad (6.12)$$

The relative degree of the complimentary sensitivity function $t_i(s)$needs to be chosen carefully so that it gives proper stabilizing controller $c_i(s)$. The stabilizing controller $C(s)$ is designed to achieve the nominal complimentary sensitivity function $T(s)$, while the actual complimentary sensitivity function $G_c(s)$ is given as follows:

$$G_c(s) = [I + G(s)C(s)]^{-1}G(s)C(s) \tag{6.13}$$

Once $C(s)$ has been designed, then it is possible to proceed to the design of the compensator matrix $F(z)$, as shown in Figure 6.1. Figure 6.1 shows the configuration of a MIMO system with DRC-1 for tracking periodic reference.

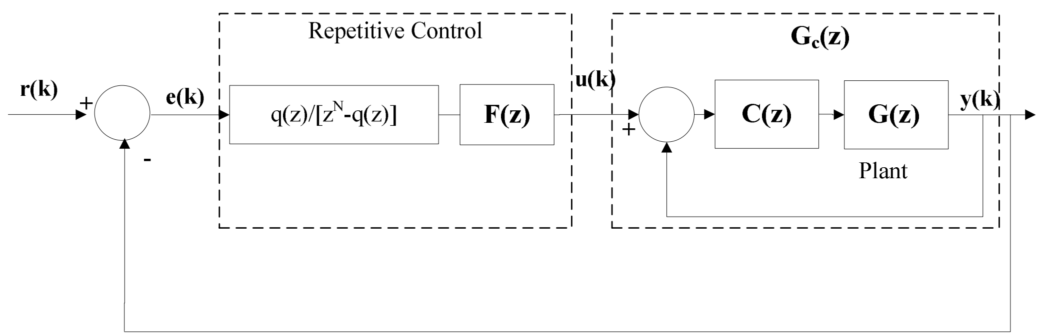

Figure 6.1 Block diagram of DRC-1

where $G_c(z)$ is the actual complimentary sensitivity function with mxm transfer functions, which is also the discrete model of (6.13)**,** $F(z)$is the compensator matrix with m transfer functions, r(k) is the periodic reference signal, e(k) is the tracking error, u(k) is the control signal, and y(k) is the tracking output. and $r(k), e(k), u(k), y(k) \in \mathbb{R}^m$

If RGA analysis suggests $[u_i, y_i]$ pairings, then the compensator matrix $F(z)$ will have elements only at the diagonal.

$$F(z) = \begin{bmatrix} f_{11}(z) & 0 & 0 \\ 0 & \ddots & 0 \\ 0 & 0 & f_{mm}(z) \end{bmatrix} \tag{6.14}$$

where $f_{11}(z) \dots f_{mm}(z)$ are stable and causal compensators.

The design of $F(z)$ is based on the information of complimentary sensitivity function $\mathrm{T(s)}$. Here, each component of matrix $F(z)$ is designed to compensate the dynamic of the respective component of $T(z)$, where $T(z)$ is the discrete model of $T(s)$ at sampling period T. The compensator $\mathrm{f}_{ii}(\mathrm{z})$ will be designed to compensate the dynamics of $\mathrm{t}_{ii}(\mathrm{z})$. As there are m pairings, then we only need to design m compensators to build matrix $F(z)$. Each component of $\mathrm{T(s)}$ can be assigned to have the same transfer function, and also in low order.

The RC compensator design mostly aims to mimics the inverse of the SISO plant model, and usually ends up with either non-causal or high order compensator. Here, the design scheme proposed in Chapter 4 can be used to obtain a low order, stable and causal compensator. Thus, the compensator $\mathrm{f}_{ii}(\mathrm{z})$ is in the following form.

$$\mathrm{f}_{ii}(\mathrm{z}) = \frac{q_0^{ii}\mathrm{z}^{\mathrm{n}} + q_1^{ii}\mathrm{z}^{\mathrm{n}-1} + \cdots + q_n^{ii}}{\mathrm{z}^{\mathrm{n}} + r_1^{ii}\mathrm{z}^{\mathrm{n}-1} + \cdots + r_n^{ii}}\ , \mathrm{n} > 0 \tag{6.15}$$

Let the period of reference signal and sampling period be T_r and T respectively. As the RC design is treated on a decentralized basis, then we have m separate RCs as follow;

$$g_{rc}^{ii}(\mathrm{z}) = \frac{\mathrm{q(z)}}{\mathrm{z}^{\mathrm{N}} - \mathrm{q(z)}}\mathrm{f}_{ii}(\mathrm{z}) \tag{6.16}$$

where $g_{rc}^{ii}(\mathrm{z})$ is the digital RC for the nominal sensitivity function $\mathrm{t}_{ii}(\mathrm{z})$, and $\mathrm{q(z)}$ is the chosen zero-phase low pass filter to improve the robustness, $N = {}^{T_r}/_{T}$.

An optimization problem similar to (4.16) is used to obtain a low order, stable and causal $f_{ii}(z)$.

$$\min_{(p_1^{ii},\dots,p_n^{ii},q_0^{ii},\dots,q_n^{ii})} h_{\text{Total}}^{ii} = \sum_{k=1}^{N/2} h_k^{ii} \ \forall\ \omega_k = 2\pi\frac{k}{NT}, k = 1,2..,N/2$$

Subject to:

$$1. \begin{bmatrix} -1+\delta \\ \cdot \\ \cdot \\ -1+\delta \end{bmatrix} < \begin{bmatrix} p_1^{ii} \\ \cdot \\ \cdot \\ p_n^{ii} \end{bmatrix} < \begin{bmatrix} 1-\delta \\ \cdot \\ \cdot \\ 1-\delta \end{bmatrix} \tag{6.17}$$

$$2.\ h_k^{ii} < 1-\tau, \forall\omega_k = 2\pi\frac{k}{NT}, k = 1,2..,N/2$$

where

$$h_k^{ii} = |(1 - t_{ii}(z)f_{ii}(z))q(z)|_{\omega=\omega_k} \tag{6.18}$$

$|.|_{\omega=\omega_k}$ stands for the magnitude at frequency ω_k

$p_1^{ii},\dots,p_n^{ii}$ are n real poles of $f_{ii}(z)$, δ and τ are small positive constants

Since $t_{ii}(z)$ and $q(z)$ are known, then the parameters of $f_{ii}(z)$ can be obtained by solving the nonlinear minimization above. If we assign $t_{ii}(z)$ to be the same for $i = 1,..,m$, then we only need to solve one optimization problem. Once the compensator $f_{ii}(z)$ have been obtained, then the compensator matrix $F(z)$ can be constructed. Each component of $F(z)$ is designed on separate SISO model, Therefore, there is no guarantee that $F(z)$ ensures the stability of a MIMO RC system. A stability check needs to be performed to ensure that the MIMO RC system is stable. The MIMO RC system shown in Fig is stable if the following condition is satisfied [73, 96].

$$\bar{\sigma}[(I - F(z)G_c(z))q(z)] < 1 \forall\ \omega \in \mathbb{R} \tag{6.19}$$

The design procedure for DRC-1 can be summarized as follows:

1. Perform RGA analysis to obtain the best pairings.
2. Choose the desired nominal complementary sensitivity function $T(s)$. Each component of $T(s)$ can be assigned to have the same transfer function, and can be chosen to be in a low order. This will result in a low order of compensator.
3. Conduct a robustness check (6.8) to analyse the impact of the neglected dynamics.
4. Obtain the decentralized stabilizing controller $C(s)$. The controller $C(s)$ is designed to achieve the nominal complementary sensitivity function $T(s)$. Each component of $C(s)$ can be obtained by solving the Diophantine Equation.
5. Solve the optimization problem (6.17). If components of $T(s)$ are assigned to have the same transfer function, only one optimization problem needs to be solved. Now, the matrix $F(z)$ can be constructed.
6. Conduct a stability check (6.19) to ensure the MIMO RC system is stable.

6.3 DECENTRALIZED RC: APPROACH 2 (DRC-2)

In DRC-1, the design consists of several steps which include obtaining the decentralized stabilizing controller $C(s)$, and assessing the stability of the MIMO RC system. In this section, we introduce a different approach to designing decentralized RC, known as DRC-2. The approach does not require a design of a decentralized stabilizing controller $C(s)$, or a stability check of MIMO RC system. The structure of the MIMO RC system with DRC-2 is shown in Figure below:

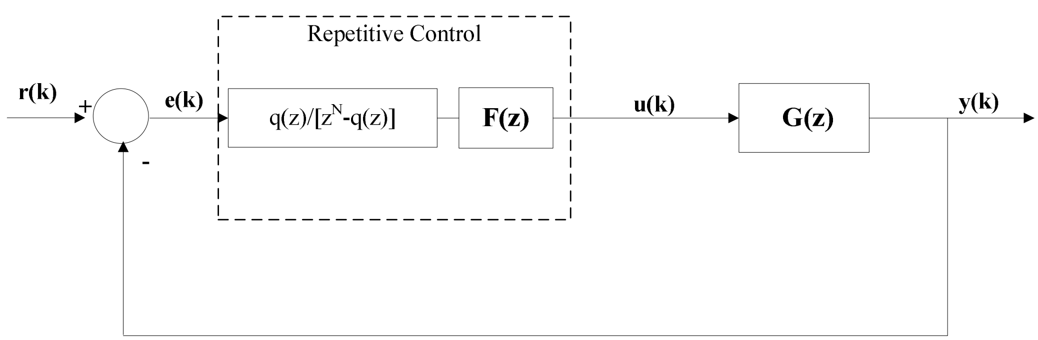

Figure 6.2 Block diagram of DRC-2

where $\mathrm{G(z)}$ is the discrete plant model with mxm transfer functions, and $F(z)$ is a compensator matrix with m transfer functions.

The transfer function from $R(z)$ to $Y(z)$, and the tracking error $E(z)$ of RC MIMO system shown in Figure 6.2 are respectively as follow:

$$\frac{\mathrm{Y(z)}}{\mathrm{R(z)}} = \frac{\mathrm{q(z)F(z)G(z)}}{[\mathrm{z^N I - (I - F(z)G(z))q(z)}]} \tag{6.20}$$

$$\mathrm{E(z)} = \frac{1}{[\mathrm{z^N I - (I - F(z)G(z))q(z)}]}[\mathrm{z^N - q(z)]R(z)} \tag{6.21}$$

Let $S(z)$ and $M(z)$ be:

$$\mathrm{S(z)} = [\mathrm{z^N I - (I - F(z)G(z))q(z)}] \tag{6.22}$$

$$\mathrm{M(z)} = \mathrm{(I - F(z)G(z))q(z)} \tag{6.23}$$

The stability of the MIMO system can be examined from the location of the zeros of its characteristic equation. The characteristic equation of MIMO RC system above can be obtained by calculating the determinant of $S(z)$. To be stable, all zeros of $\det S(z)$ have to be inside the unit circle. Calculating the determinant of $S(z)$ is troublesome because of the high order of N. Therefore, examining the location of zeros of $\det S(z)$ is very ineffective. From Equation (6.20)-(6.21), the stability of the MIMO RC system can be assessed in more simple way. The overall system stable if [73, 96]:

$$\overline{\sigma}[M(z)] < 1 \; \forall \; 0 < \omega < \frac{\pi}{\mathrm{T}} \tag{6.24}$$

where $\overline{\sigma}(.)$ stands for the maximum singular value, $M(z)$ is as shown in (6.23), and T is the sampling period

The stability condition (6.24) implies that the maximum singular value has to be less than for all frequencies up to Nyquist. The maximum singular value of $M(z)$ is a norm of the matrix $M(z)$, and also defined as the square root of the maximum eigenvalue of $M^H M$. In MIMO, the maximum singular value is considered as the gain of the system, which is also function of frequency [101].

$$\overline{\sigma}[M(z)] = \sqrt{\lambda_{max}(M^H M)} \qquad (6.25)$$

where $\lambda_{\mathrm{max}}(.)$ is the maximum eigenvalues of the Hermitian matrix $\mathrm{M^H M}$, and the notation H operates as the complex conjugate transpose.

The matrix $\mathrm{M(z)}$ is the functions of z, where z is equal to $e^{j\omega T}$. The singular value is evaluated at every frequency up to Nyquist. By replacing z with $e^{j\omega T}$, and picking a single frequency ω, the elements of matrix $\mathrm{M(z)}$ become complex numbers now. Multiplying $\mathrm{M(z)}$ with $\mathrm{M^H}(z)$ results in Hermitian matrix $\mathrm{M^H M}$. The eigenvalues of Hermitian matrix $\mathrm{M^H M}$ are real positives; $eig(\mathrm{M^H M}) = \lambda_1, \ldots, \lambda_m$, $\lambda_i > 0, i = 1, .., m$. Then, a maximum eigenvalue is simply the largest value of $(\lambda_1, \ldots, \lambda_{\mathrm{m}})$".

Xu [73] developed several stability conditions that also ensure the asymptotic stability of the MIMO RC system. One of the stability conditions proposed in [73] , which is less restrictive than (6.24) is given as follows:

$$|\det(M(z))| < 1 \; \forall \; 0 < \omega < \frac{\pi}{\mathrm{T}} \qquad (6.26)$$

Reference [73] strongly stated that the tracking error of RC MIMO system converges to zero for all possible N, and for all possible initial conditions, if only if the magnitude of the determinant of $M(z)$ is less than one for all frequencies up to Nyquist. Later on, the stability condition (6.26) is used as a constraint in the proposed optimization problem to obtain the compensator parameters.

Let $G(z)$ be a discrete plant model at sampling period T:

$$G(z) = \begin{bmatrix} g_{11}(z) & \cdots & g_{1m}(z) \\ \vdots & \ddots & \vdots \\ g_{m1}(z) & \dots & g_{mm}(z) \end{bmatrix} \tag{6.27}$$

To build the compensator matrix $F(z)$, we also need the information regarding the best pairings obtained from RGA analysis. For simplicity, suppose RGA analysis also suggest $[\mathrm{u_i}, \mathrm{y_i}]$ pairings, then matrix $F(z)$ only has elements on diagonal. Since the idea of DRC here is about designing F(z) for compensating the strong dynamics in $G(z)$, a single objective function can be formulated:

$$h_{Total} = \sum_{i=1}^{m} \sum_{\mathrm{k}=1}^{\mathrm{N}/2} |(1 - \mathrm{g}_{ii}(\mathrm{z})\mathrm{f}_{ii}(\mathrm{z}))\mathrm{q}(\mathrm{z})|_{\omega=\omega_\mathrm{k}} \ \forall\ \omega_\mathrm{k} = 2\pi \frac{\mathrm{k}}{\mathrm{NT}} \tag{6.28}$$

Supposed $\mathrm{f}_{ii}(\mathrm{z})$ has the same causal form as shown in (6.15). Let the chosen order for compensator $\mathrm{f}_{ii}(\mathrm{z})$ be n_i. Then, the number of parameters of the matrix $F(z)$ to be obtained is:

$$n_{Total} = \sum_{i=1}^{m} 2n_i + 1 \tag{6.29}$$

The optimization problem (6.30) is proposed in order to obtain the causal compensator $f_{ii}(z)$ for $i = 1, .., m$, in which the obtained matrix $F(z)$ guarantees the stability of the MIMO RC system.

$$\begin{aligned} &\min_{(p_1^{11},\dots,p_{n_1}^{11},\dots,p_1^{mm},\dots,p_{n_m}^{mm},q_0^{11},\dots,q_{n_1}^{11},\dots,q_0^{mm},\dots,q_{n_m}^{mm})} h_{Total} \\ &\text{Subject to:} \\ &1.1. \begin{bmatrix} -1+\delta \\ \cdot \\ \cdot \\ -1+\delta \end{bmatrix} < \begin{bmatrix} \mathrm{p}_1^{11} \\ \cdot \\ \cdot \\ p_{n_1}^{11} \end{bmatrix} < \begin{bmatrix} 1-\delta \\ \cdot \\ \cdot \\ 1-\delta \end{bmatrix} \\ &1.2. \begin{bmatrix} -1+\delta \\ \cdot \\ \cdot \\ -1+\delta \end{bmatrix} < \begin{bmatrix} \mathrm{p}_1^{22} \\ \cdot \\ \cdot \\ p_{n_2}^{22} \end{bmatrix} < \begin{bmatrix} 1-\delta \\ \cdot \\ \cdot \\ 1-\delta \end{bmatrix} \\ &\qquad\qquad \dots \end{aligned} \tag{6.30}$$

$$1m.\begin{bmatrix}-1+\delta\\ \cdot\\ \cdot\\ -1+\delta\end{bmatrix} < \begin{bmatrix}p_1^{mm}\\ \cdot\\ \cdot\\ p_{n_m}^{11}\end{bmatrix} < \begin{bmatrix}1-\delta\\ \cdot\\ \cdot\\ 1-\delta\end{bmatrix}$$

$$2.\ |\det(M(z))|_{\omega_k} < 1-\tau, \forall\omega_k = 2\pi\frac{k}{NT}, k = 1,2..,N/2$$

where

$p_1^{11}, \dots, p_{n_1}^{11}$ are n_1 real poles of $f_{11}(z)$

$p_1^{22}, \dots, p_{n_2}^{22}$ are n_2 real poles of $f_{22}(z)$

$p_1^{mm}, \dots, p_{n_m}^{mm}$ are n_m real poles of $f_{mm}(z)$

$|\det(M(z))|_{\omega_k}$ is the magnitude of the determinant of $M(z)$ at frequency ω_k, and

δ and τ are small positive constants.

Remark 6.1: The first condition of (6.30) consists of $\sum_{i=1}^{m} n_i$ constraints which guarantees that all poles of the elements of the matrix $F(z)$ are inside the unit circle. The positive constant δ presents a minimum distance of all poles from the unit circle. This condition ensures that the obtained compensators are stable within a safe margin.

Remark 6.2: The second condition of (6.30) guarantees that the MIMO RC system is stable within a positive margin of τ.

The optimization problem (6.30) is a class of nonlinear minimization that finds $\sum_{i=1}^{m} 2n_i + 1$ optimum variables subject to $\sum_{i=1}^{m} n_i$ bound constraints and $N/2$ (for an even N) nonlinear constraints. Solving this minimization problem (6.30) gives all parameters of $F(z)$, but at the expense of larger number of variables to optimized compared to number of variables in the optimization of DRC-1.

The design procedure of DRC-2 here can be summarized as follow:

1. Perform RGA analysis to obtain the best pairings
2. Solve the optimization problem (6.30) to obtain all parameters of $F(z)$.

The proposed DRCs are still limited for a class of mxm MIMO model. This is due to the RGA analysis and MIMO stability assessment require to calculate the inverse of the matrix. Hence, the matrix needs to be square, which means the number of inputs is similar to the number of outputs.

6.4 SIMULATION RESULTS

Simulation is now performed to validate the effectiveness of the two proposed approaches. The advantage and disadvantage of both approaches will be discussed. A comparison study conducted to PCI [96] is also given in this section.

6.4.1 SIMULATION OF DRC-1

A two-input two -output MIMO model of pick and place robot arm [100] is used to verify the effectiveness of DRC-1. The MIMO model has the following transfer functions:

$$G(s) = \begin{bmatrix} g_{11}(s) & g_{12}(s) \\ g_{21}(s) & g_{22}(s) \end{bmatrix} \tag{6.31}$$

where $g_{11}(s), g_{12}(s), g_{21}(s)$, and $g_{22}(s)$ are given as follows:

$$g_{11}(s) = \frac{0.16s^9 + 14.51s^8 + 578.2s^7 + 1.392e4s^6 + 2.26e5s^5 + \cdots}{5.3e-5s^{12} + 0.02s^{11} + 0.91s^{10} + 31.2s^9 + 714.1s^8 + 1.2e4s^7 + \cdots} \frac{2.58e6s^4 + 2.09e7s^3 + 1.17e8s^2 + 4.21e8s + 7.6e8}{1.45e5s^6 + 1.4e6s^5 + 1.01e7s^4 + 5.7e7s^3 + 2.3e8s^2 + 5.9e8s + 7.6e8} \tag{6.32}$$

$$g_{12}(s) = \frac{-0.022s^7 - 3.24s^6 - 88.3s^5 - 1347s^4 - 1.06e4s^3 + \cdots}{5.3e-5s^{10} + 0.014s^9 + 0.72s^8 + 20s^7 + 363s^6 + 4645s^5 + \cdots} \frac{-4.52e4s^2}{4.3e4s^4 + 2.9e5s^3 + 1.4e6s^2 + 4.18e6s + 6.32e6} \tag{6.33}$$

$$g_{21}(s) = \frac{-0.16s^7 - 8.7s^6 - 194s^5 - 2498s^4 - 1.78e4s^3 + \cdots}{5.2e-5s^{10} + 0.014s^9 + 0.72s^8 + 20s^7 + 363s^6 + 4645s^5 + \cdots} \qquad (6.34)$$
$$\frac{-6.64e4s^2}{4.3e4s^4 + 2.9e5s^3 + 1.4e6s^2 + 4.18e6s + 6.32e6}$$

$$g_{11}(s) = \frac{0.027s^9 + 4.95s^8 + 264s^7 + 7394s^6 + 1.3e5s^5 + \cdots}{5.3e-5s^{12} + 0.014s^{11} + 0.9s^{10} + 31s^9 + 714.1s^8 + 1.19e4s^7 + \cdots} \qquad (6.35)$$
$$\frac{1.69e6s^4 + 1.5e7s^3 + 9.4e7s^2 + 3.8e8s + 7.6e8}{1.48e5s^6 + 1.4e6s^5 + 1.04e7s^4 + 5.7e7s^3 + 2.3e8s^2 + 5.9e8s + 7.6e8}$$

We can see that each element of the matrix $G(s)$ is in high order. The zeros and poles of the plant are the zeros and poles of determinant of $G(s)$. The det $[G(s)]$ has 38 zeros and 44 poles, and all zeros and poles are on the left half plane (LHP). Thus, the continuous model (6.31) is a stable and minimum phase MIMO plant.

The RGA of $G(s)$ is calculated as follows:

$$\Lambda = \begin{bmatrix} 1 & 0 \\ 0 & 1 \end{bmatrix} .* \left(\begin{bmatrix} 1 & 0 \\ 0 & 1 \end{bmatrix}^{-1} \right)^{T} = \begin{bmatrix} 1 & 0 \\ 0 & 1 \end{bmatrix} \qquad (6.36)$$

The RGA value Λ shows that the dynamic $g_{11}(s)$ and $g_{22}(s)$ give dominant interaction to output $y_1(t)$ and $y_2(t)$ respectively. The RGA suggests that the best pairings are $[u_1, y_1]$ and $[u_2, y_2]$. This also means that we only need to consider the dynamics of $g_{11}(s)$ and $g_{22}(s)$. Before designing the decentralized stabilizing controller $C(s)$, robust analysis needs to be performed to check the impact of the neglected dynamics $g_{12}(s)$ and $g_{21}(s)$. Let the desired complimentary sensitivity function $T(s)$ be:

$$T(s) = \begin{bmatrix} t_1(s) & 0 \\ 0 & t_2(s) \end{bmatrix} \qquad (6.37)$$

where

$$t_1(s) = t_2(s) = \frac{100}{(s^2 + 6s + 16)(s + 25)} \tag{6.38}$$

The $t_1(s)$ and $t_2(s)$ are chosen to have the same transfer function with relative degree 3. The choice of the relative degree of $t_1(s)$ and $t_2(s)$ will affect the properness of the stabilizing controller $C(s)$.

If the actual model is represented as $G(s) = G_n(s)[I + G_\Delta(s)]$, then the nominal model $G_n(s)$ and the uncertainty model $G_\Delta(s)$ are given respectively as follow:

$$G_n(s) = \begin{bmatrix} g_{11}(s) & 0 \\ 0 & g_{22}(s) \end{bmatrix} \tag{6.39}$$

$$G_\Delta(s) = \begin{bmatrix} 0 & g_{12}(s)/g_{22}(s) \\ g_{21}(s)/g_{11}(s) & 0 \end{bmatrix} \tag{6.40}$$

Singular values of $G_\Delta(j\omega)T(j\omega)$ are shown in Figure 6.3

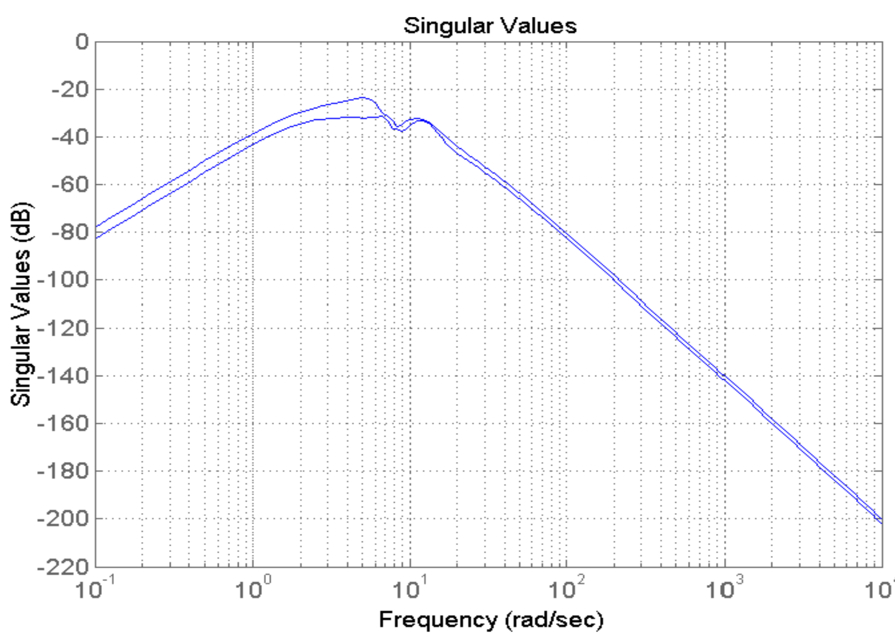

Figure 6.3 Singular values of $G_\Delta(j\omega)T(j\omega)$

The upper line in Figure 6.3 shows the maximum singular values of $G_\Delta(j\omega)T(j\omega)$, which are less than 0 dB for all frequencies. Thus, the impact of the neglected dynamics is acceptable. Now, we can proceed to design the decentralized stabilizing controller $\mathrm{C(s)}$.

The decentralized stabilizing controller $\mathrm{C(s)}$ is obtained by solving the following Diophantine Equations as follows:

$$\mathrm{nc_1(s)[ng_{11}(s)nt_1(s) - ng_{11}(s)dt_1(s] + dc_1(s)[dg_{11}(s)nt_1(s)] = 0} \qquad (6.41)$$

$$\mathrm{nc_2(s)[ng_{22}(s)nt_2(s) - ng_{22}(s)dt_2(s] + dc_2(s)[dg_{22}(s)nt_2(s)] = 0} \qquad (6.42)$$

The obtained controller $\mathrm{C(s)}$ is

$$\mathrm{C(s)} = \begin{bmatrix} \frac{\mathrm{nc_1(s)}}{\mathrm{dc_1(s)}} & 0 \\ 0 & \frac{\mathrm{nc_2(s)}}{\mathrm{dc_2(s)}} \end{bmatrix} = \begin{bmatrix} \mathrm{c_1(s)} & 0 \\ 0 & \mathrm{c_2(s)} \end{bmatrix} \qquad (6.43)$$

where $\mathrm{c_1(s)}$ and $\mathrm{c_2(s)}$ are

$$\begin{aligned}\mathrm{c_1(s)} &= \frac{5.4\mathrm{e}-5\mathrm{s}^{12} + 1.4\mathrm{e}-2\mathrm{s}^{11} + 0.93\mathrm{s}^{10} + 31.9\mathrm{s}^9 + 730\mathrm{s}^8 + 1.22\mathrm{e}4\mathrm{s}^7 + \cdots}{1.6\mathrm{e}-3\mathrm{s}^{12} + 0.19\mathrm{s}^{11} + 10.19\mathrm{s}^{10} + 319.5\mathrm{s}^9 + 6761\mathrm{s}^8 + 1.02\mathrm{e}5\mathrm{s}^7 + \cdots} \qquad (6.44) \\ &\quad \frac{1.5\mathrm{e}5\mathrm{s}^6 + 1.43\mathrm{e}6\mathrm{s}^5 + 1.03\mathrm{e}7\mathrm{s}^4 + 5.83\mathrm{e}7\mathrm{s}^3 + 2.35\mathrm{e}8\mathrm{s}^2 + 6.03\mathrm{e}8\mathrm{s} + 7.8\mathrm{e}8}{1.1\mathrm{e}6\mathrm{s}^6 + 9.3\mathrm{e}7\mathrm{s}^5 + 5.5\mathrm{e}7\mathrm{s}^4 + 2.2\mathrm{e}8\mathrm{s}^3 + 5.6\mathrm{e}8\mathrm{s}^2 + 6.1\mathrm{e}8\mathrm{s}}\end{aligned}$$

$$\begin{aligned}\mathrm{c_2(s)} &= \frac{1.6\mathrm{e}-13\mathrm{s}^{12} + 4.3\mathrm{e}-11\mathrm{s}^{11} + 2.7\mathrm{e}-9\mathrm{s}^{10} + 9.5\mathrm{e}-8\mathrm{s}^9 + 2.2\mathrm{e}-6\mathrm{s}^8 + \cdots}{8.3\mathrm{e}-13\mathrm{s}^{12} + 1.7\mathrm{e}-10\mathrm{s}^{11} + 1.2\mathrm{e}-8\mathrm{s}^{10} + 4.6\mathrm{e}-7\mathrm{s}^9 + 1.1\mathrm{e}-5\mathrm{s}^8 + \cdots} \qquad (6.45) \\ &\quad \frac{3.6\mathrm{e}-5\mathrm{s}^7 + 4.5\mathrm{e}-4\mathrm{s}^6 + 4.3\mathrm{e}-3\mathrm{s}^5 + 0.03\mathrm{s}^4 + 0.17\mathrm{s}^3 + 0.7\mathrm{s}^2 + 1.8\mathrm{s} + 2.3}{1.8\mathrm{e}-4\mathrm{s}^7 + 2.2\mathrm{e}-3\mathrm{s}^6 + 0.02\mathrm{s}^5 + 0.13\mathrm{s}^4 + 0.6\mathrm{s}^3 + 1.6\mathrm{s}^2 + 1.8\mathrm{s}}\end{aligned}$$

Let the period of reference signal and sampling period be 8 s and 0.04 s respectively. The discrete models of $\mathrm{t_1(s)}$ and $\mathrm{t_2(s)}$ are:

$$t_1(z) = t_2(z) = \frac{8.2e - 4(z + 2.88)(z + 0.2)}{(z - 0.37)(z^2 - 1.88z + 0.88)} \tag{6.46}$$

Both discrete-time $t_1(z)$ and $t_2(z)$are non-minimum phase model because they have a zero outside the unit circle.

The order of compensator $n = 3$ is chosen. This follows the suggestion in Chapter 4 that the compensator order should be equal or higher than the plant order to give good phase and magnitude compensation. The zero phase low pass filter $q(z)$, and positive constants δ and τ are chosen respectively as follows:

$$q(z) = 0.25z + 0.5 + 0.25z^{-1}, \delta = 0.075, \tau = 0.05 \tag{6.47}$$

The compensator $f_{11}(z)$ is obtained by solving the optimization problem (6.17) using an Optimization Toolbox from Matlab. Since we assign $t_1(z)$ as equal to $t_2(z)$, only one optimization problem needs to be solved.

$$F(z) = \begin{bmatrix} f_{11}(z) & 0 \\ 0 & f_{22}(z) \end{bmatrix} \tag{6.48}$$

where

$$f_{11}(z) = f_{22}(z) = \frac{475.6z^3 - 1046z^2 + 704.1z - 131.2}{z^3 + 2.10z^2 + 1.33z + 0.22} \tag{6.49}$$

Equation (6.48)-(6.49) show that two elements of $F(z)$ have the same transfer function, and they are in lower order compared to the order of $g_{11}(z)$ and $g_{22}(z)$. The compensator matrix $F(z)$ is designed to compensate low order nominal complimentary sensitivity function $T(z)$, while the actual stabilized complimentary sensitivity function is $G_c(z)$ which is the discrete model of (6.13). The stability check (6.19) is performed to ensure the stability of the MIMO RC system, and the singular values of $[(I - F(z)G_c(z))q(z)]$ is shown in Figure 6.4.

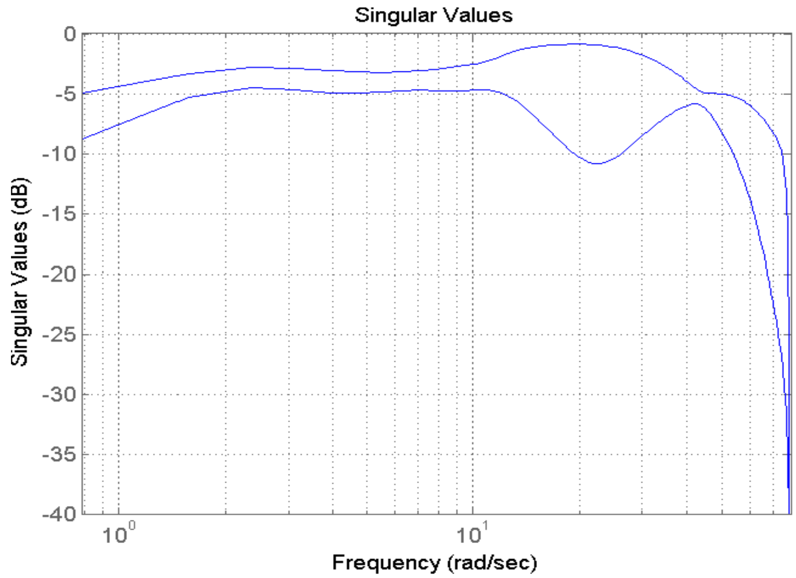

Figure 6.4 Singular values of $[(\mathrm{I}-\mathrm{F(z)G_c(z)})\mathrm{q(z)}]$

Figure 6.4 shows that the maximum singular values of $[(\mathrm{I}-\mathrm{F(z)G_c(z)})\mathrm{q(z)}]$ are less than one for all frequencies up to Nyquist. Hence, the MIMO RC system using the obtained compensator matrix $\mathrm{F(z)}$ is stable.

In the simulation, two tracking schemes are presented. In the first scheme, the first channel y_1 is required to track triangle reference signal, while the second channel y_2 needs to stay idle. In the second scheme, both channels are required to track the triangle reference signals with different amplitudes. The tracking output and tracking error for the first scheme is shown in Figure 6.5.

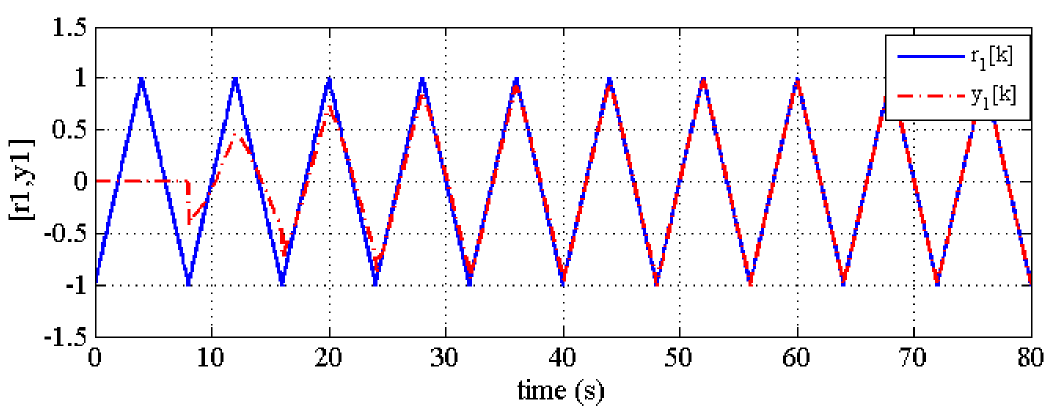

(a)

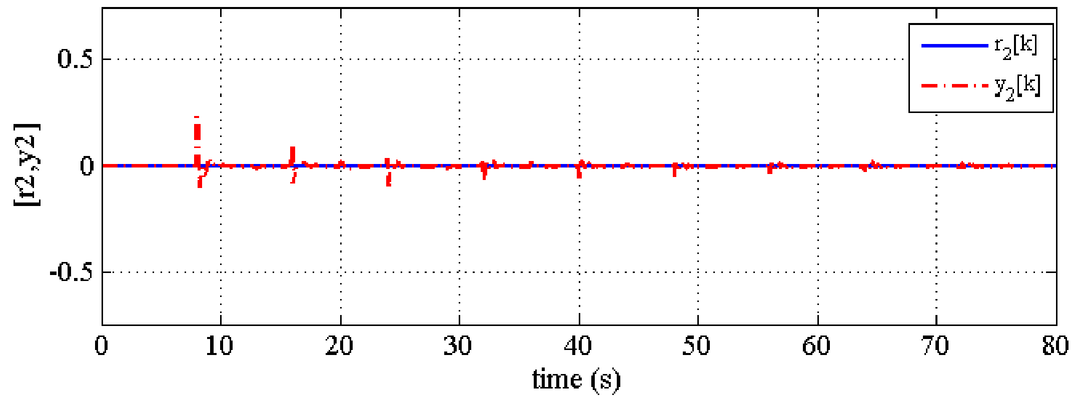

(b)

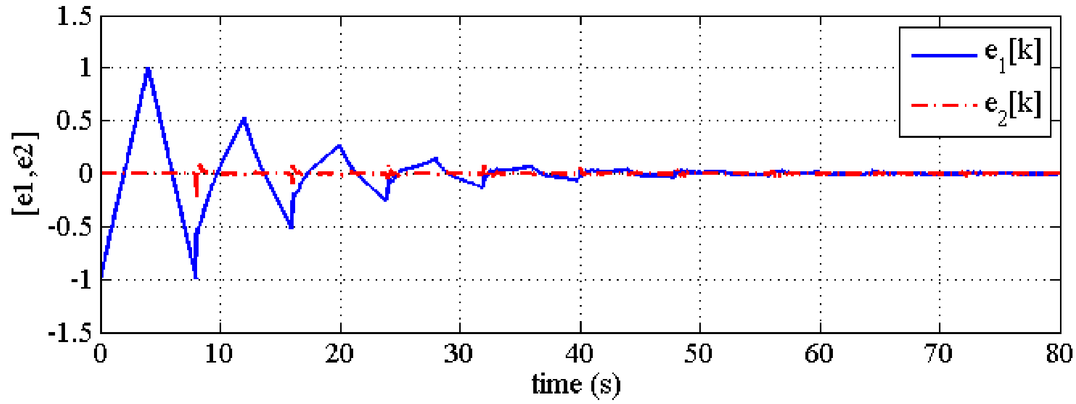

(c)

Figure 6.5 The first scheme (a) Tracking output $y_1(k)$,(b) Tracking output $y_2(k)$, (c).Tracking errors $e_1(k)$ and $e_2(k)$

The first scheme aims to emphasize the effect of neglected dynamics in this decentralized control. On Channel 1, the tracking output y_1 is able to follow periodic reference r_1 after 4 repetitions. On channel 2, a small excitation due to the coupling effect appears on output y_2. The tracking output and tracking error for the second scheme is shown in Figure 6.6. Figure 6.6 shows good tracking performance for both channel 1 and 2. The simulation results verify the effectiveness of DRC 1.

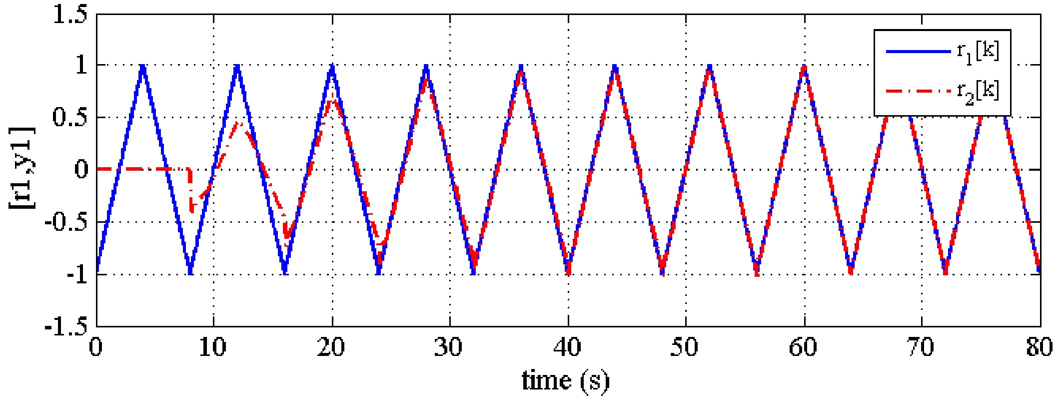

(a)

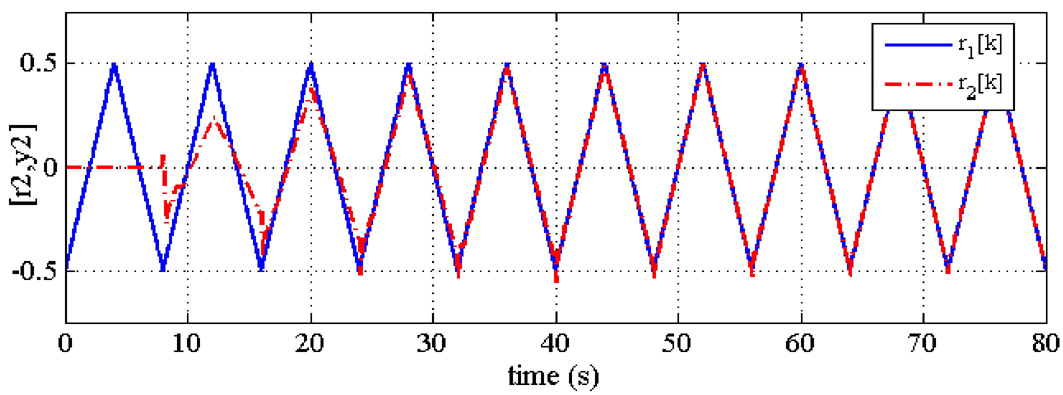

(b)

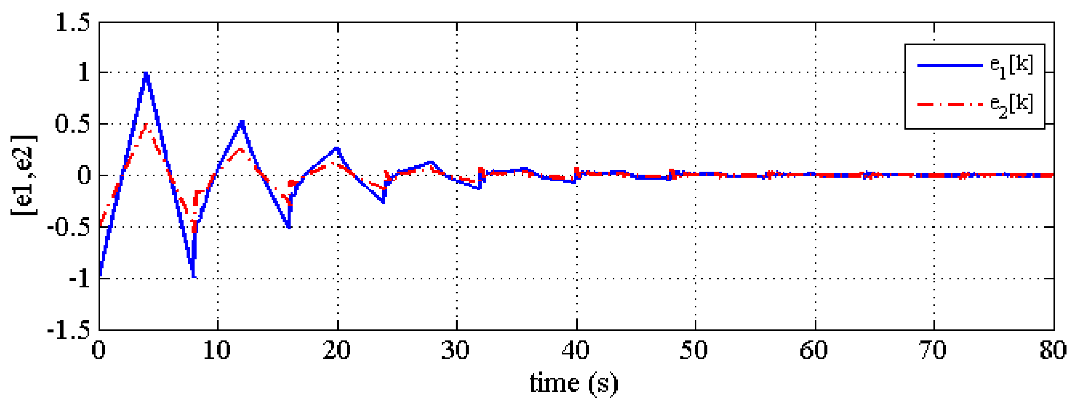

(c)

Figure 6.6 The second scheme (a) Tracking output $y_1(k)$,(b) Tracking output $y_2(k)$, (c).Tracking errors $e_1(k)$ and $e_2(k)$

6.4.2 Simulation of DRC-2

In this subsection, the DRC-2 will be used for the tracking control of a 2 DOF robot plant, which is the plant used in the experiment.

$$G(s) = \begin{bmatrix} g_{11}(s) & g_{12}(s) \\ g_{21}(s) & g_{22}(s) \end{bmatrix} \tag{6.50}$$

where $g_{11}(s), g_{12}(s), g_{21}(s)$, and $g_{22}(s)$ are also given in (3.3)-(3.6)

$$g_{11}(s) = \frac{1.0210}{0.0059s^2 + 0.1191s + 1} \tag{6.51}$$

$$g_{12}(s) = \frac{-0.0144\,s \ + \ 0.3975}{26.430s^2 + 7.2020s + 1} \tag{6.52}$$

$$g_{21}(s) = \frac{-0.002888\,s}{0.0069s^2 + \ 0.1201s + 1} \tag{6.53}$$

$$g_{22}(s) = \frac{1.003}{0.0051\,s^2 + 0.1151s + 1} \tag{6.54}$$

The RGA of $\mathrm{G(s)}$ is calculated as follows:

$$\Lambda = \begin{bmatrix} 1 & 0 \\ 0 & 1 \end{bmatrix} \tag{6.55}$$

The RGA value Λ shows that the dynamic $\mathrm{g_{11}(s)}$ and $\mathrm{g_{22}(s)}$ give dominant interaction to output $\mathrm{y_1(t)}$ and $\mathrm{y_2(t)}$ respectively. The RGA also suggests that the best pairings are $[\mathrm{u_1, y_1}]$ and $[\mathrm{u_2, y_2}]$. Therefore, the compensator matrix $F(z)$ has elements at the diagonal.

$$\mathrm{F(z)} = \begin{bmatrix} \mathrm{f_{11}(z)} & 0 \\ 0 & \mathrm{f_{22}(z)} \end{bmatrix} \tag{6.56}$$

Let the period of reference signal and the sampling period be $2\ s$ and $0.025\ s$ respectively. This gives the number of samples per reference period N as 80. The discrete model of $G(s)$ at the given sampling period is

$$G(z) = \begin{bmatrix} g_{11}(z) & g_{12}(z) \\ g_{21}(z) & g_{22}(z) \end{bmatrix} \tag{6.57}$$

where

$$g_{11}(z) = \frac{0.045z + 0.038}{z^2 - 1.522z + 0.604} \tag{6.58}$$

$$g_{12}(s) = \frac{-1e - 5(0.88z - 1.82)}{z^2 - 1.99z + 0.99} \tag{6.59}$$

$$g_{21}(s) = \frac{-0.00831z + 0.0083}{z^2 - \ 1.577z + 0.649} \tag{6.60}$$

$$g_{22}(s) = \frac{0.051z + 0.042}{z^2 - 1.476z + 0.568} \tag{6.61}$$

The chosen $q(z)$, δ and τ are similar to the previous design. The transfer function $\mathrm{f}_{11}(\mathrm{z})$ and $\mathrm{f}_{22}(\mathrm{z})$ will be designed to compensate the dynamics of $\mathrm{g}_{11}(\mathrm{z})$ and $\mathrm{g}_{22}(\mathrm{z})$ respectively. Therefore, the order of $\mathrm{f}_{11}(\mathrm{z})$ and $\mathrm{f}_{22}(\mathrm{z})$ are chosen to be equal or higher than the order of $\mathrm{g}_{11}(\mathrm{z})$ and $\mathrm{g}_{22}(\mathrm{z})$ respectively. Let the order of both $\mathrm{f}_{11}(\mathrm{z})$ and $\mathrm{f}_{22}(\mathrm{z})$ be $n_1 = n_2 = 2$. The objective function (6.28) is formulated as follows:

$$h_{Total} = \sum_{\mathrm{k}=1}^{\mathrm{N}/2} |(1 - \mathrm{g}_{11}(\mathrm{z})\mathrm{f}_{11}(\mathrm{z}))\mathrm{q}(\mathrm{z})|_{\omega_\mathrm{k}} + \sum_{\mathrm{k}=1}^{\mathrm{N}/2} |(1 - \mathrm{g}_{22}(\mathrm{z})\mathrm{f}_{22}(\mathrm{z}))\mathrm{q}(\mathrm{z})|_{\omega_\mathrm{k}} \tag{6.62}$$

There are 10 unknown parameters to be designed, and the goal is to minimize the objective function value (6.54). By solving the optimization problem (6.30), the following compensator matrix $F(z)$ is obtained:

$$F(z) = \begin{bmatrix} \dfrac{35.60z^2 - 56.91z + 24.34}{z^2 + 1.85z + 0.86} & 0 \\ 0 & \dfrac{32.29z^2 - 50.31z + 21.11}{z^2 + 1.85z + 0.86} \end{bmatrix} \qquad (6.63)$$

In this simulation, both channels are required to track triangle reference signals. The tracking outputs are shown in Figure 6.3.

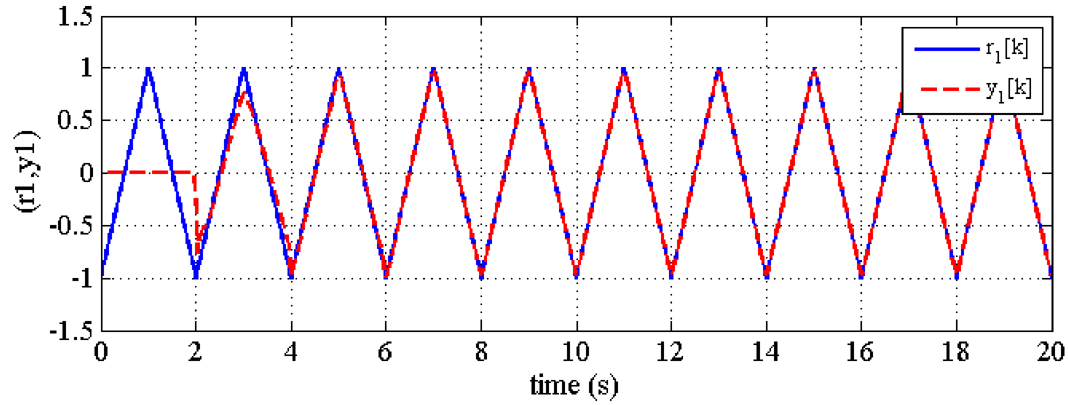

(a)

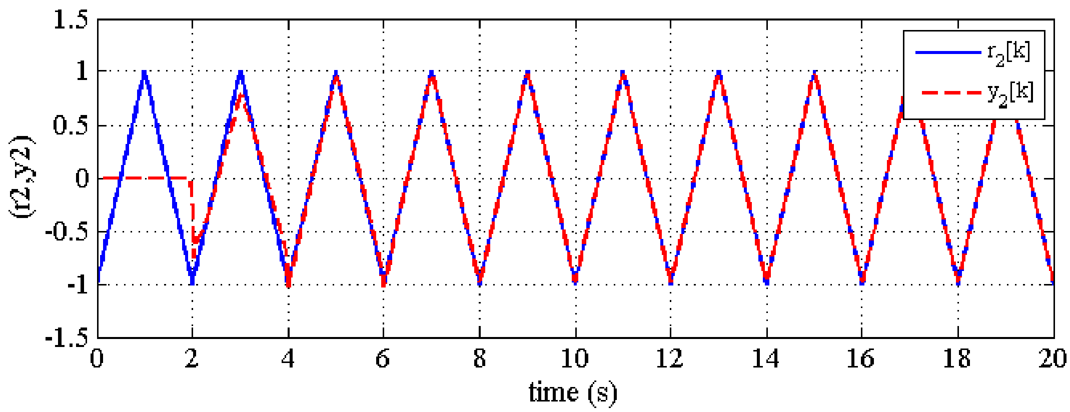

(b)

Figure 6.7 DRC-2 (a) Tracking output $y_1(k)$,(b) Tracking output $y_2(k)$

Figure 6.7(a) shows that tracking output $y_1(k)$ follows the reference $r_1(k)$ perfectly after 3 repetitions. On channel 2, the same tracking performance has been achieved. These results verify the effectiveness of DRC-2.

Compared to the DRC-1 design, the DRC-2 design is more straightforward. This is because the DRC 2 does not require the design of stabilizing controller, or separate checking of the stability condition. The stability check has been packed as a constraint in the optimization problem. This means that the obtained compensator parameters from the optimization ensure the stability of the MIMO RC system. However, the DRC-2 design is more complex if it is used for plant model (6.31). If the DRC-2 is applied for tracking control of the plant model (6.31), the compensator matrix $\mathrm{F(z)}$ will result in high order, since $\mathrm{g_{11}(s)}$ and $\mathrm{g_{22}(s)}$ are in high order. Both $\mathrm{g_{11}(s)}$ and $\mathrm{g_{22}(s)}$ of (6.31) have an order 12. The discrete model of $\mathrm{g_{11}(s)}$ and $\mathrm{g_{22}(s)}$ will also have an order 12, but with relative degree 1. Therefore, the order of $f_{11}(\mathrm{z})$ and $f_{22}(\mathrm{z})$are chosen to be at least 12 or higher. This results in large number of parameters that needs to be optimized. The computation to solve large-scale optimization is more time consuming than to solving the Diophantine Equation. Therefore, the DRC-1 design has an advantage in this case.

6.4.3 A Comparison Study of DRC

This section presents a comparison study to show the significance of the proposed DRC. The MIMO model used for the comparison is a model of a 2 DOF robot plant (6.50). The comparison study is conducted with the PCI compensator proposed by Jeong and Fabien [96]. The idea of the PCI is very similar to the Zero Phase Tracking Error Controller (ZPETC) [11] in the SISO case, which aims to perfectly cancel the phase response of the plant. The PCI is a matrix function such that [96].

$$F_{pci}(z)G(z) = I_{mxm} \tag{6.64}$$

If $G(z)$ is a square and minimum phase system, then the choice for PCI will be $G^{-1}(z)$.

$$F_{pci}(z) = \frac{1}{\det(G(z))} Adj(G(z)) \tag{6.65}$$

If $G(z)$ is a square and non-minimum phase system, then the PCI will be

$$F_{pci}(z) = Adj(G(z))\frac{\beta^{+}(z^{-1})}{\beta^{-}(z)} \tag{6.66}$$

where$F_{pci}(z)$ is the PCI matrix, $Adj(G(z))$ is the adjoint of $G(z)$, $\beta^{+}(z), \beta^{-}(z)$ are uncancellable and cancellable part of $\det[G(z)]$, and elements of $G(z)$ are in a non-causal FIR filter form.

To design PCI for the plant model (6.56), we need to examine the zeros and poles of $(G(z))$.

The determinant of $G(z)$ can be expressed as follows:

$$det(G(z)) = \frac{Z_g(z)}{P_g(z)} \tag{6.67}$$

where $Z_g(z)$ and $P_g(z)$ are the numerator and denumerator parts respectively.

The determinant of $G(z)$ has 6 zeros and 8 poles, where there are 4 zeros - poles cancellation. After the cancellation, $det[G(z)]$ will have 2 zeros and 4 poles. The number of zeros and poles of $2x2$ MIMO system with rational transfer functions can also be obtained by simple calculation as follows:

$$n_z = \max[(n_{d12} + n_{d21} + n_{n11} + n_{n22}), (n_{d11} + n_{d22} + n_{n12} + n_{n21})] \tag{6.68}$$

$$n_p = n_{d11} + n_{d22} + n_{d12} + n_{d21} \tag{6.69}$$

where

n_z and n_p are the number of zeros and poles of $det[G(z)]$respectively,

$n_{d11}, n_{d22}, n_{d12}, n_{d21}$ are the denumerator order of $g_{11}(z), g_{22}(z), g_{12}(z), g_{21}(z)$ respectively, and

$n_{n11}, n_{n22}, n_{n12}, n_{n21}$ are the numerator order of $g_{11}(z), g_{22}(z), g_{12}(z), g_{21}(z)$ respectively.

All zeros and poles of $det(G(z))$ are still inside the unit circle. Thus, the $G(z)$ is stable and a minimum phase system. Since the inverse of $Z_g(z)$ is stable, we do not need to break $Z_g(z)$ into cancellable and uncancellable parts.

The PCI matrix after zeros poles cancellation is obtained as follows:

$$F_{pci}(z) = k_r \begin{bmatrix} f_{11}(z) & f_{12}(z) \\ f_{21}(z) & f_{22}(z) \end{bmatrix} \tag{6.70}$$

where k_r is the learning rate

$$f_{11}(z) = \frac{21.94z^3 - 15.21z^2 - 14.39z + 10.97}{z^2 + 1.673z + 0.699} \tag{6.71}$$

$$f_{12}(z) = \frac{3.85z^5 - 14.32z^4 + 22.98z^3 - 18.54z^2 + 7.52z - 1.23}{z^4 + 0.097z^3 - 1.29z^2 - 0.02z + 0.45} \tag{6.72}$$

$$f_{12}(z) = \frac{1e - 2(0.38z^5 - 1.93z^4 + 3.66z^3 - 3.36z^2 + 1.51z - 0.27)}{z^4 - 0.32z^3 - 1.64z^2 + 0.27z + 0.69} \tag{6.73}$$

$$f_{22}(z) = \frac{19.65z^3 - 12.39z^2 - 13.33z + 9.44}{z^2 + 1.673z + 0.699} \tag{6.74}$$

If there is no zero pole cancellation, then the denumerator of the PCI will have an order of 6. From (6.71)-(6.74), we can see that all elements of PCI are improper, and the order of the PCI is higher than the order of (z) . The PCI can be realized because of the high causal term of the internal model.

$$G_{rc}^{pci}(z) = k_r \begin{bmatrix} \frac{q(z)}{z^N - q(z)} f_{11}(z) & \frac{q(z)}{z^N - q(z)} f_{12}(z) \\ \frac{q(z)}{z^N - q(z)} f_{21}(z) & \frac{q(z)}{z^N - q(z)} f_{22}(z) \end{bmatrix} \tag{6.75}$$

This is different to the compensator matrix $F(z)$ shown in (6.63) , where $F(z)$ has two low order, stable and proper compensators. The tracking performance of the MIMO RC system using PCI and DRC-2 is shown in Figure 6.8(a) and (b) respectively.

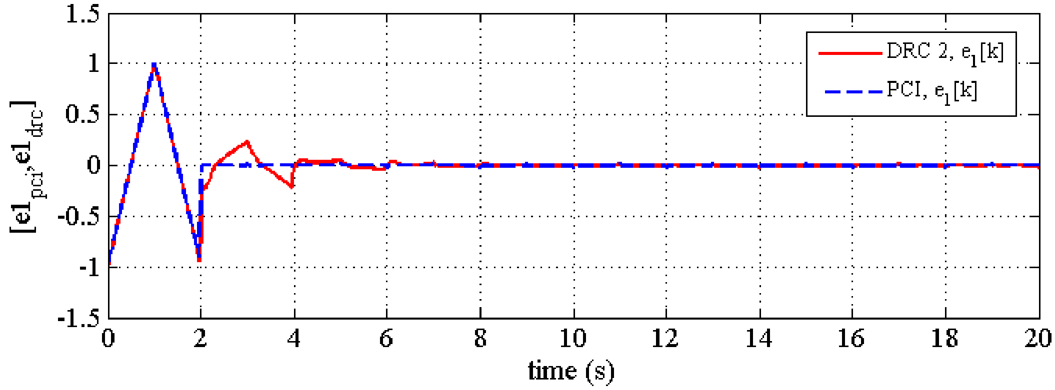

(a)

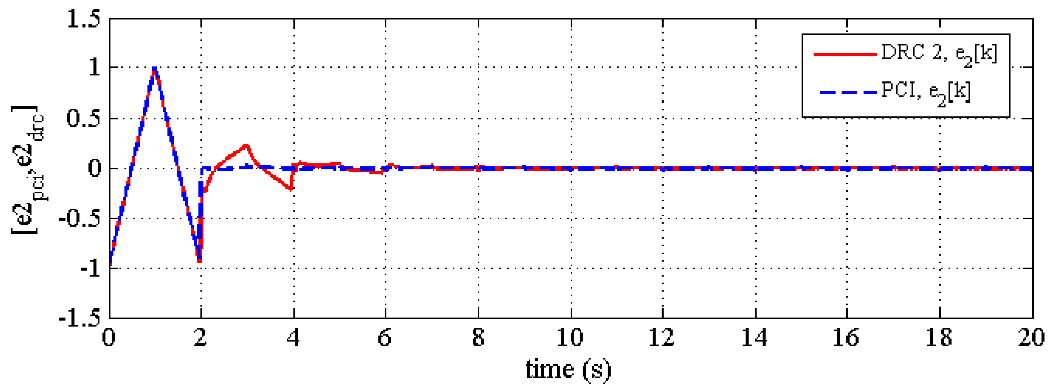

(b)

Figure 6.8 Tracking errors with PCI, $kr = 1$ and DRC-2, (a) On Channel 1 (b) On Channel 2.

Figure 6.8 shows that the tracking errors of PCI on both channels vanish completely after one repetition, while the tracking errors of DRC-2 converge to zero after three repetitions. This shows the superiority of the PCI in terms of the convergence rate. This is understandable, because the PCI is the ideal compensator as it is the exact inverse of the plant matrix. The DRC-2 here only approximates the inverse of strong dynamic elements in the plant matrix. In terms of the complexity, the DRC-2 is simpler than the PCI. In DRC-2, only m elements are needed to build the compensator matrix. Moreover, all the elements of the DRC-2 are low order, and in causal form. The complexity of the PCI design will arise significantly when the plant model is in the high order.

For instance, the use of the PCI design for the plant model (6.31) will result in very high order compensators. Each transfer function of the discrete model of (6.31) has the following order:

$$\frac{n_{n11}}{n_{d11}}=\frac{11}{12} \qquad \frac{n_{n12}}{n_{d12}}=\frac{9}{10} \qquad \frac{n_{n21}}{n_{d21}}=\frac{9}{10} \qquad \frac{n_{n22}}{n_{d22}}=\frac{11}{12} \tag{6.76}$$

Using the equation (6.70)-(6.71), the determinant of $G(z)$ has 42 zeros and 44 poles. If all the zeros are stable and there is no zero pole cancellation, the denumerator of the PCI will have an order 42, and of course the order of the numerator will be higher than 42. This complexity shows the drawback of the PCI.

6.5 EXPERIMENTAL RESULTS

This section presents the experimental results of the proposed DRCs. The real-time experiments were conducted on the 2 DOF Quanser robot plant pictured in Figure 3.5. Two servo motors mounted at a fixed distance control two arms coupled via two non-powered two-link arms. The system has 2 actuated and 3 unactuated revolute joints. The 4-bar linkage system gives a coupling effect to the actuated joints. The 2 DOF Quanser robot plant is a 2x2 MIMO system, and its transfer functions were experimentally modeled using time-domain data.

The experiments aimed to control the end effector E in order to have diamond shape movement, by giving a triangle reference signal at each channel. The reference signals are X-Y coordinates (E_{xd}, E_{yd}), where E_{xd} and E_{yd} are given on Channel 1 and 2 respectively. The period of both E_{xd} and E_{yd} are 2 s, and E_{yd} has to be started 0.5 s after E_{xd} .The proposed DRC-1 and DRC-2 are used to control the position of the end effector. The tracking outputs and tracking errors of the system using DRC-1 and DRC-2 are shown in Figure 6.9 and Figure. 6.10 respectively.

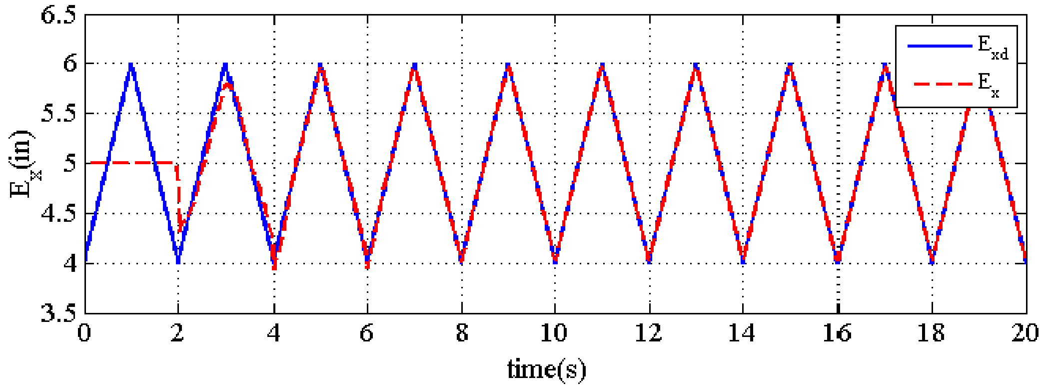

(a)

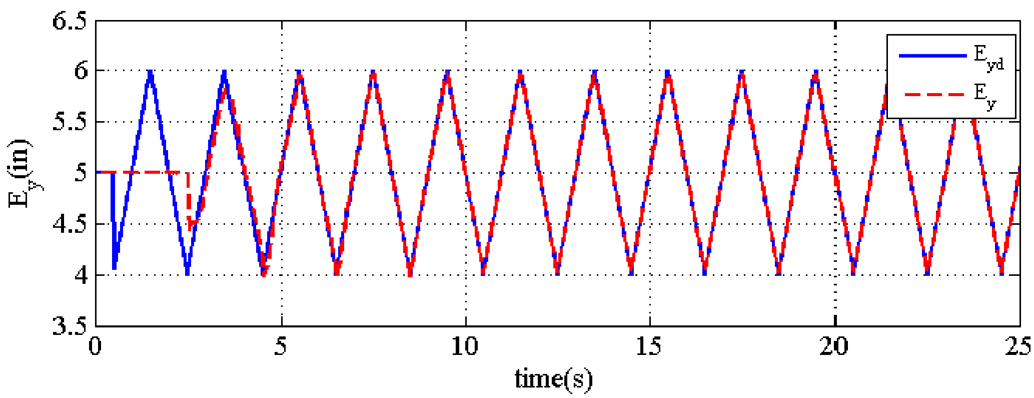

(b)

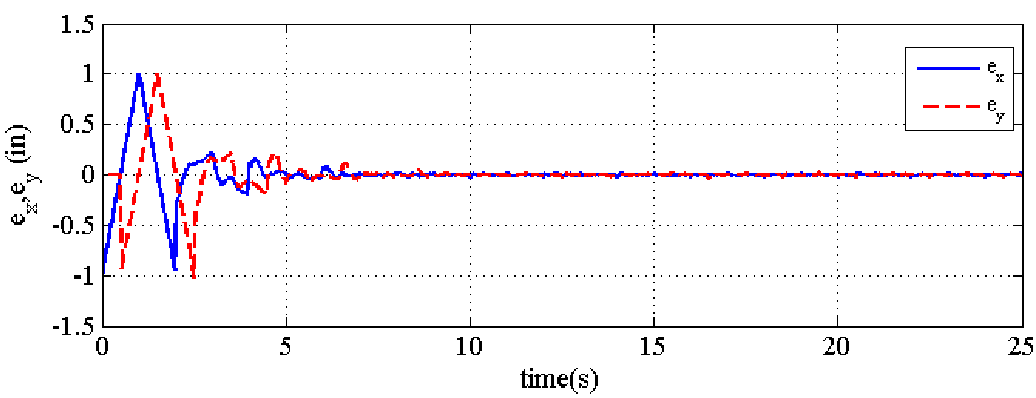

(c)

Figure 6.9 DRC-1 (a) Tracking output $E_x(k)$,(b) Tracking output $E_y(k)$, (c).Tracking errors $e_x(k)$ and $e_y(k)$

Figure 6.9(c) shows that the tracking errors on both channels converge to zero after 3 repetitions. As indicated in Figure 6.9(c), a similar performance was achieved for DRC-2.

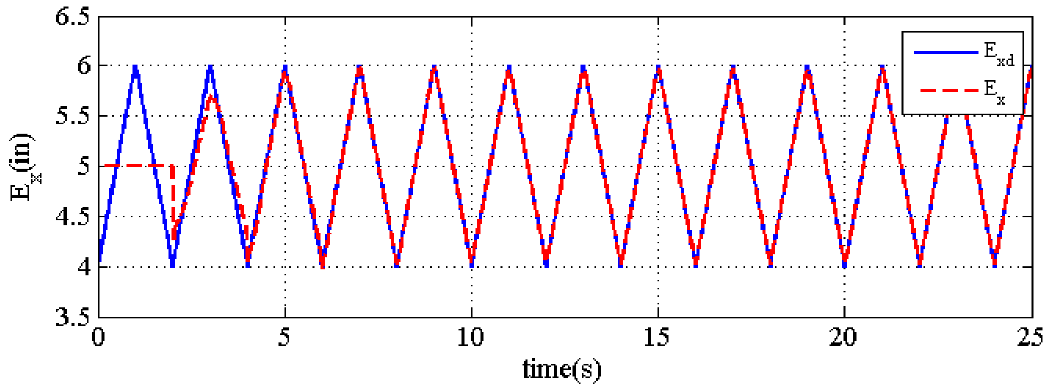

(a)

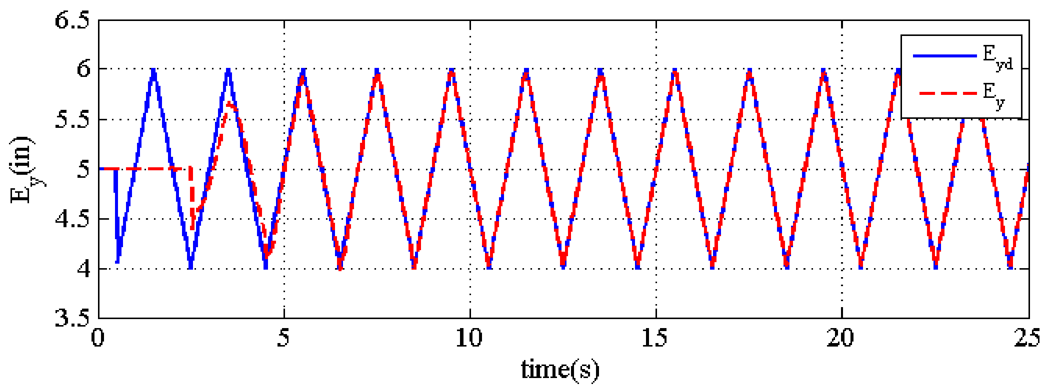

(b)

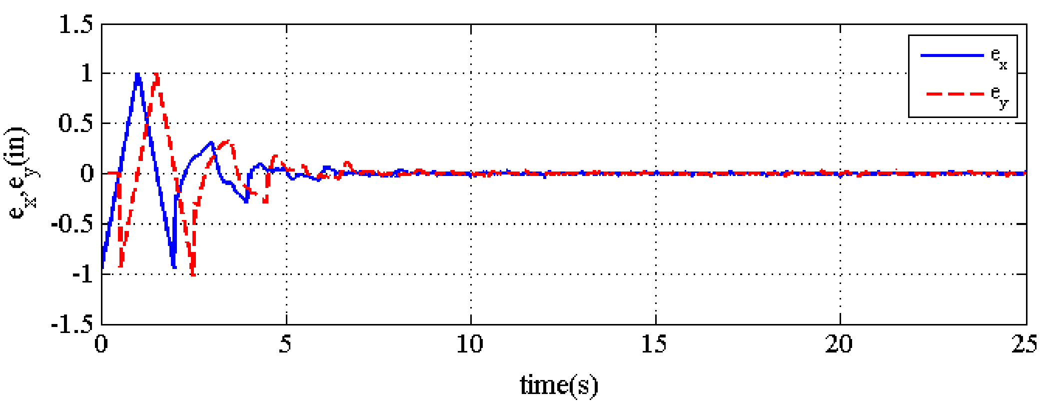

(c)

Figure 6.10 DRC-2 (a) Tracking output $E_x(k)$,(b) Tracking output $E_y(k)$,

(c).Tracking errors $e_x(k)$ and $e_y(k)$.

The end-effector X-Y position response of DRC-2 is shown in Figure 6.11. Figure 6.11 traces the end effector movement in inches after reaching a steady state. It can be seen that the trace of the end effector forms a diamond shape, and it follows the set point exactly.

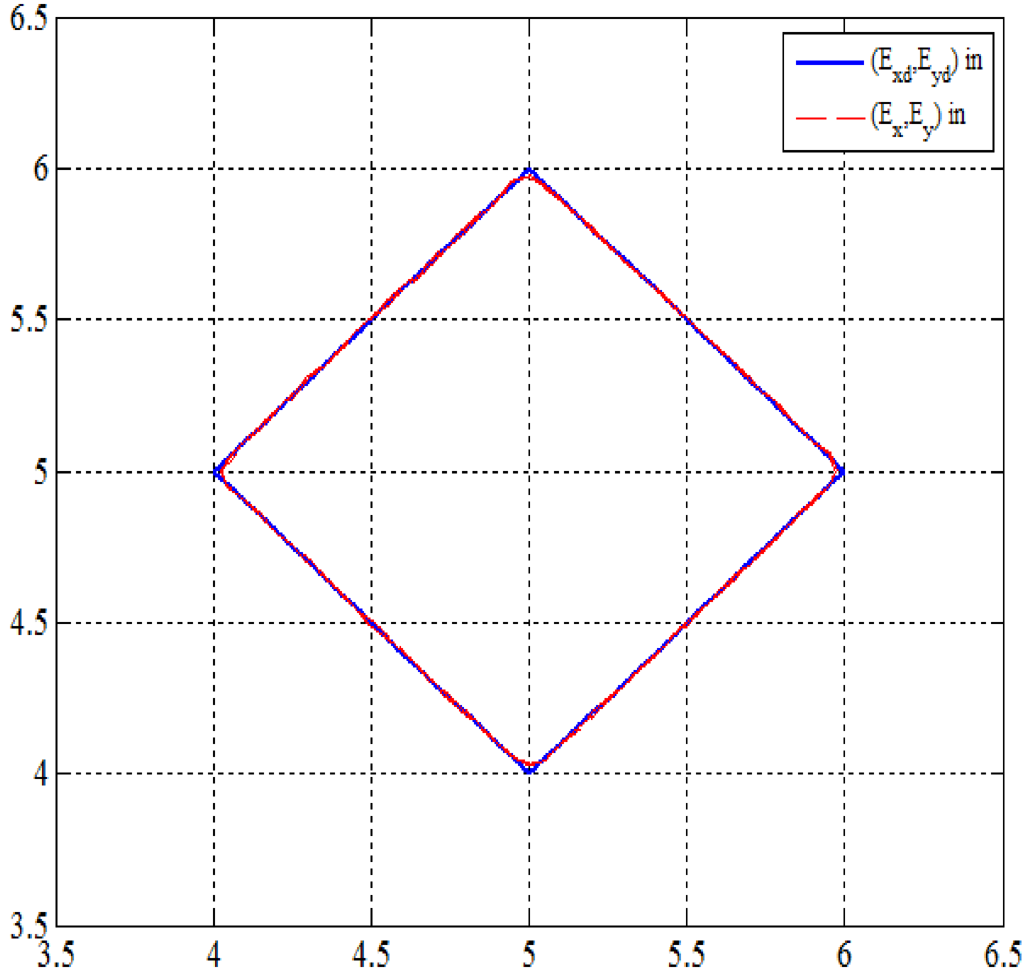

Figure 6.11 End effector X-Y position response of DRC-2

For comparison, the PCI was also implemented with $k_r = 1$. The tracking outputs and errors are shown in Figure 6.12(a)-(b) and Figure 6.12(c) respectively. Figure 6.12(c) shows that the tracking errors perfectly converge to zero after two repetitions. These results indicate that the PCI has a superior convergence rate compared to DRCs. This performance verifies the simulation results presented in subsection 6.3.4.

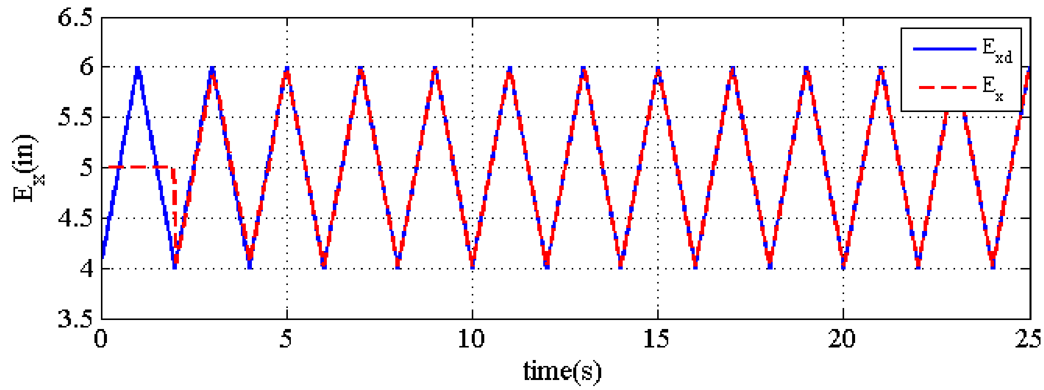

(a)

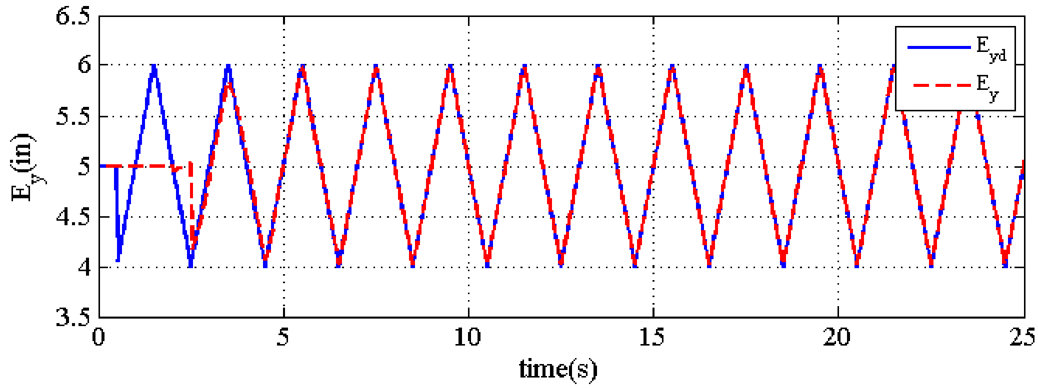

(b)

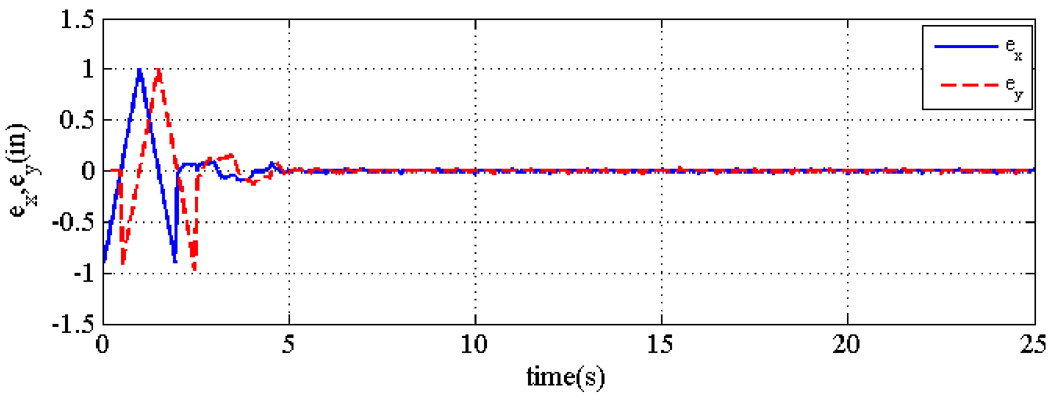

(c)

Figure 6.12 PCI (a) Tracking output $E_x(k)$,(b) Tracking output $E_y(k)$,

(c).Tracking error $e_x(k)$ and $e_y(k)$

6.6 SUMMARY

A decentralized RC design for linear MIMO system has been presented in this chapter. Two approaches have been proposed, DRC-1 and DRC-2.

In DRC-1, Relative Gain Array (RGA) analysis is used first to obtain the best pairing of inputs and outputs. A robustness check is then conducted to determine the impact of neglected couplings. Once the robustness check has been performed, then the decentralized stabilizing controller can be designed based on the chosen complimentary sensitivity function. The compensator matrix $F(z)$ is designed in discrete-time. For mxm MIMO system, there are m-elements of matrix $F(z)$ needing to be designed. Each element of $F(z)$ has been designed using optimization to obtain a low order, stable and causal compensator. If elements of $T(s)$ are chosen to have the same transfer function, then only one optimization problem needs to be solved. Once, the compensator matrix $F(z)$ has been obtained, a stability check of the MIMO RC system needs to be performed.

In DRC-2, the design does not require a stabilizing controller to be obtained, nor separate checking of the stability condition. The stability check is packed as a constraint in the optimization problem. This means that the obtained compensator parameters from the optimization ensure the stability of the MIMO RC system. The compensator matrix $F(z)$ is obtained by solving a single optimization problem. The design of DRC-2 is more straightforward than DRC-1. However, DRC-2 design requires a large number of parameters to be optimized especially for high order plant. This large-scale optimization in DRC-2 is more complex than solving the Diophantine Equation in DRC-1.

Both DRC-1 and DRC-2 have been verified by simulation and real-time experiments, and shown good tracking performance. For comparison, the PCI method was also simulated and implemented in real-time experiments. The PCI design results in a full matrix $F(z)$, in which its elements are non-causal and in high order.

CHAPTER 7

CONCLUSION AND FUTURE WORK

In this chapter, the contributions of this research are summarized, and issues that are worth future investigation are discussed.

7.1 CONCLUSION

This thesis has presented 3 groups of algorithms; a Robust RC design in Chapter 4, an Adaptive RC design in Chapter 5, and a MIMO RC design in Chapter 6. A comparison of all proposed algorithms is summarized in Table 7.1.

Chapter 4 proposed two main ideas; a new design of RC compensator, and a robust RC design that works for a time-varying sampling period. A low order, stable, and causal IIR filter based compensator was first designed using an optimization method to achieve fast convergence and high tracking accuracy. Since the compensator has a causal form, then it can be implemented independently without being merged to the internal model that is mostly in the high order. This reduces the design complexity, as most of the existing repetitive compensators are either non-causal or unstable, which makes their implementation difficult. The design works for both minimum and non-minimum phase plant, where fast convergence and high tracking accuracy have been achieved. The compensator order should be equal or higher than the plant order to give good phase and magnitude compensation.

A robust RC compensator was then designed to achieve a stable system when the sampling period varies in a defined range. In a robust design, the nominal compensator is designed at a nominal sampling period to achieve fast convergence and high tracking accuracy. Then, the robust compensator closest to the nominal one is designed using optimization, in which it has to ensure that the system is stable in the defined range of sampling period. The proposed compensators have been verified by simulation and real-time experiments.

Chapter 5 presented an MRRC and ARC design method. Both MRRC and ARC can simultaneously track the periodic reference signal and reject the periodic disturbance, where the reference period is not necessarily the same or multiples of the disturbance period. The MRRC scheme successfully works for known plant subject to periodic disturbance with fixed frequency. The MRRC is constructed of two controllers: Model Reference Control (MRC), and RC. The controller parameters of MRC are fixed, and designed based on the transfer function matching. The RC part is composed of the internal model and the compensator that is an inverse of the reference model.

An ARC has been proposed for an unknown linear system subject to periodic disturbances with time-varying frequency. The proposed ARC is based on the direct adaptive control scheme (MRAC) and the internal model principle (RC). The ARC scheme can exactly reject the disturbance since the number of samples per period remains fixed. The time-varying plant parameters are handled by the MRAC, which quickly tunes the controller parameters such that the closed-loop system is stable and the plant output tracks the reference model output. Both simulations and experiments results have been presented to verify the effectiveness of the proposed design.

Chapter 6 introduced a decentralized RC (DRC) design for a linear MIMO system. Two design approaches were presented; DRC-1 and DRC-2. In DRC-1, Relative Gain Array (RGA) analysis was used initially to obtain the best pairing of inputs and outputs. Then, a robustness check was conducted to determine the impact of neglected couplings. Once the robustness check has been performed, then the decentralized stabilizing controller can be designed based on the chosen complimentary sensitivity function. The RC compensator matrix was designed in discrete-time. For a

mxm MIMO system, there are m-elements of compensator matrix that need to be designed. Each element of the matrix was designed using optimization to obtain a low order, stable and causal compensator. If elements of the complimentary sensitivity function are chosen to have the same transfer function, then only one optimization problem needs to be solved. Once, the compensator matrix has been obtained, a stability check of RC MIMO system needs to be performed.

In DRC-2, the design does not need to obtain stabilizing controller, or separate checking of the stability condition. The stability check has been packed as a constraint in the optimization problem. This means that the obtained compensator parameters from the optimization ensure the stability of the RC MIMO system. The compensator matrix is obtained by solving a single optimization problem. The design of DRC-2 is more straightforward than DRC-1. However, the DRC-2 design requires a large number of parameters to be optimized especially for high order plant. This large-scale optimization in DRC-2 requires greater complexity than just solving Diophantine Equation in DRC-1. Both DRC-1 and DRC-2 have been verified by simulation and real-time experiments, and show good tracking performance.

Table 7.1 Comparison of all proposed algorithms

Algorithm	Chapter 4		Chapter 5		Chapter 6
	New Compensator	*Robust Compensator*	*MRRC*	*ARC*	*DRC-1 and DRC-2*
Plant Class	Linear SISO	Linear SISO	Linear SISO	Linear SISO	Linear MIMO
RC Class	Internal Model	Internal Model	Internal Model	Internal Model	Internal Model

Prior know-ledge	Parametric model of the plant, number of samples per period	Parametric model of the plant, number of samples per period , sampling period interval	Parametric model of the plant, number of samples per period	Order of the plant, number of samples per period	Parametric model of the plant, number of samples per period
Controller Design	Frequency Domain	Frequency Domain	Time Domain	Time Domain	Freq. Domain
Selective Frequency Tracking / Rejection	No (Fundamental Frequency and its harmonics up to Nyquist)	No	No	No	No
Simultaneous Tracking and Rejection	No (Tracking or Rejection)	No	Yes	Yes	No
Convergen-ce Rate	Fast (no learning gain requirement)	Fast at the nominal sampling period	Fast (depend on RC gain)	Medium (depend on both adaptive and RC gain)	Fast (no learning gain requirement)
Tracking Accuracy	Good	Good	Good	Fine	Good

7.2 FUTURE WORK

Three groups of algorithms have been proposed in this thesis; a Robust RC design, an Adaptive RC design, and a MIMO RC design. The proposed robust RC compensator described in Chapter 4 has been designed for an RC with a discrete modified internal model. The modified internal model uses Q-filter to improve robustness, but at the expense of tracking accuracy at higher frequencies. The proposed compensator in this thesis also has a low order, stable and causal transfer function. For tracking control where very high tracking accuracy is required, the internal model without a Q-filter is sometimes preferred. A stable and causal compensator for a discrete internal model without a Q-filter has not yet been proposed.

$$G_{rc}(z) = F(z)\frac{z^{-N}}{1 - z^{N}} \tag{7.1}$$

For rejection of narrow band disturbance, the finite internal model is sometimes sufficient. If the purpose is to reject a repetitive signal that consists of two dominant fundamental frequencies and their harmonics, then multi-periodic RC will be required. The stable and causal compensators for a finite and multi-periodic internal model have also not yet been investigated.

$$G_{rc}(z) = F(z)\frac{1}{(1 - \mathrm{z}^{-1})\prod_{\mathrm{k}\in\mathrm{K}}(1 - 2\cos(\mathrm{k}\omega_{\mathrm{o}}T)\,\mathrm{z}^{-1} + \mathrm{z}^{-2})} \tag{7.2}$$

$$G_{rc}(z) = F(z)\frac{1}{\prod_{k=1}^{L} 1 - Q_k(z)z^{-N_k}} \tag{7.3}$$

where $F(z)$ is a stable and causal compensator, and $\frac{1}{(1-\mathrm{z}^{-1})\prod_{\mathrm{k}\in\mathrm{K}}(1-2\cos(\mathrm{k}\omega_{\mathrm{o}}T)\mathrm{z}^{-1}+\mathrm{z}^{-2})}$ is a finite internal model as shown in (2.8) , and $\frac{1}{\prod_{k=1}^{L} 1-Q_k(z)z^{-N_k}}$ is a multi- periodic internal model as shown in (2.10).

In Adaptive RC design described in Chapter 5, the gradient adaptation law and fixed RC gain are used for each value of sampling period. It is also possible to use Least-Squares adaptation law and adaptive RC gain to achieve quick parameter convergences and faster disturbance rejection. Due to the change of plant parameters in ARC, the adaptive of RC gain is necessary to achieve fast rejection. The design of an ARC using adaptive RC gain is quite challenging, and this of course needs a new stability analysis.

The decentralized RC (DRC) proposed in Chapter 6 works for MIMO model with square matrix. The DRC for non-square matrix has not been investigated yet. The challenge will arise especially when the number of outputs is larger than the number of inputs. A new stability condition for RC system with non-square MIMO model needs to be studied too. Some of the issues discussed above could be investigated in the future.

All algorithms proposed in this thesis are designed for linear systems. The algorithms can be extended to nonlinear systems. The nonlinear system itself can be represented as a linear system with additional term. By treating an additional term as disturbance, the proposed algorithms can be employed for tracking/rejecting periodic signal in nonlinear system. In this case, a new stability condition needs to be analyzed too. Extending the proposed algorithms to nonlinear system can be another possible future work.

REFERENCES

[1] C. Li, D. Zhang, and X. Zhuang, "Theory and applications of the repetitive control," in *Proceeding of The Society of Instrument and Control Engineers Annual Conference, SICE 2004, Sapporo, Hokkaido Institute of Tecnology,* vol. 1, pp. 27-34, Japan 2004.

[2] G. Hillerström and J. Sternby, "Repetitive control theory and applications - a survey," in *Proceedings of the 13th the International Federation of Automatic Control World Congress,IFAC 1996,* vol. D, pp. 1-6, 1996.

[3] Y. X. Song, Y. H. Yu, G. R. Chen, J. X. Xu, and Y. P. Tian, "Time delayed repetitive learning control for chaotic systems," *International Journal of Bifurcation and Chaos,* vol. 12, pp. 1057-1065, May 2002.

[4] J. X. Xu and R. Yan, "On repetitive learning control for periodic tracking tasks," *IEEE Transactions on Automatic Control,* vol. 51, pp. 1842-1848, Nov 2006.

[5] B. A. Francis and W. M. Wonham, "The internal model principle for linear multivariable regulators," *Applied Mathematics & Optimization,* vol. 2, pp.170-194, 1975.

[6] T. Inoue, M. Nakano, and S. Iwai, "High accuracy control of a proton synchroton magnet power supply," in *Proceedings of the 8th the International Federation of Automatic Control World Congress*, *IFAC 1981*, pp. 3137-3142.

[7] K. K. Chew and M. Tomizuka, "Digital control of repetitive errors in disk drive systems," *IEEE Control Systems Magazine,* vol. 10, pp. 16-20, 1990.

[8] K. Kalyanam and T. Tsu-Chin, "Two-period repetitive and adaptive control for repeatable and nonrepeatable runout compensation in disk drive track following," *IEEE/ASME Transactions on Mechatronics,* vol. 17, pp. 756-766, 2012.

[9] C. Cosner, G. Anwar, and M. Tomizuka, "Plug in repetitive control for industrial robotic manipulators," in *Proceedings of IEEE International Conference on Robotics and Automation*, vol. 3, pp. 1970-1975, 1990.

[10] M. Tomizuka, T.-C. Tsao, and K.-K. Chew, "Analysis and synthesis of discrete-time repetitive controllers," *Journal of Dynamic Systems, Measurement, and Control,* vol. 111, pp. 353-358, 1989.

[11] M. Tomizuka, "Zero phase error tracking algorithm for digital control," *Journal of Dynamic Systems, Measurement and Control, Transactions of the ASME,* vol. 190, pp. 65-68, 1987.

[12] G. F. Ledwich and A. Bolton, "Repetitive and periodic controller design," *Control Theory and Applications, IEE Proceedings D,* vol. 140, pp. 19-24, 1993.

[13] G. Hillerstrom and J. Sternby, "Application of repetitive control to a peristaltic pump," in *Proceedings of American Control Conference*, pp. 136-141, 1993.

[14] B. Panomruttanarug and R. W. Longman, "Repetitive controller design using optimization in the frequency domain," in *Proceedings of AIAA/AAS Astrodynamics Specialist Conference*, pp. 1215-1236, 2004.

[15] B. Zhang, D. Wang, K. Zhou, and Y. Wang, "Linear phase lead compensation repetitive control of a CVCF PWM inverter," *IEEE Transactions on Industrial Electronics,* vol. 55, pp. 1595-1602, 2008.

[16] X. H. Wu, S. K. Panda, and J. X. Xu, "Design of a plug-in repetitive control scheme for eliminating supply-side current harmonics of three-phase PWM boost rectifiers under generalized supply voltage conditions," *IEEE Transactions on Power Electronics,* vol. 25, pp. 1800-1810, 2010.

[17] M. Sun, Y. Wang , and D. Wang, "Variable-structure repetitive control: a discrete-time strategy," *IEEE Transactions on Industrial Electronics,* vol. 52, pp. 610-616, 2005.

[18] K. Zhou and D. Wang, "Digital repetitive learning controller for three-phase CVCFPWM inverter," *IEEE Transactions on Industrial Electronics,* vol. 48, pp. 820-830, Aug 2001.

[19] K. J. Astrom, P. Hagander, and J. Sternby, "Zeros of sampled systems," in *Proceedings of the 19th IEEE Conference on Decision and Control including the Symposium on Adaptive Processes*, pp. 1077-1081, 1980.

[20] H. G. M. Dotsch, H. T. Smakman, P. M. J. Van den Hof, and M. Steinbuch, "Adaptive repetitive control of a compact disc mechanism," in *Proceedings of the 34th IEEE Conference on Decision and Control*, vol.2., pp. 1720-1725, 1995.

[21] G. Hillerstrom, "Adaptive suppression of vibrations-a repetitive control approach," in *Proceedings of the American Control Conference*, vol.5, pp. 3820-3824, 1995.

[22] T.-C. Tsao and M. Nemani, "Asymptotic rejection of periodic disturbances with uncertain period," in *Proceedings of American Control Conference* , pp. 2696-2699, 1992.

[23] I. D. Landau, A. Constantinescu, and D. Rey, "Adaptive narrow band disturbance rejection applied to an active suspension - An internal model principle approach," *Automatica,* vol. 41, pp. 563-574, 2005.

[24] Z. Cao and G. F. Ledwich, "Adaptive repetitive control to track variable periodic signals with fixed sampling rate," *IEEE/ASME Transactions on Mechatronics,* vol. 7, pp. 378-384, 2002.

[25] T. C. Tsao, Y. X. Qian, and M. Nemani, "Repetitive control for asymptotic tracking of periodic signals with an unknown period," *Transactions of the ASME, Journal of Dynamic Systems, Measurement and Control,* vol. 122, pp. 364-369, 2000.

[26] M. Steinbuch, "Repetitive control for systems with uncertain period-time," *Automatica,* vol. 38, pp. 2103-2109, 2002.

[27] Z. Cao and S. S. Narasimhulu, "Digital PLL-based adaptive repetitive control," in *Proceedings of ISSCAA 2006: 1st International Symposium on Systems and Control in Aerospace and Astronautics, Vols 1and 2,* pp. 1468-1471, 2006.

[28] S. Dasgupta, S. N. Mohan, S. K. Sahoo, and S. K. Panda, "Application of four-switch-based three-phase grid-connected inverter to connect renewable energy source to a generalized unbalanced microgrid system," *IEEE Transactions on Industrial Electronics,* vol. 60, pp. 1204-1215, 2013.

[29] C. Dong, Z. Junming, and Q. Zhaoming, "An improved repetitive control scheme for grid-connected inverter with frequency-adaptive capability," *IEEE Transactions on Industrial Electronics,* vol. 60, pp. 814-823, 2013.

[30] M. Rashed, C. Klumpner, and G. Asher, "Repetitive and resonant control for a single-phase grid-connected hybrid cascaded multilevel converter," *IEEE Transactions on Power Electronics,* vol. 28, pp. 2224-2234, 2013.

[31] J. Shuai, C. Dong, L. Yuan, and P. Fang Zheng, "Grid-connected boost-half-bridge photovoltaic microinverter system using repetitive current control and maximum power point tracking," *IEEE Transactions on Power Electronics,* vol. 27, pp. 4711-4722, 2012.

[32] D. Sha, D. Wu, and X. Liao, "Analysis of a hybrid controlled three-phase grid-connected inverter with harmonics compensation in synchronous reference frame," *IET Power Electronics,* vol. 4, pp. 743-751, 2011.

[33] Y. Yang, K. Zhou, M. Cheng, and B. Zhang, "Phase compensation multiresonant control of CVCF PWM converters," *IEEE Transactions on Power Electronics,* vol. 28, pp. 3923-3930, 2013.

[34] Y. Yunhu, Z. Keliang, and C. Ming, "Phase compensation resonant controller for PWM converters," *IEEE Transactions on Industrial Informatics,* vol. 9, pp. 957-964, 2013.

[35] Z. Keliang, W. Danwei, Z. Bin, and W. Yigang, "Plug-in dual-mode-structure repetitive controller for CVCF PWM inverters," *IEEE Transactions on Industrial Electronics,* vol. 56, pp. 784-791, 2009.

[36] Y. Ye, B. Zhang, K. Zhou, D. Wang, and Y. Wang, "High-performance cascade-type repetitive controller for CVCF PWM inverter: analysis and design," *IET Electric Power Applications,* vol. 1, pp. 112-118, 2007.

[37] C. Younghoon and L. Jih-Sheng, "Digital plug-in repetitive controller for single-phase bridgeless PFC converters," *IEEE Transactions on Power Electronics,* vol. 28, pp. 165-175, 2013.

[38] G. A. Ramos and R. Costa-Castello, "Power factor correction and harmonic compensation using second-order odd-harmonic repetitive control," *IET Control Theory & Applications,* vol. 6, pp. 1633-1644, 2012.

[39] G. Escobar, M. Hernandez-Gomez, P. R. Martinez, and M. F. Martinez-Montejano, "A repetitive-based controller for a power factor precompensator," *IEEE Transactions on Circuits and Systems I: Regular Papers,* vol. 54, pp. 1968-1976, 2007.

[40] H. Utsugi, K. Ohishi, and H. Haga, "Reduction in current harmonics of electrolytic capacitor-less diode rectifier using inverter-controlled IPM motor," in *Proceedings of the 38th Annual Conference on IEEE Industrial Electronics Society*, *IECON ,* 2012, pp. 6206-6211.

[41] Y. Xu, Y. Zhao, and Y. Xu, "Application of repetitive control technique with feedforward in shunt active power filter," in *Proceedings of the 5th IEEE Conference on Industrial Electronics and Applications, ICIEA 2010*, pp. 1067-1071, 2010.

[42] P. Mattavelli and F. P. Marafao, "Repetitive-based control for selective harmonic compensation in active power filters," *IEEE Transactions on Industrial Electronics,* vol. 51, pp. 1018-1024, 2004.

[43] Z. XiaoJian, H. Lei, C. Xiao, and C. Guozhu, "Design and implementation of compound current control strategy for improved LCL-based Shunt Active Power Filter," in *Proceedings of the 38th Annual Conference on IEEE Industrial Electronics Society*, *IECON ,* 2012, pp. 339-344.

[44] B. J. Kenton and K. K. Leang, "Design and control of a three-axis serial-kinematic high-bandwidth nanopositioner," *IEEE/ASME Transactions on Mechatronics,* vol. 17, pp. 356-369, 2012.

[45] S. Necipoglu, S. A. Cebeci, Y. E. Has, L. Guvenc, and C. Basdogan, "Robust repetitive controller for fast AFM imaging," *IEEE Transactions on Nanotechnology,* vol. 10, pp. 1074-1082, 2011.

[46] R. J. E. Merry, M. J. C. Ronde, R. van de Molengraft, K. R. Koops, and M. Steinbuch, "Directional repetitive control of a metrological AFM," *IEEE Transactions on Control Systems Technology,* vol. 19, pp. 1622-1629, 2011.

[47] K. K. Leang, S. Yingfeng, S. Song, and K. J. Kim, "Integrated sensing for IPMC actuators using strain gages for underwater applications," *IEEE/ASME Transactions on Mechatronics,* vol. 17, pp. 345-355, 2012.

[48] L. Ott, F. Nageotte, P. Zanne, and M. de Mathelin, "Robotic assistance to flexible endoscopy by physiological-motion tracking," *IEEE Transactions on Robotics,* vol. 27, pp. 346-359, 2011.

[49] L. Ott, F. Nageotte, P. Zanne, and M. de Mathelin, "Simultaneous physiological motion cancellation and depth adaptation in flexible endoscopy," *IEEE Transactions on Biomedical Engineering,* vol. 56, pp. 2322-2326, 2009.

[50] H. Liao, M. J. Roelle, C. Jyh-Shin, P. Sungbae, and J. C. Gerdes, "Implementation and analysis of a repetitive controller for an electro-hydraulic engine valve system," *IEEE Transactions on Control Systems Technology,* vol. 19, pp. 1102-1113, 2011.

[51] S. Zongxuan and K. Tang-Wei, "Transient control of electro-hydraulic fully flexible engine valve actuation system," *IEEE Transactions on Control Systems Technology,* vol. 18, pp. 613-621, 2010.

[52] H. Chuxiong, Y. Bin, C. Zheng, and W. Qingfeng, "Adaptive robust repetitive control of an industrial biaxial precision gantry for contouring tasks," *IEEE Transactions on Control Systems Technology,* vol. 19, pp. 1559-1568, 2011.

[53] O. Hui, Z. Kai, Z. Pengju, K. Yong, and X. Jian, "Repetitive compensation of fluctuating DC link voltage for railway traction drives," *IEEE Transactions on Power Electronics,* vol. 26, pp. 2160-2171, 2011.

[54] R. J. L. M. Verstappen, C. T. Freeman, E. Rogers, T. Sampson, and J. H. Burridge, "Robust higher order repetitive control applied to human tremor suppression," in *Proceedings of IEEE International Symposium on Intelligent Control , ISIC 2012*, pp. 1214-1219, 2012.

[55] M. Tomizuka, K. K. Chew, and W. C. Yang, "Disturbance rejection through an external model," *Journal of Dynamic Systems Measurement and Control-Transactions of the Asme,* vol. 112, pp. 559-564, 1990.

[56] H. Shinji, O. Tohru, and N. Michio, "Synthesis of repetitive control systems and its application," in *Proceedings of the 24th IEEE Conference on Decision and Control,* pp. 1387-1392, 1985.

[57] S. Hara, Y. Yamamoto, T. Omata, and M. Nakano, "Repetitive control system: a new type servo system for periodic exogenous signals," *IEEE Transactions on Automatic Control,* vol. 33, pp. 659-668, 1988.

[58] J. Ghosh and B. Paden, "Nonlinear repetitive control," *IEEE Transactions on Automatic Control,* vol. 45, pp. 949-954, 2000.

[59] D. Zhang, M. Zeng, and B. Su, "Rejection of states-dependent nonlinear disturbance torques in servomechanisms with finite-dimensional repetitive control," in *Proceedings of 2003 IEEE Conference on Control Applications, CCA 2003,* vol.2, pp. 803-807, 2003.

[60] M. Nagahara, M. Ogura, and Y. Yamamoto, "A novel approach to repetitive control via sampled-data H_∞ filters," in *Proceedings of the 7th Asian Control Conference, ASCC 2009*, pp. 160-165, Hong Kong 2009.

[61] M. Nakano and S. Hara, "Microprocessor-based repetitive control," in *Microprocessor-Based Control Systems*. vol. 4, N. Sinha, Ed., ed: Springer Netherlands, pp. 279-296, 1986.

[62] K. K. Chew and M. Tomizuka, "Steady-state and stochastic performance of a modified discrete-time prototype repetitive controller," *Journal of Dynamic Systems, Measurement and Control, Transactions of the ASME,* vol. 112, pp. 35-41, 1990.

[63] G. Hillerstrom and J. Sternby, "Repetitive control using low order models," in *Proceedings of the 1994 American Control Conference* , pp. 1873-1878, 1994.

[64] R. Griñó and R. Costa-Castelló, "Digital repetitive plug-in controller for odd-harmonic periodic references and disturbances," *Automatica,* vol. 41, pp. 153-157, 2005.

[65] C. Woo Sok and S. Il Hong, "Analysis and design of digital dual-repetitive controllers," in *Proceedings of the 35th IEEE Conference on Decision and Control,* vol.3, pp. 2495-2500, 1996.

[66] R. W. Longman, J. W. Yeol, and Y. S. Ryu, "Improved methods to cancel multiple unrelated periodic disturbances by repetitive control," in *Proceedings of the AAS/AIAA Astrodynamics Conference,* vol. 123 I, pp. 199-218, 2006.

[67] M. Yamada, Z. Riadh, and Y. Funahashi, "Design of robust repetitive control system for multiple periods," in *Proceedings of the 39th IEEE Conference on Decision and Control,* vol.4, pp. 3739-3744, 2000.

[68] G. Weiss, *Repetitive control systems: Old and new ideas* , Systems and Control in the Twenty-First Century, vol. 22, 1997.

[69] N. O. Pérez-Arancibia, T. C. Tsao, and J. S. Gibson, "Multiple-period adaptive-repetitive control of a hard disk drive," in *Proceedings of the 48th IEEE Conference on Decision and Control/ 28th Chinese Control Conference*, pp. 5432-5439, 2009.

[70] M. Yamada, Z. Riadh, and Y. Funahashi, "Design of discrete-time repetitive control system for pole placement and application," *IEEE/ASME Transactions on Mechatronics,* vol. 4, pp. 110-118, 1999.

[71] T. Mi-Ching and Y. Wu-Sung, "Design of a plug-in type repetitive controller for periodic inputs," *IEEE Transactions on Control Systems Technology,* vol. 10, pp. 547-555, 2002.

[72] C. L. Roh and M. J. Chung, "Design of repetitive control system for an uncertain plant," *IEE Electronics Letters,* vol. 31, pp. 1959-1960, 1995.

[73] K. Xu, "Multi-input multi-output repetitive control theory and Taylor series based repetitive control design," *Phd Thesis*, Graduate School of Arts and Sciences, Columbia University, 2012.

[74] E. Kurniawan, Z. Cao, and Z. Man, "Robust design of repetitive control system," in *Proceedings of 37th Annual Conference on IEEE Industrial Electronics Society*, *IECON 2011*, pp. 722-727, 2011.

[75] K. Xu and R. W. Longman, "Use of Taylor expansions of the inverse model to design FIR repetitive controllers," in *Proceedings of the 19th AAS/AIAA*, pp. 1073-1088, 2009.

[76] M. Tomizuka, "Dealing with periodic disturbances in controls of mechanical systems," *Annual Reviews in Control,* vol. 32, pp. 193-199, 2008.

[77] K. K. Tan, S. Zhao, S. Huang, T. H. Lee, and A. Tay, "A new repetitive control for LTI systems with input delay," *Journal of Process Control,* vol. 19, pp. 711-716, 2009.

[78] B. S. Kim and T. C. Tsao, "An integrated feedforward robust repetitive control design for tracking near periodic time varying signals," in *Proceedings of Japan–USA symposium on flexible automation* , pp. 875–882, 2002.

[79] J. H. She, M. Wu, Y. H. Lan, and Y. He, "Simultaneous optimisation of the low-pass filter and state-feedback controller in a robust repetitive-control system," *IET Control Theory & Applications,* vol. 4, pp. 1366-1376, 2010.

[80] J. V. Flores, J. M. Gomes da Silva, L. F. A. Pereira, and D. Sbarbaro, "Robust repetitive control with saturating actuators: a LMI approach," in *Proceedings of American Control Conference (ACC),* pp. 4259-4264, 2010.

[81] D. Sbarbaro, M. Tomizuka, and B. L. de la Barra, "Repetitive Control System Under Actuator Saturation and Windup Prevention," *Journal of Dynamic Systems, Measurement, and Control,* vol. 131, pp. 044505-8, 2009.

[82] L. Chi-Ying and L. Yen-Chung, "Precision tracking control and constraint handling of mechatronic servo systems using model predictive control," *IEEE/ASME Transactions on Mechatronics,* vol. 17, pp. 593-605, 2012.

[83] Y. Yang, K. Zhou, and W. Lu, "Robust repetitive control scheme for three-phase constant-voltage-constant-frequency pulse-width modulated inverters," *Power Electronics, IET,* vol. 5, pp. 669-677, 2012.

[84] T-C. Tsao and Y-X. Qian, "Adaptive repetitive control scheme for tracking periodic signals with unknown period," in *Proceedings of American Control Conference*, pp. 1736-1740, 1993.

[85] Z. Cao and G. Ledwich, "Tracking variable periodic signals with fixed sampling rate," in *Proceedings of the 40th IEEE Conference on Decision and Control,* vol.5, pp. 4885-4890, 2001.

[86] Y. H. Kim, C. I. Kang, and M. Tomizuka, "Adaptive and optimal rejection of non-repeatable disturbance in hard disk drives," in *Proceedings of IEEE/ASME Int.Conf. Adv. Intell. Mechatronics* , pp. 1-6, 2005.

[87] G. Hillerstrom and J. Sternby, "Rejection of periodic disturbances with unknown period-a frequency domain approach," in *Proceedings of American Control Conference,* vol.2 , pp. 1626-1631 , 1994.

[88] N. O. Perez Arancibia, L. Chi-Ying, T. Tsu-Chin, and J. S. Gibson, "Adaptive-repetitive control of a hard disk drive," in *Proceedings of the 46th IEEE Conference on Decision and Control*, pp. 4519-4524, 2007.

[89] C. Y. Lin, Y. G. Chen, T. C. Tsao, and S. Gibson, "Laser beam tracking by repetitive and variable-order adaptive control," in *Proceedings of the American Control Conference, ACC 2008,* pp. 2371-2376, Seattle, WA, 2008.

[90] Z. Lu, F. Xu, and X. Dai, "Periodic disturbance restraint based on adaptive finite-dimensional repetitive control," in *Proceedings of the 2nd International Symposium on Systems and Control in Aerospace and Astronautics, ISSCAA 2008*, pp. 1-5, 2008.

[91] J. M. Olm, G. A. Ramos, and R. Costa-Castelló, "Adaptive compensation strategy for the tracking/rejection of signals with time-varying frequency in digital repetitive control systems," *Journal of Process Control,* vol. 20, pp. 551-558, 2010.

[92] E. Kurniawan, Z. Cao, and Z. Man, "Adaptive repetitive control of system subject to periodic disturbance with time-varying frequency," in *Proceedings of the First International Conference on Informatics and Computational Intelligence, ICI 2011*, pp. 185-190, 2011.

[93] A. Cataliotti, V. Cosentino, and S. Nuccio, "A Phase-Locked Loop for the synchronization of power quality instruments in the presence of stationary and transient disturbances," *IEEE Transactions on Instrumentation and Measurement,* vol. 56, pp. 2232-2239, 2007.

[94] G. A. Ramos, J. M. Olm, and R. Costa-Castello, "Digital repetitive control under time-varying sampling period: An LMI stability analysis," in *Proceedings of the 2009 IEEE Conference on* C*ontrol Applications (CCA) & Intelligent Control (ISIC),* pp. 782-787, 2009.

[95] N. Sadegh, "A discrete-time MIMO repetitive controller," in *Proceedings of the 1992 American Control Conference,* pp. 2671-2675, 1992.

[96] D. Jeong and B. C. Fabien, "A discrete time repetitive control system for MIMO plants," in *Proceedings of the 1999 American Control Conference,* vol.6, pp. 4295-4299, 1999.

[97] D. H. Owens, L. M. Li, and S. P. Banks, "Multi-periodic repetitive control system: a Lyapunov stability analysis for MIMO systems," *International Journal of Control,* vol. 77, pp. 504-515, March 2004.

[98] H. Dang and D. H. Owens, "MIMO multi-periodic repetitive control system: Universal adaptive control schemes," *International Journal of Adaptive Control and Signal Processing,* vol. 20, pp. 409-429, 2006.

[99] J. V. Flores, J. M. G. da Silva, L. F. A. Pereira, and D. G. Sbarbaro, "Repetitive control design for MIMO systems with saturating actuators," *IEEE Transactions on Automatic Control,* vol. 57, pp. 192-198, 2012.

[100] L. Wang, S. Chai, E. Rogers, and C. T. Freeman, "Multivariable Repetitive-Predictive Controllers Using Frequency Decomposition," *IEEE Transactions on Control Systems Technology,* vol. 20, pp. 1597-1604, 2012.

[101] G. C. Goodwin, S. F. Graebe, and M. E. Salgado, *Control System Design* Prentice Hall, 2000.

[102] Quanser, "SRV02 User Manual," Canada: Quanser Inc., 2010.

[103] Quanser, "2 DOF Robot position control using QUARC - intructor manual," Canada: Quanser Inc., 2010.

[104] Quanser, "Q8-USB Data Acquisition Board user manual," Canada: Quanser Inc., 2010.

[105] Quanser, "VoltPAQ-X1 user manual," Canada: Quanser Inc., 2010.

[106] *Optimization Toolbox Matlab 7.8.0*. Massachusetts: The Mathworks Inc., 2009.

[107] H. Elci, R. W. Longman, M. Q. Phan, J. Jer-Nan, and R. Ugoletti, "Simple learning control made practical by zero-phase filtering: applications to robotics," *IEEE Transactions on Circuits and Systems I: Fundamental Theory and Applications,* vol. 49, pp. 753-767, 2002.

[108] M. Q. Phan, H. M. Brown, S. C. Lee, and R. W. Longman, "Frequency domain based design of iterative learning controllers for monotonic convergence," in *Proceedings of the 17th The International Federation of Automatic Control World Congress*, vol. 17, pp. 12454-12459 , Seoul, Korea, 2008.

[109] D. Wang and Y. Yongqiang, "Design and experiments of anticipatory learning control: frequency-domain approach," *IEEE/ASME Transactions on Mechatronics,* vol. 10, pp. 305-313, 2005.

[110] M. Comanescu and L. Xu, "An improved flux observer based on PLL frequency estimator for sensorless vector control of induction motors," *IEEE Transactions on Industrial Electronics,* vol. 53, pp. 50-56, 2006.

[111] G. Tao, *Adaptive Control Design and Analysis* Wiley-IEEE Press; 1 edition, 2003.

[112] E. Bristol, "On a new measure of interaction for multivariable process control," *IEEE Transactions on Automatic Control,* vol. 11, pp. 133-134, 1966.

[113] M. T. Tham, "Multivariable control: an introduction to decoupling control " *Report*, Dept.Of Chemical and Process Engineering, University of Newcastle upon Tyne, 1999.

APPENDIX

MATLAB CODES AND SIMULINK MODELS USED IN SIMULATIONS AND EXPERIMENTS

(A) LIST OF MATLAB CODES AND SIMULINK MODELS

CHAPTER 4: Design of Robust RC with Time-varying Sampling Periods			
No	**Name**	**Description**	**Used in**
1.	*compobjfun_lead_quanser.m*	m- file function to formulate the objective function in (4.18) for Quanser servo plant (minimum phase system).	Simulation
2.	*compconfun_lead_quanser.m*	m- file function to formulate the optimization nonlinear constraints no.2 in (4.18) for Quanser servo plant. The boundary constraint (no.1) is given in the optimtool (GUI of optimization toolbox)	Simulation
3.	*compobjfun_lead_robot_nmp.m*	m- file function to formulate the objective function in (4.18) for 7 degree of freedom robot (non-minimum phase system).	Simulation
4.	*compconfun_lead_robot_nmp.m*	m- file function to formulate the constraints in (4.18) for 7 degree of freedom robot (non-minimum phase system).	Simulation
5.	*sim_quanser_new_compensator_nominalTs.mdl*	Simulink model to simulate the proposed new compensator for Quanser servo plant.	Simulation

6.	*sim_robot_nmp_new_compensator_nominalTs.mdl*	Simulink model to simulate the proposed new compensator for 7 degree of freedom robot	Simulation
7.	*robobjfun_lead_quanser.m*	m- file function to formulate the objective function in (4.30) for Quanser servo plant.	Simulation
8.	*robconfun_lead_quanser.m*	m- file function to formulate the constraints function no.2 and 3 in (4.30) for Quanser servo plant. The boundary constraint (no.1) is given in the optimtool (GUI of optimization toolbox)	Simulation
9.	*sim_quanser_robust_compensator.mdl*	Simulink model to simulate the proposed robust compensator for Quanser servo plant.	Simulation
10.	*real_quanser_new_compensator_nominalTs.mdl*	Simulink model to run the RC system with the proposed new compensator in real-time.	Experiment
11	*real_quanser_lead_compensator_nominalTs.mdl*	Simulink model to run the RC system with the lead compensator $k_r z^m$ in real-time.	Experiment
12	*real_quanser_robust_compensator.mdl*	Simulink model to run the RC system with the robust compensator in real-time.	Experiment

CHAPTER 5: Design of Adaptive RC of Linear Systems with Time-varying Periodic Disturbances			
No	**Name**	**Description**	**Used in**
1.	*sim_quanser_MRRC.mdl*	Simulink model to simulate the proposed model reference repetitive control (MRRC) for Quanser model.	Simulation
2.	*adaptive_law_theta_grad_est_Sbuilder_1st_new.c*	C-S function for updating theta each sampling time, where theta has four parameters to be adapted.	Simulation and Experiment

3.	*adaptive_law_rho_grad_est_Sbuilder_1st.c*	C-S function for updating rho each sampling time, where rho has single parameter to be adapted.	Simulation and Experiment
4.	*rep_control_out_states.c*	C-S function to generate RC control law, and also RC states. With this function, not just RC output, but each state of RC can be saved to the workspace.	Simulation and Experiment
5.	*sim_quanser_ARC.mdl*	Simulink model to simulate the proposed adaptive repetitive control (ARC) for quanser model.	Simulation
6.	*sim_RC_fixed_Ts_vary_dist.mdl*	Simulink model to simulate the prototype RC with fixed sampling period and time-varying disturbance.	Simulation
7.	*sim_MRAC_fixed_Ts_vary_dist.mdl*	Simulink model to simulate the model reference adaptive control (MRAC) with fixed sampling period and time-varying disturbance.	Simulation
8.	*gen_dist.m*	m-file function to generate time-varying disturbance. Input of this function is a vector of sampling period.	Simulation
9.	*real_quanser_ARC.mdl*	Simulink model to run the proposed ARC in real-time.	Experiment
10.	*real_fixed_RC_fixed_Ts_vary_dist:*	Simulink model to run the prototype RC with fixed sampling period and time-varying disturbance in real-time	Experiment

CHAPTER 6: Design of Decentralized RC of Linear MIMO Systems			
No	**Name**	**Description**	**Used in**
1.	*compobjfun_lead_mimo_pp_robot.m*	m- file function to formulate the objective function of DRC-1 for pick and place robot model.	Simulation

2.	*compconfun_lead_mimo_pp_robot.m*	m- file function to formulate the nonlinear constraints of DRC-1 for pick and place robot model. The boundary constraint is given in the optimtool (GUI of the optimization toolbox)	Simulation
3.	*stab_control_pp_robot.m*	m- file function to obtain the decentralized stabilizing controller for pick and place robot model.	Simulation
4.	*stab_control_quanser.m*	m- file function to obtain the decentralized stabilizing controller for 2 DOF Quanser robot model.	Simulation
5.	*compobjfun_lead_mimo_quanser_one.m*	m- file function to formulate the objective function of DRC-1 for 2 DOF quanser robot model.	Simulation
6.	*compconfun_lead_mimo_quanser_one.m*	m- file function to formulate the nonlinear constraints of DRC-1 for 2 DOF Quanser robot model.	Simulation
7.	*robust_check_mimo_quanser.m*	m-file function to assess the stability of quanser RC system using DRC-1	Simulation
8.	*compobjfun_lead_mimo_quanser_two.m*	m- file function to formulate the objective function of DRC-2 for 2 DOF Quanser robot model.	Simulation
9.	*compconfun_lead_mimo_quanser_two.m*	m- file function to formulate the nonlinear constraints of DRC-2 for 2 DOF Quanser robot model.	Simulation
10.	*pci_matrix_quanser.m*	m- file function to obtain the phase cancellation inverse (PCI) matrix for 2 DOF Quanser robot model.	Simulation
11.	*s_RC_MIMO_decentralized_pp_robot.mdl*	Simulink model to simulate the proposed DRC-1 for pick and place robot model	Simulation
12.	*s_RC_MIMO_PCI_quanser.mdl*	Simulink model to simulate the PCI for 2 DOF quanser robot model.	Simulation

13.	*s_MIMO_RC_quanser_two.mdl*	Simulink model to simulate the proposed DRC 2 for 2 DOF Quanser robot model.	Simulation
14.	*real_MIMO_RC_quanser_m1.mdl*	Simulink model to run the proposed DRC 1 for 2 DOF Quanser robot model in real-time	Experiment
15.	*real_MIMO_RC_quanser_m2.mdl*	Simulink model to run the proposed DRC 2 for 2 DOF Quanser robot model in real-time.	Experiment
16.	*real_MIMO_RC_quanser_PCI.mdl*	Simulink model to run the PCI for 2 DOF Quanser robot model in real-time.	Experiment

(B) MATLAB CODES TO FORMULATE OPTIMIZATION PROBLEM (4.18) – NEW DESIGN OF RC COMPENSATOR

```
function [f,fi,ci] = compobjfun_lead_quanser(x)
% Objective function for Quanser servo model
% x = parameters to be optimized
% f = total objetive function value
% fi = objective function value at harmonics i
% ci = constraint value at harmonics i
Ts = 0.005;
s= tf('s');
% Second Order Quanser Servo (Minimum Phase)
Kp = 10;
Gs=1.74/(0.0268*s^2+s);
G = c2d(Gs,Ts);
Gstab = G/(1+Kp*G);
Gstab = minreal(Gstab);
%------------------------------------------
[a,b]=tfdata(Gstab,'v');
z = tf('z',Ts);
```

```
q = [0.25 0.5 0.25];% Q-filter coefficients
%%%%--------------Picking up the order of compensator----------------------
%%%%--------------1st Order Compensator-----------------------------------
% p1 = x(1);
% b0 =x(2); b1=x(3);
%%%%----------------------------------------------------------------------
%%%%--------------2nd Order Compensator-----------------------------------
p1 = x(1);p2 = x(2);
b0=x(3); b1=x(4); b2=x(5);
%%%%----------------------------------------------------------------------
%%%%--------------3rd Order Compensator-----------------------------------
% p1 = x(1);p2 = x(2);p3 = x(3);
% b0=x(4); b1=x(5); b2=x(6);b3=x(7);
%%%%----------------------------------------------------------------------
%%%%--------------4th Order Compensator-----------------------------------
% p1 = x(1);p2 = x(2);p3 = x(3);p4 = x(4);
% b0=x(5); b1=x(6); b2=x(7); b3=x(8); b4=x(9);
%%%%----------------------------------------------------------------------
%%%%--------------5th Order Compensator-----------------------------------
% p1 = x(1);p2 = x(2);p3 = x(3);p4 = x(4);p5 = x(5);
% b0=x(6); b1=x(7); b2=x(8); b3=x(9); b4=x(10);b5=x(11);
%%%%----------------------------------------------------------------------

freq=0.8:0.8:100; % picking frequencies at all harmonics up to Nyquist
Ws=2*pi*freq*Ts;
f = 0;fi=[];
ci = 0.95*ones(1,length(freq));

%%%%--------------Obtaining total objective value -------------------------
%%%%%---- For 1st Order (3 Parameters)------------------------------------
% for k=1:1:length(freq);
%     numF = b0*exp(i*1*Ws(k))+b1;
%     numG = a(2)*exp(i*Ws(k))+a(3);
```

```
%     num = numF*numG;
%     denF = (exp(i*Ws(k)) - p1);
%     denG = exp(i*2*Ws(k))+b(2)*exp(i*Ws(k))+b(3);
%     denum = denF*denG;
%     f0 = ((1-num/denum))*conj((1-num/denum));
%     f1 = sqrt(f0);
%     numq = q(1)*exp(-i*Ws(k))+q(2)+q(3)*exp(i*Ws(k));
%     c1 = abs(numq);
%     ft = f1*c1;
%     f = f+ft;
%     fi = [fi ft];
% end
%%%%---------------------------------------------------------------------

%%%%%---- For 2nd Order (5 Parameters)------------------------------------
for k=1:1:length(freq);
   numF = b0*exp(i*2*Ws(k))+b1*exp(i*1*Ws(k))+b2;
   numG = a(2)*exp(i*Ws(k))+a(3);
   num = numF*numG;
   denF = (exp(i*Ws(k)) - p1)*(exp(i*Ws(k)) - p2);
   denG = exp(i*2*Ws(k))+b(2)*exp(i*Ws(k))+b(3);
   denum = denF*denG;
   f0 = ((1-num/denum))*conj((1-num/denum));
   f1 = sqrt(f0);
   numq = q(1)*exp(-i*Ws(k))+q(2)+q(3)*exp(i*Ws(k));
   c1 = abs(numq);
   ft = f1*c1;
   f = f+ft;
   fi = [fi ft];
end
%%%%---------------------------------------------------------------------

%%%%---- For 3rd Order (7 Parameters) ------------------------------------
```

```
% for k=1:1:length(freq);
%     numF = b0*exp(i*3*Ws(k))+b1*exp(i*2*Ws(k))+b2*exp(i*1*Ws(k))+b3;
%     numG = ( a(2)*exp(i*Ws(k))+a(3) );
%     num = numF*numG;
%     denF = (exp(i*Ws(k)) - p1)*(exp(i*Ws(k)) - p2)*(exp(i*Ws(k)) - p3);
%     denG = exp(i*2*Ws(k))+b(2)*exp(i*Ws(k))+b(3);
%     denum = denF*denG;
%     f0 = ((1-num/denum))*conj((1-num/denum));
%     f1 = sqrt(f0);
%     numq = q(1)*exp(-i*Ws(k))+q(2)+q(3)*exp(i*Ws(k));
%     c1 = abs(numq);
%     ft = f1*c1;
%     f = f+ft;
%     fi = [fi ft];
% end
%%%%---------------------------------------------------------------------

%%%%---- For 4th Order (9 Parameters) -------------------------------------
% for k=1:1:length(freq);
%     numF = b0*exp(i*4*Ws(k))+b1*exp(i*3*Ws(k))+b2*exp(i*2*Ws(k))+…
%                b3*exp(i*1*Ws(k))+b4;
%     numG = (a(2)*exp(i*Ws(k))+a(3));
%     num = numF*numG;
%     denF = (exp(i*Ws(k)) - p1)*(exp(i*Ws(k)) - p2)*(exp(i*Ws(k)) - p3)*…
%               (exp(i*Ws(k)) - p4);
%     denG = exp(i*2*Ws(k))+b(2)*exp(i*Ws(k))+b(3);
%     denum = denF*denG;
%     f0 = ((1-num/denum))*conj((1-num/denum));
%     f1 = sqrt(f0);
%     numq = q(1)*exp(-i*Ws(k))+q(2)+q(3)*exp(i*Ws(k));
%     c1 = abs(numq);
%     ft = f1*c1;
%     f = f+ft;
```

```
%     fi = [fi ft];
% end
%%%%---------------------------------------------------------------------

%%%%-- For 5th Order (11 Parameters) ---------------------------------------
% for k=1:1:length(freq);
%     numF = b0*exp(i*5*Ws(k))+b1*exp(i*4*Ws(k))+b2*exp(i*3*Ws(k))+…
%                b3*exp(i*2*Ws(k))+b4*exp(i*1*Ws(k))+b5;
%     numG = a(2)*exp(i*Ws(k))+a(3);
%     num = numF*numG;
%     denF = (exp(i*Ws(k)) - p1)*(exp(i*Ws(k)) - p2)*(exp(i*Ws(k)) - p3)*…
%               (exp(i*Ws(k)) - p4)*(exp(i*Ws(k)) - p5);
%     denG = exp(i*2*Ws(k))+b(2)*exp(i*Ws(k))+b(3);
%     denum = denF*denG;
%     f0 = ((1-num/denum))*conj((1-num/denum));
%     f1 = sqrt(f0);
%     numq = q(1)*exp(-i*Ws(k))+q(2)+q(3)*exp(i*Ws(k));
%     c1 = abs(numq);
%     ft = f1*c1;
%     f = f+ft;
%     fi = [fi ft];
% end
%%%%---------------------------------------------------------------------

function [c, ceq] = compconfun_lead_quanser(x)
% Optimzation constraints function for quanser servo model

[f,fi,ci] = compobjfun_lead_quanser(x);
cf = fi-ci;
c = [cf];
ceq=[];
```

(C) MATLAB CODES TO FORMULATE OPTIMIZATION PROBLEM (4.30) – ROBUST RC COMPENSATOR

```
function f = robobjfun_lead_quanser(x)

% Objective function of robust compensator for quanser servo model

%%%-------- Compensator coefficients at nominal Ts-------------------------

x0 = [-0.925 -0.925 1922.8   -3567.9    1671.2];

%%%%--------------2nd Order Robust Compensator-----------------------------

a1 = x(1); a2=x(2);

b0=x(3); b1=x(4); b2=x(5);

%%%%--------------the objective function----------------------------------

f = (a1-x0(1))^2 + (a2-x0(2))^2+(b0-x0(3))^2+(b1-x0(4))^2+...

        (b2-x0(5))^2;


function [c, ceq] = robconfun_lead_quanser(x)

%%% Optimzation constraints function of robust compensator

%%% for quanser servo model

%%% the aim is to stabilize plant for h=[0.0025,0.0085] s

a1 = x(1); a2=x(2); b0=x(3);b1=x(4);b2=x(5);

u = [a1 a2 b0 b1 b2]';

q = [0.25 0.5 0.25]; % Q-filter coefficients

s= tf('s');
```

```
%%% Discrete model at low sampling period

hl = 0.0025;

Kp = 10;

Gs=1.74/(0.0268*s^2+s);

Gl = c2d(Gs,hl);

z = tf('z',hl);

Gstab_low = minreal(Gl/(1+Kp*Gl));

%-------------------------------------------

[a,b]=tfdata(Gstab_low,'v');

freq = 1/(hl*250):1/(hl*250):1/(2*hl);

Ws=2*pi*freq*hl;

fi=[];ci=0.9*ones(1,length(freq));

for k=1:1:length(freq);

    numF =u(3)*exp(i*2*Ws(k))+u(4)*exp(i*1*Ws(k))+u(5);

    numG = a(2)*exp(i*Ws(k))+a(3);

    num = numF*numG;

    denF = (exp(i*Ws(k)) - u(1))*(exp(i*Ws(k)) - u(2));

    denG = exp(i*2*Ws(k))+b(2)*exp(i*Ws(k))+b(3);

    denum = denF*denG;

    f0 = ((1-num/denum))*conj((1-num/denum));

    f1 = sqrt(f0);

    numq = q(1)*exp(-i*Ws(k))+q(2)+q(3)*exp(i*Ws(k));

    c1 = abs(numq);
```

```
    ft = (f1*c1);

    fi = [fi ft];

end

%%% Discrete model at up sampling period

hu = 0.0085;

Kp = 10;

Gu = c2d(Gs,hu);

z = tf('z',hu);

Gstab_high = minreal(Gu/(1+Kp*Gu));

%-------------------------------------------

[a,b]=tfdata(Gstab_high,'v');

freq = 1/(hu*250):1/(hu*250):1/(2*hu);

Ws=2*pi*freq*hu;

fk=[];ck=0.9*ones(1,length(freq));

for k=1:1:length(freq);

    numF =u(3)*exp(i*2*Ws(k))+u(4)*exp(i*1*Ws(k))+u(5);

    numG = a(2)*exp(i*Ws(k))+a(3);

    num = numF*numG;

    denF = (exp(i*Ws(k)) - u(1))*(exp(i*Ws(k)) - u(2));

    denG = exp(i*2*Ws(k))+b(2)*exp(i*Ws(k))+b(3);

    denum = denF*denG;

    f0 = ((1-num/denum))*conj((1-num/denum));

    f1 = sqrt(f0);
```

```
    numq = q(1)*exp(-i*Ws(k))+q(2)+q(3)*exp(i*Ws(k));

    c1 = abs(numq);

    ft = (f1*c1);

    fi = [fi ft];

end

f_all = [fi fk];

c_all = [ci ck];

c = f_all - c_all;

ceq = [];
```

(D) MATLAB CODES TO FORMULATE OPTIMIZATION PROBLEM (6.30) – DECENTRALIZED RC-2 (DRC-2)

```
function [f,fi,ci] = compobjfun_lead_mimo_quanser_two(x)

% Objective function for DRC-2

% x = parameters to be optimized

% f = total objetive function value

% fi = objective function value at harmonics i

% ci = constraint value at harmonics i

Ts = 0.025; % sampling rate

s= tf('s');

% Continous model of 2 DOF Quanser robot plant

B11 =  1.021;

A11 = [0.005907  0.1191  1];

B21 = [-0.002888 0 ];

A21 = [ 0.006947  0.1201  1];
```

```
B12 = [ -0.01438  0.3975];
A12 = [26.43  7.202  1];
B22 = 1.003;
A22 = [0.005095  0.1151  1];
Gs = [tf(B11,A11) tf(B12,A12);tf(B21,A21) tf(B22,A22)];
% Discrete model of 2 DOF Quanser robot plant
G = c2d(Gs,Ts);
Gstab = minreal(G);
[a12,b12]=tfdata(Gstab(1,2),'v');
[a21,b21]=tfdata(Gstab(2,1),'v');
[a11,b11]=tfdata(Gstab(1,1),'v');
[a22,b22]=tfdata(Gstab(2,2),'v');
q = [0.25 0.5 0.25]; % Q-filter coefficients
z = tf('z',Ts);
%%%%--------------2nd Order Compensators- 10 unknown parameters-----------
p1 = x(1); p2 = x(2);p1_2 = x(3); p2_2 = x(4);
b0 = x(5); b1 = x(6); b2 = x(7);
b0_2 = x(8); b1_2 = x(9); b2_2 = x(10);
%%%%%---- 2 lead compensators - 10 parameters to be optimized-------------
freq = 1/(Ts*80):1/(Ts*80):1/(2*Ts);
Ws = 2*pi*freq*Ts;
f = 0;fi=[];
ci = 0.95*ones(1,length(freq));
%%%%--------------Obtaining total objective value ----------------------------
for k=1:1:length(freq);
   numF1 = b0*exp(i*2*Ws(k))+b1*exp(i*1*Ws(k))+b2;
   numF2 = b0_2*exp(i*2*Ws(k))+b1_2*exp(i*1*Ws(k))+b2_2;
```

```
numG1 =  a11(2)*exp(i*Ws(k))+a11(3);
numG2 =  a22(2)*exp(i*Ws(k))+a22(3);
num1 = numF1*numG1;
num2 = numF2*numG2;
denF1 = (exp(i*Ws(k)) - p1)*(exp(i*Ws(k)) - p2);
denF2 = (exp(i*Ws(k)) - p1_2)*(exp(i*Ws(k)) - p2_2);
denG1 = exp(i*2*Ws(k))+b11(2)*exp(i*Ws(k))+b11(3);
denG2 = exp(i*2*Ws(k))+b22(2)*exp(i*Ws(k))+b22(3);
denum1 = denF1*denG1;
denum2 = denF2*denG2;
numq = q(1)*exp(-i*Ws(k))+q(2)+q(3)*exp(i*Ws(k));
f0_1 = ((1-num1/denum1))*conj((1-num1/denum1));
f1_1 = sqrt(f0_1);
f0_2 = ((1-num2/denum2))*conj((1-num2/denum2));
f1_2 = sqrt(f0_2);
c1 = abs(numq);
ft = f1_1*c1;
ft_2=f1_2*c1;
f = f+ft+ft_2;
numG3 =  a12(2)*exp(i*Ws(k))+a12(3);
denG3 =  exp(i*2*Ws(k))+b12(2)*exp(i*Ws(k))+b12(3);
numG4 =  a21(2)*exp(i*Ws(k))+a21(3);
denG4 =  exp(i*2*Ws(k))+b21(2)*exp(i*Ws(k))+b21(3);
F  = [numF1/denF1 0; 0 numF2/denF2];
G  = [(numG1/denG1) (numG3/denG3);(numG4/denG4) (numG2/denG2)];
P = (eye(2,2)-F*G)*numq;
detP = P(1,1)*P(2,2)-P(1,2)*P(2,1);
```

```
    fs = abs(detP);
    fi = [fi fs];
end

function [c, ceq] = compconfun_lead_mimo_quanser_two(x)
% Optimization constraints for mimo model of 2 DOF robot
[f,fi,ci] = compobjfun_lead_mimo_quanser_two(x);
cf = fi-ci;
c = [cf];
ceq=[];
```

LIST OF PUBLICATIONS

Journal Papers:

[1] E. Kurniawan, Z. Cao, and Z. Man, "Design of Robust Repetitive Control with Time Varying Sampling Periods " *IEEE Transactions on Industrial Electronics*, 2013**, accepted**.

[3] E. Kurniawan, Z. Cao, and Z. Man, "Decentralized Repetitive Control of MIMO Systems with Application to 2 DOF robot", *International Journal of Control , Automation and Systems,* **submitted**.

[2] E. Kurniawan, Z. Cao, and Z. Man, "Digital Design of Adaptive Repetitive Control of Linear Systems with Time-Varying Periodic Disturbances", *IET Control Theory and Applications,* **to be submitted**.

Conference Papers:

[4] E. Kurniawan, Z. Cao, and Z. Man,“Design of Decentralized Repetitive Control of Linear MIMO System",in *Proceedings of the 8th IEEE Conference on Industrial Electronics and Application*, pp. 427-432, Australia, June 2013.

[5] E. Kurniawan, Z. Cao, and Z. Man, "Robust design of repetitive control system," in *Proceedings of 37th Annual Conference on IEEE Industrial Electronics Society*, *IECON 2011*, pp. 722-727, Australia, Novermber 2011.

[6] E. Kurniawan, Z. Cao, and Z. Man, "Adaptive Repetitive Control of System Subject to Periodic Disturbance with Time-Varying Frequency," in *Proceedings of the First International Conference on Informatics and Computational Intelligence, ICI 2011*, pp. 185-190, December 2011.